Resilience of Residential Wooden Structures against Wind Hazards

by

Ahmed U. Abdelhady

A dissertation submitted in partial fulfillment
of the requirements for the degree of
Doctor of Philosophy
(Civil Engineering and Scientific Computing)
in The University of Michigan
2021

Doctoral Committee:

Associate Professor Jason McCormick, Co-Chair
Associate Professor Seymour M.J. Spence, Co-Chair
Professor Sherif El-Tawil
Professor Seth Guikema

Ahmed U. Abdelhady
auhady@umich.edu
ORCID iD: 0000-0002-5274-0129

This dissertation is dedicated to my parents, my brother and my wife whose unyielding love, support, and encouragement have enriched my soul and inspired me to pursue and complete this research.

ACKNOWLEDGEMENTS

This study has been financially supported by the National Science Foundation (NSF), the Rackham International Student Fellowship, and the Rackham Graduate Student Research Grant. These supports are gratefully acknowledged.

I would like to express my sincere appreciation to Dr. Jason McCormick and Dr. Seymour Spence for their consistent support and instant feedback on my work, especially during the pandemic. I would like to express my gratitude to Dr. Sherif El-Tawil and Dr. Seth Guikema for taking the time to evaluate this research study and providing constructive feedback that helps enrich the dissertation.

During my Ph.D. journey, I have received technical, societal, and emotional support from my family (Usama, Youssria, Hazem, and Hannah), my friends (Bakry, Zaky, Omar, Amr, Essam, Osama, Abdelhamid, Fatma, Hiba, Mostafa, and Ali), my in-laws (David, Cameron, Meredith, Elizabeth, Gregory, Christie, Joshua, Esme, Taran, Teilo, Emma, Eli, Elyse, and Amy), my labmates (Dr. Wei-Chu, Dr. Arthriya, Dr. Zhicheng, Dr. Jason, Dr. Alyssa, Bowei, and Srinivasan), and my colleagues (Andrew, Dr. Donghui, Dr. Szu-Yun, and Xi). I would like to thank all of you for being part of this achievement.

TABLE OF CONTENTS

LIST OF FIGURES

Figure

LIST OF TABLES

Table

ABSTRACT

Extreme windstorms, such as hurricanes and tornadoes, can have adverse social and economic impacts which pose a great challenge for a community's economic prosperity and quality of life. From 1997 to 2016, tornado events made up 39.9% of total insured losses due to catastrophic events while hurricanes and tropical storms comprised 38.2% of the losses. Consequently, over the past four decades, governments and decision-makers adopted policies and mitigation plans to enhance the resilience of communities against such hazards. The quantification of the impact of these mitigation policies toward reducing the gap between the current and target resilience levels is a computationally challenging problem.

To address this problem, research is undertaken to develop computational frameworks to quantify the impact and effectiveness of policies and mitigation plans on the resilience of residential wooden structures against wind hazards. These computational frameworks are able to quantify the response of a residential neighborhood to the hazard immediately after its impact and during the recovery process. Damage to the residential wooden buildings, that composes the neighborhood, immediately after a hurricane is estimated considering dynamic wind pressure and the impact of windborne debris. To model this damage for a certain subset of houses, debris generated in neighboring areas, defined as exogenous debris, must be taken into account. The estimated damage is then integrated with a probabilistic recovery model which enables a fully probabilistic quantification of the resilience of residential wooden buildings.

Hurricanes typically produce severe widespread rainfall. This rainfall can cause significant damage to the built environment and its supporting infrastructure. To extend the developed frameworks to account for the impact of hurricane rainfall, estimates of water ingress due to wind-driven rain and inland flooding are included. Finally, this dissertation presents a three-dimensional six-degree-of-freedom debris trajectory model for tornadoes. The trajectory model can be used to determine the landing locations of windborne debris as well as the impact energy upon landing which are essential in quantifying the damage to buildings due to tornadoes. These frameworks can help decision-makers identify the performance of residential wooden buildings against wind hazards and optimally prioritize the mitigation plans.

CHAPTER I

Introduction

1.1 Motivation

Severe windstorms, such as hurricanes and tornadoes, can have adverse social and economic impacts which pose a challenge for a community's economic prosperity and quality of life. Moreover, risk-prone areas around the globe have experienced population growth, migration, and increased wealth concentration, all of which inevitably lead to increased risk of future losses. While recent improvements in forecasting and early warning systems have resulted in a decrease in fatalities resulting from windstorms; the impact on the mental health of survivors, the environment, as well as the economy cannot be mitigated through the aforementioned strategies (*Bourque et al.*, 2006; *Deborah D'Souza*, 2019; *Espinel et al.*, 2019; *Harriet Torry and Sarah Chaney*, 2018; *Kyle Grammatica*; *Rhodes et al.*, 2010; *Robert M. Horkovich*, 2017; *Sallenger*; *Strobl*, 2011; *Wetsman*, 2019).

A more comprehensive and robust approach to windstorms risk mitigation (in terms of risk reduction, transfer of risk, and better preparedness and response effectiveness) can be achieved through implementing strategies that increase community resilience, a concept that has recently been used to mitigate risk from various natural hazards (e.g., *Ceskavich and Sasani*, 2018; *Disse et al.*, 2020; *Haggag et al.*, 2020; *Han et al.*, 2020; *Hassan et al.*, 2020; *Lu et al.*, 2020; *Masoomi et al.*, 2018; *McClymont*

et al., 2020; *Nofal and van de Lindt*, 2020; *Ribeiro and Pena Jardim Gonçalves*, 2019; *Sediek et al.*, 2020; *Sen et al.*, 2021; *Sharma et al.*, 2018; *Stochino et al.*, 2019; *van de Lindt et al.*, 2020). Over the past two decades, research has focused on developing an understanding of the concept of resilience by introducing definitions as well as identifying measures, properties, and dimensions (*Haimes*, 2009; *Hosseini et al.*, 2016b; *Meerow et al.*, 2016; *Rosowsky*, 2020). The following definition of community resilience is provided by the National Academy of Science "*Community resilience is the ability to prepare and plan for, absorb, recover from, and more successfully adapt to actual or potential adverse events.*"

Quantifying community resilience against windstorms, in light of the previous definition, requires the development of computational frameworks that can capture the response of the community during and after the windstorm event by (1) estimating the amount of damage and losses immediately after the windstorm, and (2) modeling the community recovery process. A community, which is viewed as a socio-technical system, is composed of various interdependent systems (e.g., buildings, electrical power grid, water pipelines, gas pipelines, people, etc.). The buildings of a community constitute a critical system within the community and quantifying their response and performance under windstorms is a fundamental step towards quantifying and enhancing the resilience of the community. Within this context, this dissertation focuses on multi-disciplinary computational frameworks for quantifying the performance of residential wooden buildings against hurricanes and tornadoes.

1.2 Objectives

The goal of this research is to develop computational frameworks and detailed numerical models to be used to estimate the damage sustained by residential buildings

during hurricanes and tornadoes as well as their recovery trajectory. In particular, the main objectives are listed as follows:

Objective I: Accurately account for damage from exogenous windborne debris within physics-based hurricane vulnerability models and incorporate this damage into the resilience quantification of residential wooden buildings. A major challenge in the quantification of damage due to hurricanes is modeling the damage from exogenous windborne debris. Exogenous debris is the windborne debris generated from neighboring communities that can potentially impact buildings in the considered community. A comprehensive approach that can account for damage to wooden residential structures from exogenous windborne debris is required.

Objective II: Performance and risk assessment of residential wooden buildings under hurricane winds. Evaluating the resilience of residential wooden buildings to hurricanes hinges on the assessment of their performance as well as the hurricane-imposed risks associated with residential structures. A fragility analysis methodology is used to achieve this objective.

Objective III: Probabilistic quantification of the resilience of residential wooden buildings against hurricane winds. A probabilistic recovery model is developed and integrated with a physics-based vulnerability model to estimate the resilience of residential wooden buildings against hurricane winds.

Objective IV: Estimation of water ingress due to hurricane rainfall. A comprehensive framework to estimate the amount of water ingress into residential wooden buildings due to wind-driven rain and the consequent in-land flooding is developed to quantify the impact of hurricane rainfall on residential neighborhoods.

Objective V: Account for windborne debris damage during tornadoes through a six-degree-of-freedom debris trajectory model. The problem of estimating the damage caused by windborne debris in tornadoes requires a debris trajectory model to identify the landing location and impact energy or momentum of the windborne debris. This challenge is addressed through a six-degree-of-freedom (6DOF) debris trajectory model that can trace the trajectory of windborne debris of various geometric shapes.

1.3 Dissertation Structure

The dissertation is organized into 7 chapters.

Chapter 2 presents a methodology to to account for exogenous windborne debris generated in neighboring subdivisions (*Abdelhady et al.*, 2021b). The proposed methodology is applied to analyze a hypothetical residential community in Miami, FL. Analysis results quantify the required extent of the neighboring area that must be modeled in light of hurricane maximum wind speed, floor-area ratio and capacity of the building envelope components. A regression model is provided that can be used to estimate the size of the neighboring area needed in damage estimation models.

Chapter 3 integrates the methodology developed in chapter 2 into an engineering-based vulnerability model to accurately estimate the damage due to dynamic wind pressure and windborne debris impact (*Abdelhady et al.*, 2021c, 2022). The developed vulnerability model is used for risk and performance assessment of residential buildings under hurricane winds using fragility analysis. The resulting fragility curves highlight: (1) the effect of the floor-area ratio on enhancing the performance of the residential building due to the shielding effect; and (2) the variation of the signifi-

cance of windborne debris on increasing the estimated hurricane risk. The estimated fragility curves can be used directly to model residential buildings in community resilience frameworks.

Chapter 4 integrates damage estimated immediately after a hurricane through the developed vulnerability model with a probabilistic recovery model (*Abdelhady et al.*, 2019a,b, 2020, 2021a, 2019c). A fully probabilistic quantification of the resilience of residential neighborhoods against hurricane winds is achieved. The framework is illustrated with a case study consisting of a typical residential neighborhood in Miami, FL.

Chapter 5 presents a comprehensive framework that estimates the amount of water ingress into residential buildings due to wind-driven rain and consequent inland flooding (*Abdelhady et al.*, 2021d). The developed framework is illustrated by modeling the impact of Hurricane Harvey on Houston, TX.

Chapter 6 presents a six-degree-of-freedom (6DOF) debris trajectory model that can trace the trajectory of windborne debris of various geometric shapes (*Abdelhady et al.*, 2021e). The proposed model is used to show the significant difference in modeling debris trajectory in tornado wind fields as compared to straight line winds.

Finally, **chapter 7** presents general conclusions and contributions of this work. Future research directions in the area of community resilience against hurricanes and tornadoes are also provided.

1.4 Publications from this Dissertation

In accordance with the University of Michigan's doctoral degree requirements, this dissertation is presented as a series of journal papers. The papers comprising chapters 2-6 are:

Abdelhady, A.U., Spence, S.M.J. and McCormick, J. (2020). "Modeling the effect of exogenous windborne debris in hurricanes," *Engineering Structures*, Submitted.

Abdelhady, A.U., Spence, S.M.J. and McCormick, J. (2020). "Risk and performance assessment of residential wooden buildings under hurricane winds," *Structural Safety*, Submitted.

Abdelhady, A.U., Spence, S.M.J. and McCormick, J. (2020). "A framework for the probabilistic quantification of the resilience of communities to hurricane winds," *Journal of Wind Engineering & Industrial Aerodynamics*, 206, 104376.

Abdelhady, A.U., Xu, D., Ouyang, Z., Spence, S.M.J., McCormick, J. and Ivanov, V.Y. (2020). "A framework for the estimate of water ingress due to hurricane rainfall," *Building and Environment*, Under Preparation.

Abdelhady, A.U., Spence, S.M.J. and McCormick, J. (2020). "Three-dimensional six-degree-of-freedom windborne debris trajectory model for tornadoes," *Journal of Wind Engineering & Industrial Aerodynamics*, Submitted.

CHAPTER II

Modeling the Effect of Exogenous Windborne Debris in Hurricanes[1]

Abstract

Modeling and estimating the damage to the built environment caused by hurricane winds is an essential requirement to enhance community resilience. Consideration of damage to a building's envelope caused by windborne debris impact is necessary. To model this damage for a certain subdivision of houses, debris generated in neighboring subdivisions, defined as exogenous debris, must be taken into account. Existing physics-based damage estimation models do not consider the effect exogenous windborne has on the estimated damage due to hurricane winds. This paper provides a methodology to identify the extent of the neighboring subdivisions that needs to be considered during damage simulation to accurately account for exogenous windborne debris. The presented methodology is based on first identifying the extent of the neighboring subdivisions through a simulation-based strategy which follows an iterative scheme. For each size increment, the iterative scheme estimates the number of exogenous windborne debris using a physics-based damage estimation model. The single building solution is then generalized to a subdivision of any arbitrary shape. The proposed methodology is applied to analyze a hypothetical residential commu-

[1] Abdelhady, A.U., Spence, S.M.J. and McCormick, J. (2021). "Modeling the effect of exogenous windborne debris in hurricanes," *Engineering Structures*, Submitted.

nity in Miami, FL. Analysis results show the effect on the required extent of the neighboring subdivisions of the hurricane maximum wind speed, the floor-area ratio and the resistance of the building envelope components. The analysis concludes with a regression model that can be used to estimate the size of the neighboring subdivisions to be used in damage estimation models.

2.1 Introduction

Windborne debris is one of the major causes of damage to the built environment during severe windstorms, such as hurricanes and tornadoes. Damage caused by debris is cascading in nature. Once flying debris breaches the building envelope, internal pressurization can cause more damage which leads to the generation of more windborne debris (*Lin et al.*, 2010b). The cascading nature of the windborne debris damage increases the complexity of its estimation which is a fundamental step in quantifying and mitigating risks associated with windstorms. The problem of estimating damage from windborne debris has been studied by researchers over the past four decades. In the Florida Public Hurricane Loss Projection Model (FPHLPM), only unprotected windows are assumed to be vulnerable to windborne debris impact (*Gurley et al.*, 2005). Impact loads on unprotected windows are estimated empirically by modeling the likelihood of a piece of flying debris impacting and breaking an unprotected window using an exponential distribution. Parameters controlling the exponential distribution are chosen empirically based on engineering judgment. HAZUS-MH follows a similar approach to estimate the windborne debris damage to vulnerable envelope components (e.g., windows, doors, and garage doors) of residential wooden buildings. In this case, the exponential distribution parameters are evaluated from the results of a physics-based damage estimation model (*Vickery*

et al., 2006a,b). The damage estimation model explicitly models the windborne debris trajectory, from generation until impact, for a neighborhood of around 140 buildings subject to 36 hurricanes of various categories.

With the aim of providing a better understanding of the damage caused by windborne debris and its interaction with damage from dynamic wind pressure, physics-based damage estimation models that account for both damage mechanisms have been developed (*Abdelhady et al.*, 2019a,b,c; *Grayson et al.*, 2013; *Lin and Vanmarcke*, 2010b; *Lin et al.*, 2010b; *Yau*, 2011; *Yau et al.*, 2011). *Lin and Vanmarcke* (2010b) use a 3-degree-of-freedom (3DOF) model to trace windborne debris trajectories, while *Grayson et al.* (2013) uses a 6DOF model to account for the aerodynamic shape of the debris object (*Grayson et al.*, 2012a). Despite the advantages of using physics-based models, one of the biggest challenges that limit their applicability is computational run-time since these simulations are computationally expensive. This challenge poses a limit on the number of buildings that can be modeled within a simulation.

Modeling a subdivision of a neighborhood without the surrounding buildings can result in an underestimation of damage. This damage underestimation is due to ignoring the windborne debris generated from outside the considered subdivision that can potentially land and impact buildings within the considered subdivision. This type of debris is referred to as exogenous windborne debris. The significance of exogenous windborne debris in estimating damage has been recognized in previous studies (*Abdelhady et al.*, 2020; *Grayson*, 2014). *Abdelhady et al.* (2020) accounts for exogenous windborne debris by including in the simulation all neighboring buildings that are within the maximum possible flight distance of potential windborne debris. However, due to the cascading nature of windborne debris damage, including

surrounding buildings beyond this distance may lead to further damage in buildings that are within this maximum debris flight distance therefore generating further exogenous windborne debris.

Within the context outlined above, this paper provides a comprehensive methodology to account for the effect of exogenous windborne debris through physics-based damage estimation models for residential neighborhoods. The proposed methodology explicitly accounts for the following factors that affect the amount of exogenous windborne debris: (1) factors related to the surrounding subdivisions: size and extension, pressure and impact resistance of the buildings' envelope, floor-area ratio (FAR), and building configuration; (2) factors related to the hurricane hazard impacting the community: size of the hurricane defined by its radius to maximum wind speeds (R_{max}), the location of the considered subdivision with respect to the hurricane track defined by the minimum distance from the track to the considered subdivision (d_{min}) and the hurricane heading (θ), the hurricane maximum wind speed (V_{max}), and the change in direction of the wind speed as the hurricane approaches the considered subdivision. The proposed methodology is applied to study a hypothetical subdivision which consists of representative gable-roof buildings in Miami, FL. A regression analysis of the simulation results provides a mathematical expression for estimating the extent of the surrounding subdivisions that must be modeled to accurately capture damage from exogenous windborne debris.

2.2 Problem definition

Figure 2.1(a) shows a neighborhood of residential wooden buildings that have an arbitrary configuration. Assuming this neighborhood is in a hurricane-prone region, estimation of damage caused by hurricane winds ideally considers two mechanisms:

(1) dynamic wind pressure and (2) impact of windborne debris. The damage susceptibility of a representative subdivision of the neighborhood can be modeled using a physics-based damage estimation model (e.g. *Abdelhady et al.* (2020); *Grayson et al.* (2013)) that can account for both mechanisms. The domain of the considered subdivision (Ω_{cs}) and its boundary ($\partial\Omega_{cs}$) can be defined as follows:

$$\begin{aligned} \Omega_{cs} &= \{(x,y) \in \mathbb{R}^2 \mid \Gamma_{cs}(x,y) \leq 0\} \\ \partial\Omega_{cs} &= \{(x,y) \in \mathbb{R}^2 \mid \Gamma_{cs}(x,y) = 0\} \end{aligned} \tag{2.1}$$

where Γ_{cs} is an implicit function that passes through the floor plan centroid of all buildings on the boundary of the considered subdivision.

Only modeling the considered subdivision, i.e. the buildings in Ω_{cs}, will in general lead to an underestimation of the total damage since neighboring buildings around the considered subdivision can also experience damage during a hurricane. Damage to these external buildings will generate exogenous windborne debris. To account for this, a subset of buildings in the surrounding subdivisions need to be included in the model. The domain Ω_{ns}, and associated boundary $\partial\Omega_{ns}$, that includes all buildings of neighboring subdivisions (ns) necessary for capturing the effect of exogenous windborne debris can be defined as:

$$\begin{aligned} \Omega_{ns} &= \{(x,y) \in \mathbb{R}^2 \mid \Gamma_{ns}(x,y) \leq 0\} \\ \partial\Omega_{ns} &= \{(x,y) \in \mathbb{R}^2 \mid \Gamma_{ns}(x,y) = 0\} \end{aligned} \tag{2.2}$$

where Γ_{ns} is an implicit function that defines the boundary of the neighboring subdivisions.

To account for exogenous windborne debris, Γ_{ns} needs to be chosen such that it will include all neighboring buildings that act as a source of exogenous windborne debris. This requirement can be stated as follows:

$$\Gamma_{ns}(x,y) = \Gamma_{cs}(x,y) + \alpha(x,y) \tag{2.3}$$

where $\alpha(x, y)$ is an enlargement function that expands the boundary of the considered subdivision to include buildings from neighboring subdivisions. The required enlargement function (α_{exo}) sets a boundary such that all possible exogenous windborne debris impacting the considered subdivision is captured, while including the minimum number of neighboring buildings to minimize computational run-time. This enlargement function can be estimated mathematically as follows:

$$\begin{aligned} \alpha_{exo} &= \arg\min_{\alpha} A_{\Omega_{ns}} \\ \text{subject to} \\ N_{exo}(\alpha = \alpha_{exo}; \cdots) &= \max_{\alpha} N_{exo}(\alpha; \cdots) \end{aligned} \tag{2.4}$$

where N_{exo} is the total number of exogenous windborne debris for the considered subdivision and $A_{\Omega_{ns}}$ is the area enclosed by the boundary $\partial\Omega_{ns}$. $A_{\Omega_{ns}}$ can be calculated using Green's Theorem as follows:

$$A_{\Omega_{ns}} = \frac{1}{2} \int_{\partial\Omega_{ns}} x dy - y dx \tag{2.5}$$

2.3 Simulation-based Approach

2.3.1 Single building formulation

Solving eqs. (2.3) and (2.4) directly for Γ_{ns} generally defines a computationally intractable problem. This section is focused on the development of a computationally tractable algorithm for the identification of Γ_{ns}. With this aim, it can be observed that as α_{exo} is a function of the shape of the boundary of the considered subdivision (Γ_{cs}), an α_{exo} for each specific Γ_{cs} will be required. As a result, a considered subdivision must be picked that when eqs. (2.3) and (2.4) are solved for Γ_{ns}, the solution can be generalized to any arbitrarily shape of the considered subdivision's boundary. A subdivision consisting of a single building is considered first as shown in fig. 2.1(b).

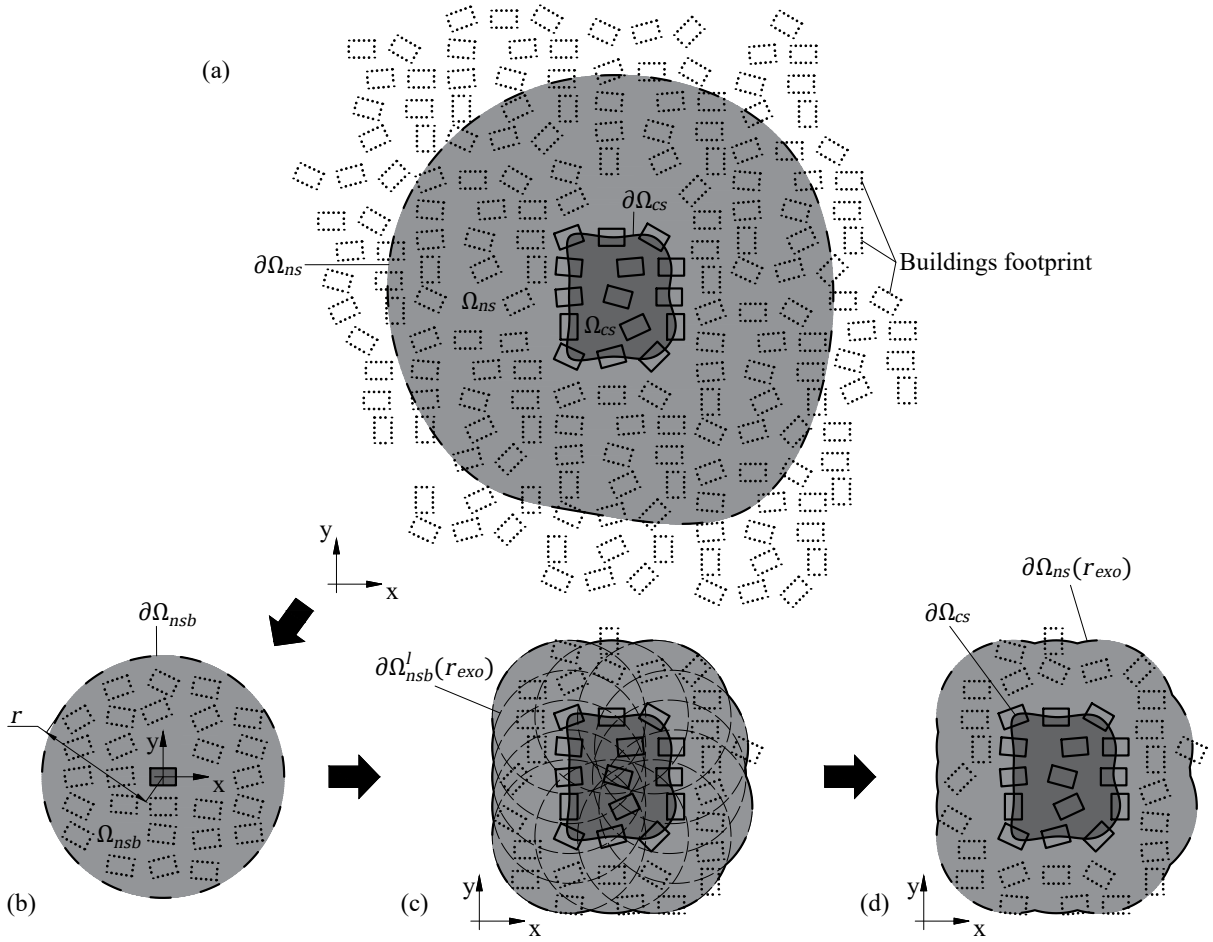

Figure 2.1: Schematic of the problem definition and the proposed methodology: (a) a neighborhood of buildings of arbitrary configuration; (b) the single building case with a circular boundary for inclusion of buildings in neighboring subdivisions; (c) graphical resolution of the boundary; and (d) the final required boundary to account for exogenous windborne debris from buildings in neighboring subdivisions.

Equation (2.2) can be re-written, for the single building case, as follows:

$$\begin{aligned} \Omega_{nsb} &= \{(x,y) \in \mathbb{R}^2 \mid \Gamma_{nsb}(x,y) \leq 0\} \\ \partial\Omega_{nsb} &= \{(x,y) \in \mathbb{R}^2 \mid \Gamma_{nsb}(x,y) = 0\} \end{aligned} \tag{2.6}$$

where Γ_{nsb} is an implicit function that defines the boundary of the domain defining the buildings of neighboring subdivisions that must be considered.

The shape of $\partial\Omega_{nsb}$ depends on the direction from which the exogenous windborne debris originates, as shown in fig. 2.2. The direction of the hurricane wind field with respect to the considered subdivision is the main factor that controls the origination direction of the exogenous windborne debris. Since the approach of hurricanes is variable, the shape of $\partial\Omega_{nsb}$ is assumed to be circular, as illustrated in fig. 2.1(b). This ensures there is equal chances for the exogenous windborne debris to come from any direction. Γ_{nsb} can therefore be defined as follows:

$$\Gamma_{nsb}(x,y) = x^2 + y^2 - r^2 \tag{2.7}$$

where r is the radius of the boundary identifying the buildings of neighboring subdivisions to include. Equation (2.4) can be re-written for the single building case as follows:

$$\begin{aligned} r_{exo} &= \arg\min_{r} A_{\Omega_{nsb}} \\ &\text{subject to} \\ n_{exo}(r = r_{exo}; \cdots) &= \max_{r} n_{exo}(r; \cdots) \end{aligned} \tag{2.8}$$

where r_{exo} is the radius that captures all exogenous windborne debris that can potentially impact the considered building while including the minimum number of neighboring buildings; $A_{\Omega_{nsb}}$ is the area enclosed by r_{exo}, i.e. πr^2; while n_{exo} is the number of exogenous windborne debris impacting the considered building.

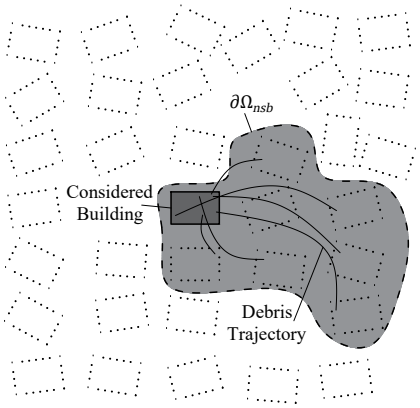

Figure 2.2: An example of a possible shape of the boundary $\partial\Omega_{nsb}$ for the single building case.

2.3.2 Simulation strategy

Solving eq. (2.8) requires estimating the number of exogenous windborne debris, n_{exo}, as a function of r. The source of the exogenous windborne debris is the damaged building envelope components of neighboring buildings, while the driving force for the generated debris flight is the hurricane wind velocity. For any given extent of the neighboring subdivisions (r), n_{exo} depends on the following factors:

- **Neighborhood-related factors:** the configuration and the structural characteristics of the buildings. These factors control the generation of debris as buildings in the considered and surrounding subdivisions are damaged.
- **Hurricane-related factors:** the shape of the storm track and its location with respect to the considered subdivision, the size of the storm and the pressure drop within its eye. These factors control the evolution of wind speeds and direction during the hurricane event which is the driving force for the flight of the debris.

To account for these factors while estimating n_{exo}, the scenario of a hurricane impacting the considered building surrounded by the neighboring buildings (within radius r) needs to be simulated using a physics-based damage estimation model. Due to the uncertainty associated with these factors, eq. (2.8) will be re-written as

follows:

$$r_{exo} = \arg\min_{r} A_{\Omega_{nsb}}$$

$$\text{subject to} \tag{2.9}$$

$$\mathrm{E}\left[n_{exo}(r = r_{exo}; \cdots)\right] = \max_{r} \mathrm{E}\left[n_{exo}(r; \cdots)\right]$$

where $\mathrm{E}\left[n_{exo}\right]$ is the expected value of n_{exo}.

Figure 2.3 illustrates the proposed simulation-based strategy to solve eq. (2.9). It follows an iterative scheme to find r_{exo} which keeps increasing r incrementally, using a predefined step Δr, until the value of $\mathrm{E}\left[n_{exo}\right]$ stabilizes. The $\mathrm{E}\left[n_{exo}\right]$ is estimated using a Monte Carlo simulation where n_{MC} is the number of simulations. Based on a predefined maximum hurricane wind speed of interest (V_{max}), the Monte Carlo simulation generates hurricanes having a maximum wind speed equal to V_{max} using the specified hurricane hazard statistics. To this end, the single-site probabilistic hurricane hazard model introduced by *Vickery and Twisdale* (1995a) is used. Uncertainties in the buildings' structural characteristics are considered by sampling the components' pressure and impact resistances from provided distributions. The damage estimation model creates models of both the considered building as well as the neighboring buildings within the current region of interest, i.e. for buildings within current radius r^j. From this model, the progression of damage from wind pressure and windborne debris impact is estimated using a time-stepping approach. At the final time step, the number of exogenous windborne debris that hit the considered building (i.e. the middle building) over the duration of the hurricane event is counted and the expected number of relevant exogenous windborne debris is calculated as shown in fig. 2.3.

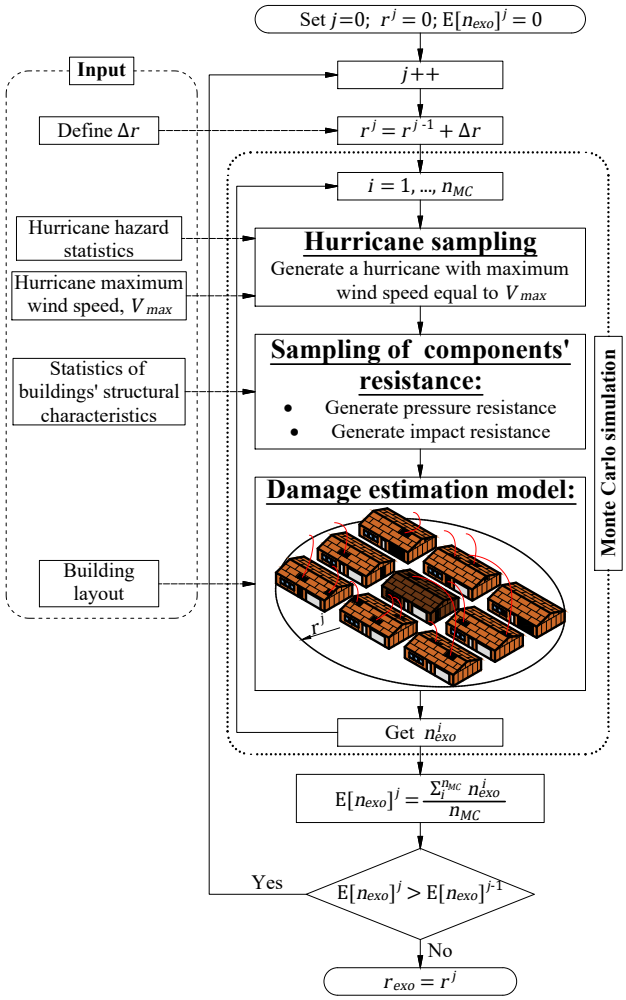

Figure 2.3: Flowchart of the simulation-based strategy.

2.3.3 Damage estimation model

The physics-based damage estimation model presented by *Grayson et al.* (2013) is used to estimate $\mathrm{E}[n_{exo}]$. The model is implemented with the following modifications:

- **External pressure coefficients:** compiled from the wind tunnel database provided by *Tokyo Polytechnic University* (2007);
- **Internal pressure coefficients:** calculated using the internal pressure model provided by *Holmes* (2017);
- **Debris impact:** checked for all the components (i.e., windows, doors, garage

doors, roof sheathing, etc.) of the buildings' envelope by solving for the point of intersection of the debris trajectory and the building envelope. This approach allows for consideration of debris hitting the building even if the estimated debris landing location is not within the perimeter of the building plan, as illustrated in fig. 2.4.

The windborne debris trajectories are traced using the probabilistic 6DOF debris trajectory model presented by *Grayson et al.* (2012a). The model solves the equations of motion for flying debris numerically using the Modified Euler method. The location of a debris object at landing ($\mathbf{D}_L$) as well as the time step immediately prior to landing ($\mathbf{D}_P$) are used to determine which component is hit by the windborne debris. The debris trajectory between $\mathbf{D}_P$ and $\mathbf{D}_L$ can be assumed linear and is represented using the following parametric form:

$$\mathbf{D}_P + t\mathbf{D}_{PL}; \quad t \in \mathbb{R} \tag{2.10}$$

where $\mathbf{D}_{PL} = \mathbf{D}_L - \mathbf{D}_P$. The parametric equation of the planes of the components of the building envelope is written as:

$$\mathbf{C}_2^k + u\mathbf{C}_{21}^k + v\mathbf{C}_{23}^k; \quad u, v \in \mathbb{R} \;\&\; k = 1, \cdots, n_C \tag{2.11}$$

where $\mathbf{C}_1^k$, $\mathbf{C}_2^k$ and $\mathbf{C}_3^k$ are the coordinates of the first, second and third vertices of the k^{th} component, respectively; n_C is the total number of components in the building; and $\mathbf{C}_{21}^k = \mathbf{C}_1^k - \mathbf{C}_2^k$ while $\mathbf{C}_{23}^k = \mathbf{C}_3^k - \mathbf{C}_2^k$.

The point of intersection of the debris trajectory and the k^{th} component is obtained by solving eqs. (2.10) and (2.11) simultaneously. The values of the parameters

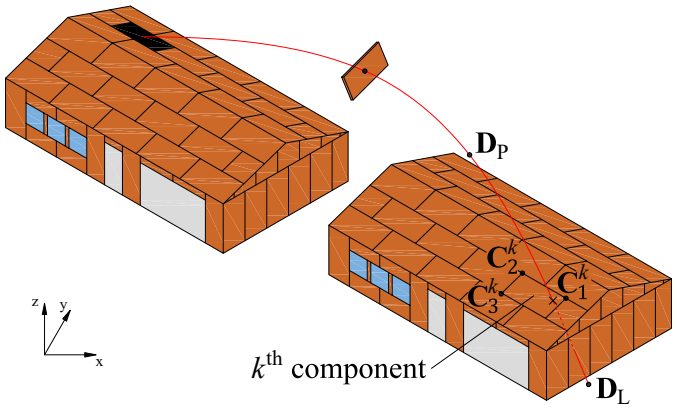

Figure 2.4: A piece of windborne debris hitting a building envelope component.

at the intersection point are given as follows:

$$
\begin{aligned}
t^k &= \frac{\left(\mathbf{C}_{21}^k \times \mathbf{C}_{23}^k\right) \cdot \left(\mathbf{D}_P - \mathbf{C}_2^k\right)}{-\mathbf{D}_{PL} \cdot \left(\mathbf{C}_{21}^k \times \mathbf{C}_{23}^k\right)} \\
u^k &= \frac{\left(\mathbf{C}_{23}^k \times -\mathbf{D}_{PL}\right) \cdot \left(\mathbf{D}_P - \mathbf{C}_2^k\right)}{-\mathbf{D}_{PL} \cdot \left(\mathbf{C}_{21}^k \times \mathbf{C}_{23}^k\right)} \\
v^k &= \frac{\left(-\mathbf{D}_{PL} \times \mathbf{C}_{21}^k\right) \cdot \left(\mathbf{D}_P - \mathbf{C}_2^k\right)}{-\mathbf{D}_{PL} \cdot \left(\mathbf{C}_{21}^k \times \mathbf{C}_{23}^k\right)}
\end{aligned}
\tag{2.12}
$$

For components of rectangular shape, the debris object hits the k^{th} component if $u^k, v^k \in [0, 1]$. In the case of triangular components, an additional condition of $(u^k + v^k) \leq 1$ needs to be satisfied at the intersection point for the debris object to hit the building envelope component. The value of t^k is used if the debris trajectory intersects two components. In this case, the component with a lower value of t^k (i.e. hit first) is the one that is considered impacted by the debris.

2.3.4 Solution generalization

The single building case can be generalized to any considered subdivision of any arbitrary shape as show in fig. 2.1(c,d). This generalization is described mathematically as follows:

$$
\Omega_{ns} = \bigcup_{l=1}^{n_{cb}} \Omega_{nsb}^l \tag{2.13}
$$

where n_{cb} is the number of the buildings in the considered subdivision while Ω^l_{nsb} is the domain identifying the required buildings of the neighboring subdivisions for the l^{th} building. From the boundaries, $\partial\Omega^l_{nsb}$, of the domains Ω^l_{nsb}, it is straight forward to estimate the boundary of Ω_{ns}. The domain, Ω^l_{nsb}, and associated boundary, $\partial\Omega^l_{nsb}$, of the l^{th} building are defined as:

$$\begin{aligned} \Omega^l_{nsb} &= \{(x,y) \in \mathbb{R}^2 \mid \Gamma^l_{nsb}\left(x - x^l_{cb}, y - y^l_{cb}\right) \leq 0\} \\ \partial\Omega^l_{nsb} &= \{(x,y) \in \mathbb{R}^2 \mid \Gamma^l_{nsb}\left(x - x^l_{cb}, y - y^l_{cb}\right) = 0\} \end{aligned} \tag{2.14}$$

where x^l_{cb} and y^l_{cb} are the $x-$ and $y-$ coordinates of the l^{th} building in the considered subdivision; Γ^l_{nsb} is the implicit function defined by eq. (2.7) and evaluated at $r = r_{exo}$.

Equations (2.13) and (2.14) are solved using alg. 1 to obtain the buildings that need to be included in the damage estimation model to account for exogenous wind-borne debris. In alg. 1, x^o_{nb} and y^o_{nb} are the $x-$ and $y-$ coordinates of the o^{th} building in a neighboring subdivision; n_{nb} is the total number of the buildings in the neighboring subdivision; while x_{mod} and y_{mod} are the $x-$ and $y-$ coordinates of the buildings to be modeled while estimating the damage in the considered neighborhood.

Algorithm 1: Generalization of the single building solution

Input: r_{exo}; $(x^l_{cb}, y^l_{cb}), \cdots, (x^{n_{cb}}_{cb}, y^{n_{cb}}_{cb})$; $(x^1_{nb}, y^1_{nb}), \cdots, (x^{n_{nb}}_{nb}, y^{n_{nb}}_{nb})$
Output: $(x^1_{mod}, y^1_{mod}), \cdots, (x^{n_{mod}}_{mod}, y^{n_{mod}}_{mod})$

```
count = 1
for l = 1, ..., n_cb do
    for o = 1, ..., n_nb do
        d_lo = sqrt((x^l_cb - x^o_nb)^2 + (y^l_cb - y^o_nb)^2)
        if d_lo ≤ r_exo and (x^o_nb, y^o_nb) ∉ [x_mod, y_mod] then
            x^count_mod = x^o_nb
            y^count_mod = y^o_nb
            count = count + 1
        end if
    end for
end for
```

2.4 Exogenous windborne debris for gable-roof buildings

The approach presented in section 2.3 is used in this section to analyze a neighborhood that consists of gable-roof buildings in Miami, FL, as shown in figs. 4.4 and 5.5. The main objective is to understand the impact of various factors, such as wind speed, floor-area ratio and building strength, on the required extent of the neighboring subdivisions to accurately model the effect of the exogenous windborne debris. This gained understanding is used to perform a regression analysis which results in a mathematical expression that relates the required extent of modeling neighboring subdivisions to the aforementioned factors.

2.4.1 Description

2.4.1.1 Community layout and building archetype

The extent of the neighboring subdivisions required to accurately model the effect of exogenous windborne debris for a hypothetical residential community, illustrated in fig. 4.4(a), located in Miami, FL is investigated. Figure 4.4(b) shows the reduction of the community to the single building case which is a fundamental step in the described methodology.

Buildings, that constitute the neighborhood, are modeled using the archetype shown in fig. 5.5 and are arranged on a rectangular grid with spacing s_x and s_y between the grid lines in the $x-$ and $y-$ directions, respectively. To study the effect of the floor-area ratio, $FAR = {}^{\text{building area}}/_{s_x s_y}$, on modeling the exogenous windborne debris, three cases are considered (1) $FAR = 0.1$: $s_x = 38.55$ m and $s_y = 33.88$ m, (2) $FAR = 0.3$: $s_x = 23.33$ m and $s_y = 18.66$ m, and (3) $FAR = 0.6$: $s_x = 17.27$ m and $s_y = 12.60$ m.

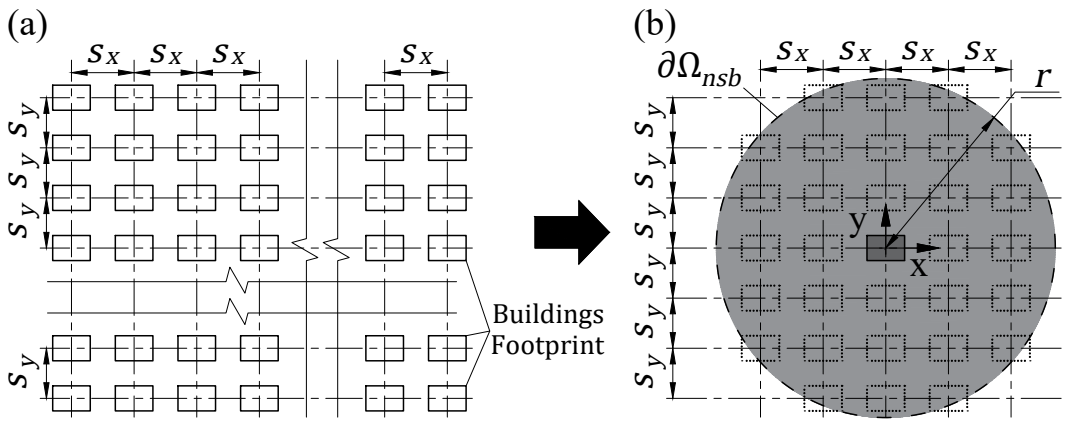

Figure 2.5: The hypothetical residential community: (a) community layout, and (b) the single building case for the considered community.

2.4.1.2 Construction cases

There are numerous types and construction methods for the components of a building envelope (e.g., windows, doors, sheathing, etc.) which result in a wide range of wind pressure and debris impact resistances. To study the effect of the strength of the building defined by the resistances of its components to both wind pressure and debris impact, the resistance ranges are taken from available literature (e.g. *Datin et al.*, 2011; *Grayson et al.*, 2013; *Gurley et al.*, 2005; *Unnikrishnan and Barbato*, 2016; *Vickery et al.*, 2006b). Ten construction cases are defined based on the identified ranges such that the resistance is increasing gradually from case one (the weakest) to case ten (the strongest).

Tables 3.2 and 3.3 summarize the resistances for wind pressure and debris impact, respectively. Component resistances are modeled as normal random variables with coefficients of variation equal 0.2 for the wind pressure resistance of the windows, door, garage doors, and roof-wall connections and 0.4 for the wind pressure resistance of the roof and wall sheathing, roof and wall cover, and the impact resistance of all components.

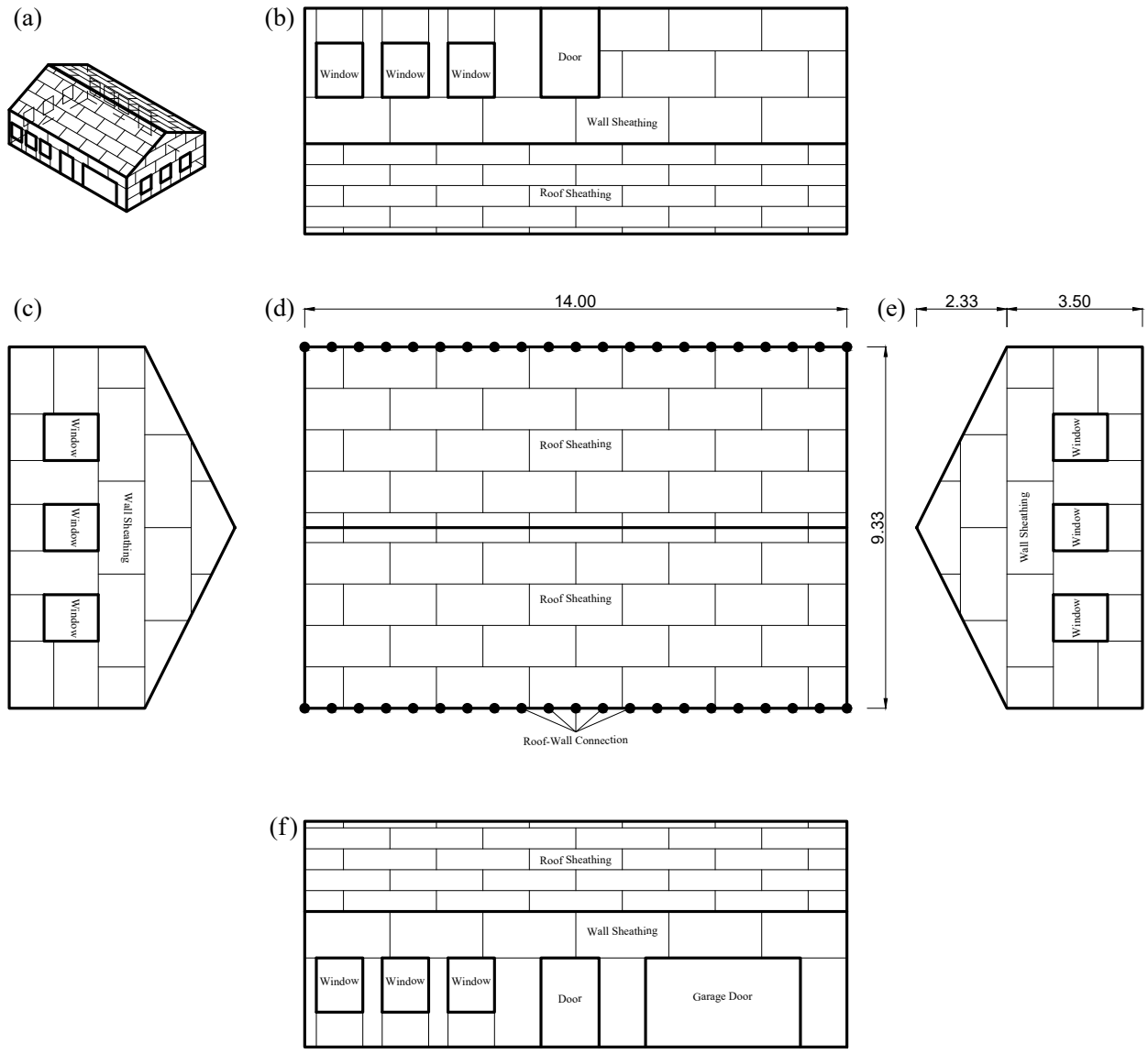

Figure 2.6: Residential gable-roof building archetype: (a) isometric projection, (b) back view, (c) left-side view, (d) top view, (e) right-side view, (f) front view.

Table 2.1: Mean wind pressure resistance for the considered construction cases.

Building component	Case 1	Case 2	Case 3	Case 4	Case 5	Case 6	Case 7
Window (kPa)	2.5	2.8	3.2	3.5	3.8	4.2	4.5
Door (kPa)	3.0	3.3	3.6	3.8	4.1	4.4	4.7
Garage door (kPa)	2.0	2.2	2.4	2.7	2.9	3.1	3.3
Wall sheathing (kPa)	1.0	1.9	2.8	3.7	4.6	5.4	6.3
Roof sheathing (kPa)	1.0	1.9	2.8	3.7	4.6	5.4	6.3
Wall cover (kPa)	2.5	2.8	3.2	3.5	3.8	4.2	4.5
Roof cover (kPa)	2.5	2.8	3.2	3.5	3.8	4.2	4.5
Roof-wall connection (kN)	1.0	2.7	4.4	6.2	7.9	9.6	11.3

Table 2.1: Mean wind pressure resistance for the considered construction cases (*Continued*).

Building component	Case 8	Case 9	Case 10
Window (kPa)	4.8	5.2	5.5
Door (kPa)	4.9	5.2	5.5
Garage door (kPa)	3.6	3.8	4.0
Wall sheathing (kPa)	7.2	8.1	9.0
Roof sheathing (kPa)	7.2	8.1	9.0
Wall cover (kPa)	4.8	5.2	5.5
Roof cover (kPa)	4.8	5.2	5.5
Roof-wall connection (kN)	13.1	14.8	16.5

Table 2.2: Mean debris impact resistance (in kJ) for the considered construction cases.

Building component	Case 1	Case 2	Case 3	Case 4	Case 5	Case 6	Case 7
Window	0.05	0.10	0.15	0.26	0.36	0.47	0.57
Door	0.10	0.15	0.30	0.51	0.72	0.93	1.14
Garage door	0.10	0.15	0.30	0.51	0.72	0.93	1.14
Wall sheathing	0.10	0.25	0.50	1.04	1.59	2.13	2.68
Roof sheathing	0.10	0.25	0.50	1.04	1.59	2.13	2.68
Wall cover	0.10	0.25	0.50	1.04	1.59	2.13	2.68
Roof cover	0.10	0.25	0.50	1.04	1.59	2.13	2.68

Table 2.2: Mean debris impact resistance (in kJ) for the considered construction cases (*Continued*).

Building component	Case 8	Case 9	Case 10
Window	0.68	0.78	1.00
Door	1.36	1.57	2.00
Garage door	1.36	1.57	2.00
Wall sheathing	3.22	3.77	5.00
Roof sheathing	3.22	3.77	5.00
Wall cover	3.22	3.77	5.00
Roof cover	3.22	3.77	5.00

2.4.1.3 Hurricane hazard statistics

Hurricane wind velocity is an important factor in estimating the required extent of neighboring subdivisions in a simulation model. In this context, the considered com-

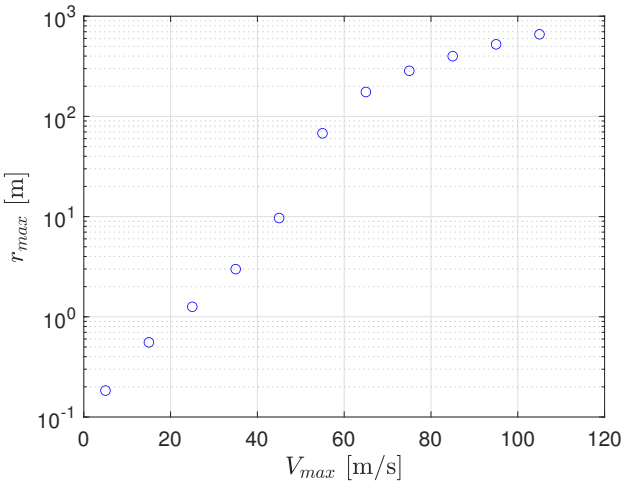

Figure 2.7: Maximum flying distance of a 4 ft × 8 ft roof sheathing panel.

munity is subject to hurricanes with $V_{max} = \{5, 15, 25, 35, 45, 55, 65, 75, 85, 95, 105\}$ m/s. For each V_{max}, 200 hurricanes (i.e. $n_{MC} = 200$) are generated. Parameters defining track and intensity of these hurricanes are sampled from the probabilistic hurricane hazard model defined by *Vickery and Twisdale* (1995a).

2.4.1.4 Radius step consideration

As mentioned in section 2.3.2, the presented methodology requires a predefined radius increment (Δr) to solve for r_{exo}. Since the analysis is carried out for various cases of V_{max} (11 cases), Δr is defined by normalizing it with respect to the maximum flight distance of windborne debris (r_{max}) for the given V_{max}. A typical 4 ft × 8 ft roof sheathing panel is used to estimate r_{max}. Figure 2.7 summarizes the values of r_{max} for each V_{max} case. The following values of $r/r_{max} = \{0.5, 1.0, 1.2, 1.4, 1.6, 1.8, 2.0, 2.2, 2.4, 2.6, 2.8, 3.0\}$ are then used as the iteration steps in the simulation.

2.4.2 Results and discussion

2.4.2.1 Overview

The analysis is conducted for a combination of 3 values of FAR, 10 construction cases, 11 values of V_{max} with 200 hurricanes (i.e., Monte Carlo simulations) considered for each V_{max}, and 12 iterations on r. This results in 792,000 simulations to comprehensively study the factors influencing the extent of the neighboring subdivisions that must be modeled to fully capture all potential exogenous windborne debris.

2.4.2.2 Effect of wind speed

Figure 2.8 shows the expected number of exogenous windborne debris impacting the considered single building, shown in fig. 4.4(b), for each V_{max} over all iterations of r (additional iterations were added for lower wind speeds to further refine r_{exo}).

No exogenous windborne debris (i.e., $\mathrm{E}[n_{exo}] = 0$) is observed for the cases of $V_{max} < 55$ m/s as the maximum debris flight distance is 9.7 m for $V_{max} = 45$ m/s, fig. 2.7, which is to short to impact any of the surrounding buildings. As expected, $\mathrm{E}[n_{exo}]$ increases as V_{max} or r/r_{max} increase. The increasing rate of $\frac{\partial(\mathrm{E}[n_{exo}])}{\partial(r/r_{max})}$ keeps declining as the extent of the modeled neighboring subdivision increases until $\mathrm{E}[n_{exo}]$ eventually plateaus, identifying the value of r_{exo}.

Figure 2.9 summarizes the values of r_{exo}/r_{max} for $V_{max} \geq 55$ m/s. For $V_{max} < 55$ m/s, r_{exo}/r_{max} can be assumed zero meaning that only the considered neighborhood needs to be modeled. The plot shows that r_{exo}/r_{max} is directly proportional to V_{max}. This direct proportionality can be explained by the fact that as V_{max} increases, the number of debris objects flying in the wind field increases. More objects in the wind field increases the potential of damage due to windborne debris. Due to the cascading nature of the windborne debris damage, the extent of neighboring

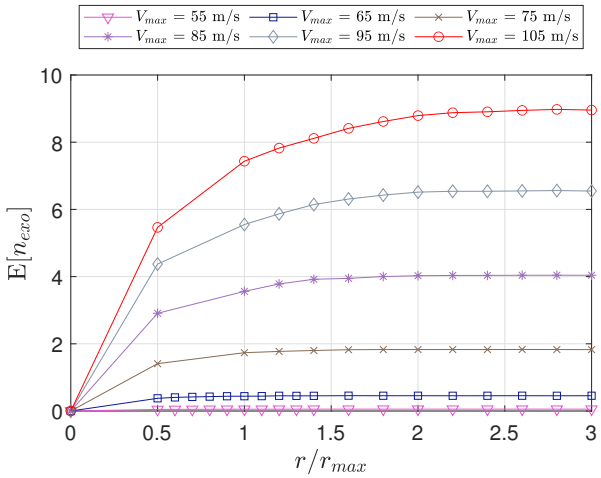

Figure 2.8: Expected number of exogenous windborne debris for cases of $V_{max} \geq 55$ m/s.

subdivisions required to account for exogenous windborne debris increases as well.

2.4.2.3 Effect of floor-area ratio (FAR)

The FAR indicates the level of urbanization in a neighborhood (i.e. higher FAR means more buildings for a given area). The expected number of windborne debris increases with increasing FAR as the increase in the density of buildings increases the sources of windborne debris, as shown in fig. 2.10. However, fig. 2.11 suggests that r_{exo}/r_{max} is inversely proportional to FAR. This inverse proportionality is due to the increase in the number of buildings as FAR increases (e.g. $FAR = 0.6$ has six times the number of buildings as when $FAR = 0.1$). Smaller extents of neighboring subdivisions (i.e. smaller r_{exo}/r_{max} values) become sufficient to capture all exogenous windborne debris for larger FAR values.

2.4.2.4 Effect of building strength

The building strength factor (BSF) is defined as an indicator of the resistance of the entire building to damage from both wind-related damage mechanisms:

$$BSF = \frac{\sum_k^{n_C} \bar{R}_P^k A^k + \sum_k^{n_C} \bar{R}_I^k A^k}{A_t} \tag{2.15}$$

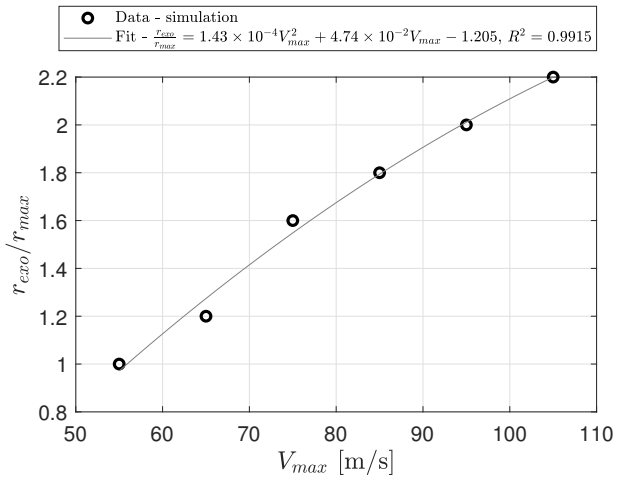

Figure 2.9: The relationship between the required extent of neighboring subdivisions to model exogenous windborne debris (r_{exo}) and V_{max}.

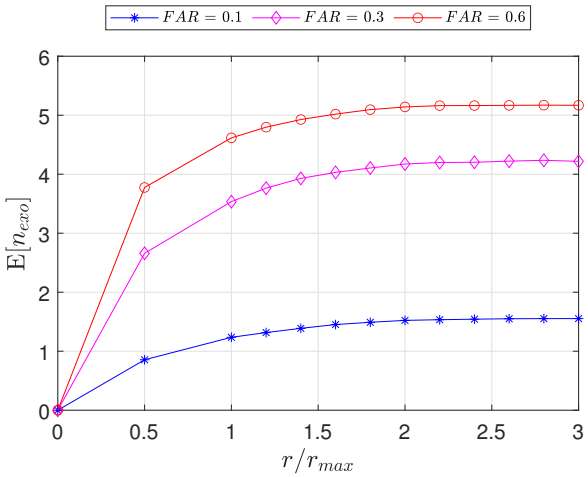

Figure 2.10: Expected number of exogenous windborne debris for each FAR case.

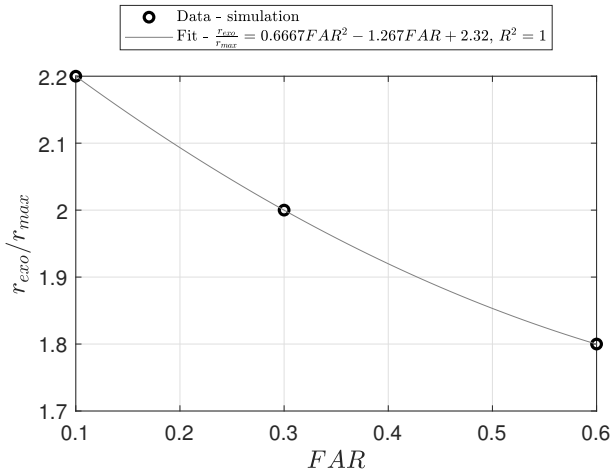

Figure 2.11: The relationship between the required extent of neighboring subdivisions to model exogenous windborne debris (r_{exo}) and FAR.

where $\bar{R}_P^k$ is the mean wind pressure resistance of the k^{th} building envelope component in kPa; $\bar{R}_I^k$ is the mean debris impact resistance of the k^{th} building envelope component in kJ; A^k is the surface area of the k^{th} building envelope component; and A_t is the total surface area of the building envelope.

Figure 2.12 shows the values of the BSF for the ten construction cases which are sorted from weakest (case 1) to strongest (case 10) in ascending order. It can be observed that as the building strength factor increases, E[n_{exo}] decreases (i.e., more strength leads to less damage and less windborne debris) while r_{exo}/r_{max} remains unchanged, figs. 2.13 and 2.14. This observation is consistent with all construction cases except 1 and 2. The difference for these cases is due to the very low value of BSF for cases 1 and 2 which indicates that the building components are damaged at very low wind speeds. Because the wind speeds are low, the hurricane wind field is not sufficient to carry dislodged components far enough to impact the considered building. As a result, increasing r/r_{max} for cases 1 and 2 does not significantly change E[n_{exo}] compared to other construction cases.

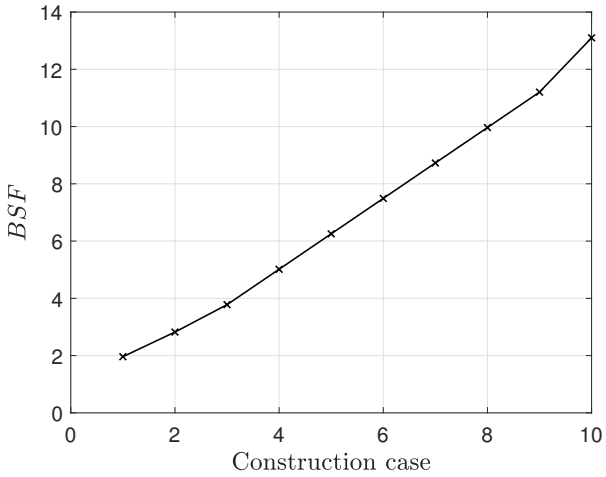

Figure 2.12: The building strength factor.

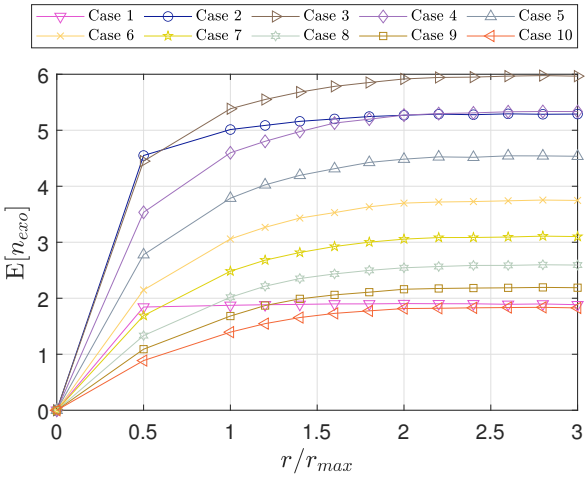

Figure 2.13: Expected number of exogenous windborne debris for each construction case.

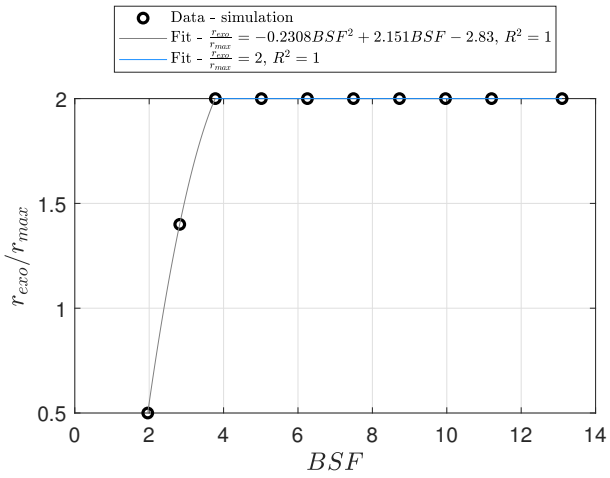

Figure 2.14: Expected number of exogenous windborne debris for various values of BSF.

2.4.3 Regression analysis

The discrete r_{exo}/r_{max} simulation results are used in a linear regression analysis to provide a mathematical expression to estimate r_{exo}/r_{max} as a function of V_{max}, FAR, and BSF. r_{exo}/r_{max} is shown to be zero for $V_{max} < 55$ m/s and constant for $3.7 \leq BSF \leq 13.1$. For all other cases, r_{exo}/r_{max} varies with respect to V_{max}, FAR, and BSF with the studied parameters. Based on these observations, the following mathematical expression is proposed to estimate r_{exo}/r_{max}:

$$\frac{r_{exo}}{r_{max}} = \begin{cases} 0 & V_{max}, FAR, BSF \in D_1 \\ a_1 V_{max}^2 + a_2 V_{max} + a_3 FAR^2 + a_4 FAR & \\ +a_5 BSF^2 + a_6 BSF + a_7 & V_{max}, FAR, BSF \in D_2 \\ b_1 V_{max}^2 + b_2 V_{max} + b_3 FAR^2 + b_4 FAR + b_5 & V_{max}, FAR, BSF \in D_3 \end{cases} \tag{2.16}$$

where V_{max} is in m/s; $D_1 = \{(V_{max}, FAR, BSF) \in \mathbb{R}^3 \mid 0 \leq V_{max} < 55,\ 0.1 \leq FAR \leq 0.6\ \&\ 1.90 \leq BSF \leq 13.10\}$, $D_2 = \{(V_{max}, FAR, BSF) \in \mathbb{R}^3 \mid 55 \leq V_{max} \leq 105,\ 0.1 \leq FAR \leq 0.6\ \&\ 1.90 \leq BSF < 3.77\}$, and $D_3 = \{(V_{max}, FAR, BSF) \in$

$\mathbb{R}^3 \mid 55 \leq V_{max} \leq 105,\ 0.1 \leq FAR \leq 0.6\ \&\ 3.77 \leq BSF < 13.10\}$; and $a_1, \cdots, a_7$ and $b_1, \cdots, b_5$ are the regression parameters which can be estimated using the ordinary least square method. The estimated values of the regression parameters are summarized in table 2.3.

Figure 2.15 shows the values of r_{exo}/r_{max} estimated from eq. (2.16) for three levels of FAR: 0.1, 0.3, and 0.6. The average relative error (ε) of these estimations equals 3.9% which is defined as follows:

$$\varepsilon = \sum_{p=1}^{n_{cases}} \left| \frac{\frac{r_{exo}}{r_{max}}^{p} - \frac{\hat{r_{exo}}}{r_{max}}^{p}}{\frac{r_{exo}}{r_{max}}^{p} n_{cases}} \right| \times 100\% \tag{2.17}$$

where n_{cases} is the number of studied cases (330 cases), $\frac{r_{exo}}{r_{max}}^{p}$ is the true value (i.e., obtained from the simulations) of the p^{th} studied case, and $\frac{\hat{r_{exo}}}{r_{max}}^{p}$ is the estimated value (i.e., obtained from eq. (2.16)) of the p^{th} studied case. By combining the values of r_{exo}/r_{max} obtained from eq. (2.16) with the generalization methodology described by eq. (2.13), the extent of the neighboring subdivisions required to capture the effect of exogenous windborne debris can be obtained for neighborhoods of any arbitrarily boundary shape in Miami, FL.

Table 2.3: Estimated values of the regression parameters.

Parameter	Estimated value	Parameter	Estimated value
a_1	-3.95×10^{-4}	b_1	-1.78×10^{-4}
a_2	6.99×10^{-2}	b_2	6.08×10^{-2}
a_3	-0.704	b_3	1.486
a_4	-0.441	b_4	-1.969
a_5	-0.331	b_5	-1.744
a_6	2.424		
a_7	-5.456		

2.5 Conclusions

A methodology for estimating the extent of the neighboring subdivisions required to account for exogenous windborne debris is presented. The underlying idea behind

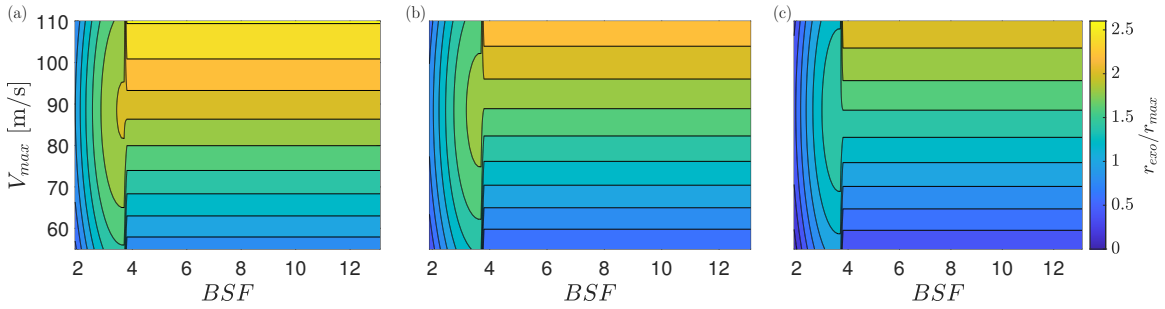

Figure 2.15: Estimated r_{exo}/r_{max} for all studied cases: (a) $FAR = 0.1$, (b) $FAR = 0.3$, and (c) $FAR = 0.6$.

the presented methodology is to reduce the problem from a representative subdivision to a single building. This reduction allows for the generalization of the solution to any subdivision with any arbitrary boundary shape. For the single building case, the required extent of the neighboring subdivisions is estimated using a simulation-based strategy. The simulation-based strategy accounts for the neighborhood-related factors and the hurricane-related factors which affect the number of exogenous windborne debris. The simulation strategy is based on an iterative technique that increases the extent of neighboring subdivisions incrementally until the number of the exogenous windborne debris plateaus (i.e., the required extent of the neighboring subdivision that needs to be modeled is obtained). The expected number of the exogenous windborne debris is estimated using a physics-based damage estimation model. The damage estimation model propagates uncertainties associated with estimating wind pressure damage and windborne debris damage using Monte Carlo simulation. Finally, an algorithm is proposed to generalize the single building solution to a subdivision with any arbitrary boundary shape.

The presented methodology is applied to analyze a hypothetical community in Miami, FL. The analysis comprehensively considers the problem of estimating the required extent of the neighboring subdivisions to model exogenous windborne debris by investigating the effect of the maximum hurricane wind speed, the floor-area ratio,

and the resistance of the building envelope components to wind pressure and debris impact. Results show that the required extent of the neighboring subdivisions is directly proportional to the maximum hurricane wind speed and inversely proportional to the floor-area ratio. The required extent of the neighboring subdivisions is not a function of the resistance of the building envelope except for very weak construction cases for which direct proportionality is seen. Based on these results, a regression model is derived that estimates the required extent of the neighboring subdivisions to account for exogenous windborne debris.

CHAPTER III

Risk and Performance Assessment of Residential Wooden Buildings Subject to Hurricane Winds[1]

Abstract

Hurricanes are the major cause of damage and losses to residential wooden buildings in the United States. Thus, studying hurricane-imposed risks on the residential-wooden buildings, as well as their performance against hurricanes, is a fundamental step to mitigate these risks. Within this context, a fragility analysis methodology is proposed to estimate the building performance probabilistically. Two damage mechanisms are considered in the proposed methodology, excessive dynamic wind pressure; and impact from windborne debris. Unlike existing frameworks, the proposed methodology defines the geometric configuration, and the required extension of the neighboring buildings to accurately estimate the damage from both mechanisms. The proposed methodology is applied to the gable-roof archetype. Ten construction cases are defined to cover the existing ranges of the resistance of the building components to both damage mechanisms, as well as three floor-area ratios (FAR). The resulting fragility curves highlight: (1) the effect of the FAR on enhancing the performance of the residential building due to the shielding effect; and (2) the variation of the significance of windborne debris on increasing the estimated hurricane risk.

[1] Abdelhady, A.U., Spence, S.M.J. and McCormick, J. (2021). "Risk and performance assessment of residential wooden buildings subject to hurricane winds," *Structural Safety*, Submitted.

The estimated fragility curves can be used directly to model residential buildings in community resilience frameworks.

3.1 Introduction

Light-frame wooden buildings represent the majority of the residential buildings in the United States. This type of construction is vulnerable to windstorms (e.g. hurricanes) as reported by post-disaster surveys (*Beason et al.*, 1984; *Masters et al.*, 2010; *Minor*, 1994), and the consequent damage of these houses represents a significant portion of the losses caused by hurricanes (*Congressional Budget Office*, 2019). Observations from these surveys suggest that excessive dynamic wind pressure, and impact of windborne debris are the prevailing damage mechanisms.

Both damage mechanisms are interdependent, progressive, and of cascading nature. As the hurricane approaches the community, dynamic wind pressure starts breaching the buildings' envelope. Damaged components of the building envelope are then carried by the wind-field and cause more damage to buildings in the downwind which leads to the generation of more windborne debris. Breaching the building envelope leads to internal pressurization and rainwater intrusion which increases the amount of monetary loss. Within this context, studying the performance of the building envelope during this damage scenario is a fundamental step to mitigate hurricane-imposed risks and enhance residential communities resilience against hurricanes.

Several studies developed fragility analysis frameworks to assess the performance of residential wooden buildings under wind loads. Some studies focused on the component-level fragilities (eg. *Ellingwood et al.* (2004); *Lee and Rosowsky* (2005); *van de Lindt and Dao* (2009)) and others on the building-level fragilities (e.g. *Dong*

and Li (2016); *Masoomi et al.* (2018); *Memari et al.* (2018)). These studies account for the excessive dynamic wind pressure damage mechanism and simplifies the progressive nature of the damage scenario by modeling the maximum wind speed only. The Florida Public Hurricane Loss Projection Model (FPHLPM) uses a similar approach while accounting for windborne debris impacts on unprotected windows empirically *Gurley et al.* (2005).

To estimate the damage of residential wooden buildings due to both damage mechanisms, researchers developed relatively higher-fidelity frameworks that simulate the aforementioned damage scenario (e.g. *Abdelhady et al.* (2019a,b, 2020, 2019c); *Grayson et al.* (2013); *Lin and Vanmarcke* (2010b); *Lin et al.* (2010b); *Vickery et al.* (2006b); *Yau et al.* (2011); *Zhang et al.* (2014)). Windborne debris trajectory is traced using a 3-degree-of-freedom (3DOF) trajectory model in (*Lin and Vanmarcke*, 2010b; *Lin et al.*, 2010b; *Yau et al.*, 2011; *Zhang et al.*, 2014) while (*Abdelhady et al.*, 2019a,b, 2020, 2019c; *Grayson et al.*, 2013) use a 6-degree-of-freedom (6DOF) trajectory model to more realistically account for various shapes of debris objects. Both models account for uncertainties in the calculated trajectory using different approaches, *Lin and Vanmarcke* (2010b) models the landing location using a two-dimensional Gaussian distribution while *Grayson et al.* (2012a) randomizes the flow angles to match landing locations from wind tunnel tests. With the aim of enhancing the community resilience against hurricanes, *Abdelhady et al.* (2020) studied integrates the community vulnerability with the community recovery to quantify the community resilience against hurricane winds. It should be mentioned that the computational run-time is one of the major challenges that face developments in the aforementioned high-fidelity damage estimation models.

In this paper, the performance of residential wooden buildings is assessed using

a building-level fragility analysis approach. Unlike previous fragility analysis frameworks, the proposed methodology accounts for the interdependency, progression and cascading nature of the two damage mechanisms by modeling the hurricane full damage scenario using a high-fidelity time-stepping damage estimation model. Developed fragility curves are then convoluted with the hurricane hazard curve to assess the hurricane-imposed risks on residential wooden buildings. The proposed methodology is then applied to perform a parametric study on a gable-roof archetype, considering various construction cases and floor-to-area (FAR) ratios. Outcomes from this study highlight the significance of including damage from windborne debris, and the effect of FAR on the estimated hurricane risks.

3.2 Problem setting

3.2.1 Performance analysis

3.2.1.1 Damage states

The performance of residential wooden building under hurricane winds is typically described qualitatively using a hierarchy criteria as in HAZUS-MH (*Vickery et al.*, 2006b). The descriptive format of this criteria is stated as "no damage", "minor damage", "moderate damage", "severe damage", and "destruction". These qualitative measures are quantified using damage states which are governed by the performance of the building envelope. Table 3.1 summarizes the mapping between the qualitative measures and the performance of building envelope components using damage states. It should be noted that the building is considered in the damage state if any of the damage indicators in the corresponding row occurs.

Table 3.1: Damage states for residential wooden buildings

Damage state	Qualitative measure	Roof/Wall cover failure	Window/Door failure	Roof/Wall sheathing failure	Roof-Wall connection failure
0	No damage	$\leq 2\%$	No	No	No
1	Minor damage	$> 2\%$ and $\leq 15\%$	1	No	No
2	Moderate damage	$> 15\%$ and $\leq 50\%$	2 or 3	1-3	No
3	Severe damage	$> 50\%$	> 3 and ≤ 8	> 3 and $\leq 25\%$	No
4	Destruction	Typically $> 50\%$	> 8	$> 25\%$	Yes

3.2.1.2 Fragility analysis

A probabilistic quantification of the building performance, based on the predefined damage states, requires performing fragility analysis (*Ellingwood et al.*, 2004). Building fragility can be defined as the likelihood of the damage to exceed a certain damage level (i.e. damage state) as a function of a hazard intensity measure. The hazard intensity measure is the maximum 3-sec gust wind speed (V_{max}) experienced by the building during the passage of the hurricane, and the building fragility can be written as follows:

$$F_{Ri}(v) = P\left[DS \geq ds_i | V_{max} = v\right] \qquad \forall i \in \{0, \cdots, n_{DS} - 1\} \tag{3.1}$$

where DS is the damage state defined in table 3.1; and n_{DS} is the number of the defined damage states which equals 5 in this work.

Deriving an analytical solution for $F_{Ri}(v)$ is intractable, instead, a stochastic simulation approach is proposed in this paper which will be described later.

3.2.2 Risk analysis

The hurricane-imposed risks on residential wooden buildings can be defined as the annual probability of failure (i.e. exceeding a certain damage state), which is written for the i^{th} damage state as follows:

$$P_{fi} = P\left[DS \geq ds_i\right] \tag{3.2}$$

To calculate P_{fi}, the building fragility defined in eq. (3.1) is convoluted with the probability density function of the annual maximum hurricane wind speed, $f_V(v)$, as follows:

$$P_{fi} = \int_0^\infty F_{Ri}(v) \cdot f_V(v)\,\mathrm{d}v \tag{3.3}$$

$f_V(v)$ can be obtained using hurricane hazard models provided by (*Vickery and Twisdale*, 1995a,b; *Vickery et al.*, 2000), which are the basis of the development of the design wind speed maps for the *ASCE/SEI 7-16* (2017). However, the Weibull distribution is found to be a reasonable fit for maximum wind speeds at the south-east coast of the United States (*Li and Ellingwood*, 2006). Therefore, the Weibull distribution will be used in this paper to model $f_V(v)$ as follows:

$$f_V(v) = \begin{cases} \frac{\alpha}{\beta}\left(\frac{v}{\beta}\right)^{\alpha-1} \exp\left[-\left(\frac{v}{\beta}\right)^{\alpha}\right] & v \geq 0 \\ 0 & v < 0 \end{cases} \tag{3.4}$$

where α and β are the shape and scale parameters, respectively, of the Weibull distribution. α and β are site-specific and can be determined from published wind speed maps (e.g *ASCE/SEI 7-16*, 2017).

3.3 Proposed methodology for fragility modeling

3.3.1 Overview

Figure 3.1 shows the flowchart of the proposed stochastic simulation methodology to estimate eq. (3.1). The proposed methodology is based on the Monte Carlo simulation method which estimates F_{Ri} for discreet values of V_{max}. The discreet values of V_{max} are input to the proposed methodology as: (1) a range: defined by the lowest ($V_{max,l}$) and highest ($V_{max,h}$) value of V_{max}; and (2) a velocity step (ΔV_{max}): which is required to define the j^{th} value of V_{max}. Within this context, eq. (3.1) can be

re-written as follows:

$$F_{Ri}^{j}(v^{j}) \approx \frac{1}{n_{MC}} \sum_{k=1}^{n_{MC}} \mathbb{1}_{DS^{k} \geq ds_{i}} \tag{3.5}$$

where v^{j} is the j^{th} value of V_{max}; n_{MC} is the number of samples used in the Monte Carlo simulation; and $\mathbb{1}$ is the indicator function.

A common practice is to express the fragility function using a log-normal cumulative distribution function (e.g. *Ellingwood et al.*, 2004; *Lee and Rosowsky*, 2005; *Masoomi et al.*, 2018). The estimated values of F_{Ri}^{j} from eq. (3.5) will be used to fit a log-normal CDF with a logarithmic median λ, and a log-normal standard deviation ζ.

$$F_{Ri}(v) = \Phi\left(\frac{\ln(v) - \lambda_{i}}{\zeta_{i}}\right) \tag{3.6}$$

3.3.2 Geometric model

Neighboring buildings influence the dynamic wind pressure on the considered building as well as the windborne debris impact. Therefore, defining their geometric configuration in the three-dimensional (3D) space, with respect to the considered building, is an essential requirement for the accurate estimation of the damage to the considered building. Concerning the dynamic wind pressure, it can be accurately estimated based on the floor-to-area ratio (FAR), and the orientation of the neighboring buildings *Tokyo Polytechnic University* (2007). In addition to these two factors, the extension of the modeled neighboring buildings, fig. 3.2, is required to be defined for the accurate estimation of the damage from windborne debris impact.

Figure 3.2 shows the extension of the modeled neighboring buildings which is defined by r. The r required for the accurate estimation of windborne debris damage needs to capture all possible windborne debris that could impact the considered building while modeling the minimum number of neighboring buildings. This prob-

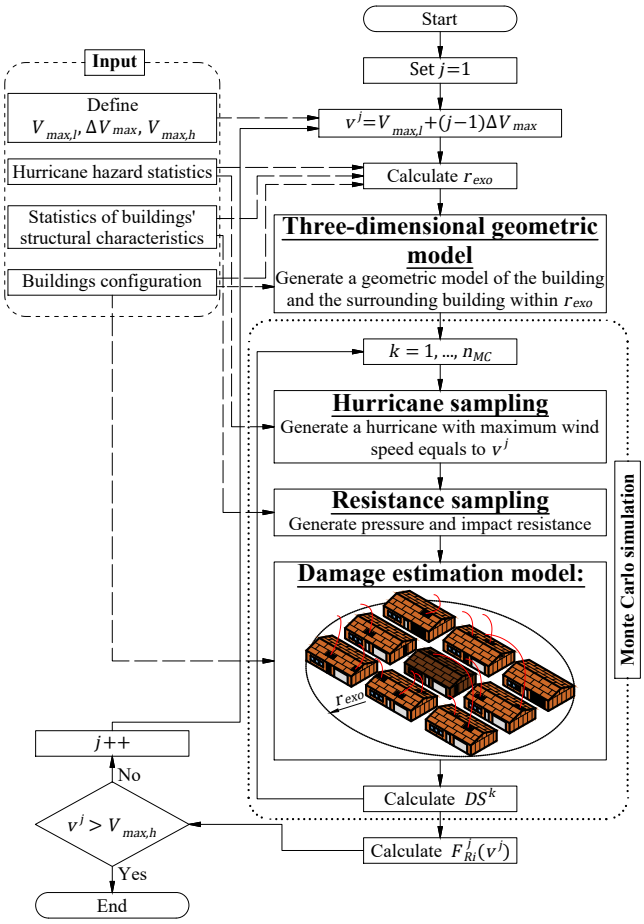

Figure 3.1: Flowchart of the proposed simulation-based fragility modeling.

lem has been addressed by **?** who provide a methodology to estimate the required r (r_{exo}). This methodology is incorporated in this work to estimate r_{exo}.

3.3.3 Damage estimation

Damage for the building envelope components is estimated using the framework presented by *Grayson et al.* (2013) with the enhancements outlined in (*Abdelhady et al.*, 2020; **?**) as follows:

$$D_l^{jk} = \mathbb{1}_{\max_{m=1}^{n_t} W_l^{jkm} > \mathcal{W}_l^k \ \vee \ \max_{m=1}^{n_t} I_l^{jkm} > \mathcal{I}_l^k} \tag{3.7}$$

where D_l^{jk} is the damage of the l^{th} building envelope component in the k^{th} sample of the Monte Carlo simulation which is subject to the j^{th} value of V_{max}; $\mathbb{1}$ is the

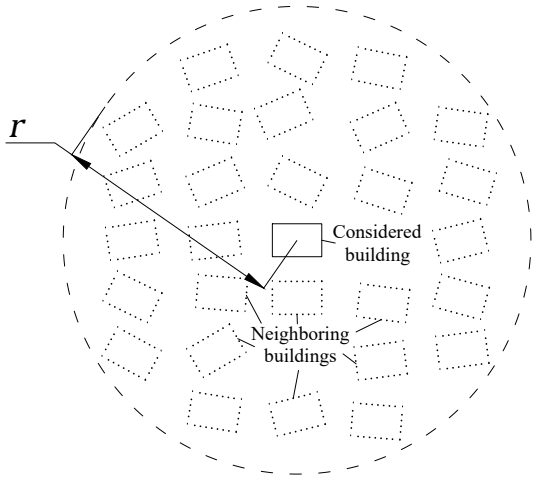

Figure 3.2: Plan of the considered building surrounded by the modeled neighboring buildings within a radius r.

indicator function; n_t is the number of time steps used in the damage estimation model; W is the dynamic wind pressure; $\mathcal{W}$ is the resistance of the component to wind pressure; I is the maximum debris impact energy or momentum at the m^{th} time step; and $\mathcal{I}$ is the resistance of the component to debris impact.

The damage estimation framework uses a time-stepping approach to model the damage scenario of a hurricane impacting a residential neighborhood. Hurricane modeling and generation follows the single-site hazard model presented by *Vickery and Twisdale* (1995a). The estimated damage is used to determine the building damage state, according to table 3.1.

3.4 Application to gable-roof archetype

3.4.1 Description

3.4.1.1 Building Archetype and construction cases

Figure 3.3 shows the residential building archetype used in this study. Ten construction cases are assigned to this archetype to cover the broad range of the resistance of the building components that exist in literature (**?**). Construction cases are

ranked ascendingly based on their strength (i.e. construction case 1 has the lowest resistance while case 10 has the highest resistance). The mean pressure and impact resistance of the building components associated with each construction case are summarized in tables 3.2 and 3.3, respectively. Components resistance are modeled as normal random variables with Coefficients of Variation of: 0.2 for the wind pressure resistance of windows, door, garage doors, and roof-wall connections; and 0.4 for the wind pressure resistance of roof and wall sheathing, roof and wall cover, and the impact resistance of all components.

Table 3.2: Mean wind pressure resistance for the considered construction cases.

Building component	Case 1	Case 2	Case 3	Case 4	Case 5	Case 6	Case 7
Window (kPa)	2.5	2.8	3.2	3.5	3.8	4.2	4.5
Door (kPa)	3.0	3.3	3.6	3.8	4.1	4.4	4.7
Garage door (kPa)	2.0	2.2	2.4	2.7	2.9	3.1	3.3
Wall sheathing (kPa)	1.0	1.9	2.8	3.7	4.6	5.4	6.3
Roof sheathing (kPa)	1.0	1.9	2.8	3.7	4.6	5.4	6.3
Wall cover (kPa)	2.5	2.8	3.2	3.5	3.8	4.2	4.5
Roof cover (kPa)	2.5	2.8	3.2	3.5	3.8	4.2	4.5
Roof-wall connection (kN)	1.0	2.7	4.4	6.2	7.9	9.6	11.3

Table 3.2: Mean wind pressure resistance for the considered construction cases (*Continued*).

Building component	Case 8	Case 9	Case 10
Window (kPa)	4.8	5.2	5.5
Door (kPa)	4.9	5.2	5.5
Garage door (kPa)	3.6	3.8	4.0
Wall sheathing (kPa)	7.2	8.1	9.0
Roof sheathing (kPa)	7.2	8.1	9.0
Wall cover (kPa)	4.8	5.2	5.5
Roof cover (kPa)	4.8	5.2	5.5
Roof-wall connection (kN)	13.1	14.8	16.5

3.4.1.2 Hurricane maximum wind speed

As previously discussed, V_{max} is input as a range, and a step. In this study, the range is $[5, 105]$ m/s, and the ΔV_{max} is 10 m/s. The number of Monte Carlo samples used is 200 for each V_{max}. Hurricane sampling is carried out by generating hurricanes

Table 3.3: Mean debris impact resistance (in kJ) for the considered construction cases.

Building component	Case 1	Case 2	Case 3	Case 4	Case 5	Case 6	Case 7
Window	0.05	0.10	0.15	0.26	0.36	0.47	0.57
Door	0.10	0.15	0.30	0.51	0.72	0.93	1.14
Garage door	0.10	0.15	0.30	0.51	0.72	0.93	1.14
Wall sheathing	0.10	0.25	0.50	1.04	1.59	2.13	2.68
Roof sheathing	0.10	0.25	0.50	1.04	1.59	2.13	2.68
Wall cover	0.10	0.25	0.50	1.04	1.59	2.13	2.68
Roof cover	0.10	0.25	0.50	1.04	1.59	2.13	2.68

Table 3.3: Mean debris impact resistance (in kJ) for the considered construction cases (*Continued*).

Building component	Case 8	Case 9	Case 10
Window	0.68	0.78	1.00
Door	1.36	1.57	2.00
Garage door	1.36	1.57	2.00
Wall sheathing	3.22	3.77	5.00
Roof sheathing	3.22	3.77	5.00
Wall cover	3.22	3.77	5.00
Roof cover	3.22	3.77	5.00

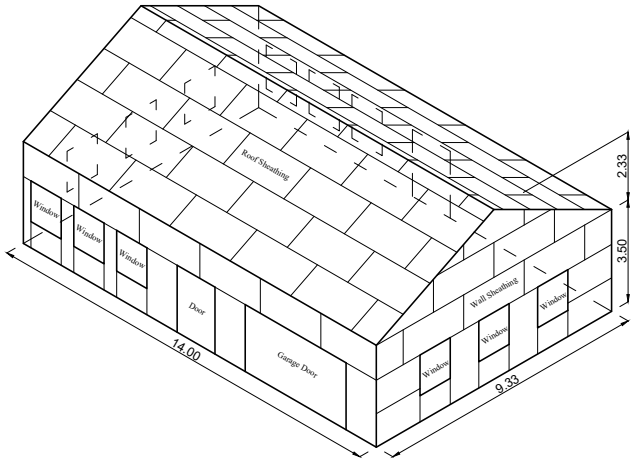

Figure 3.3: Gable-roof building archetype.

with maximum 3-sec gust wind speed that matches the considered V_{max} using the hurricane hazard model parameters for Miami, FL (*Vickery and Twisdale*, 1995a).

3.4.1.3 Geometric model generation

Buildings are arranged on a rectangular grid with the considered building in the middle as shown in fig. 3.4. The spacing between the grid lines in $x-$ and $y-$

directions are chosen so that FAR equals to 0.1, 0.3, and 0.6. The extension of the modeled neighboring buildings (r_{exo}) is determined based on the regression model presented by **?**. A sample of the calculated r_{exo} is shown in fig. 3.4.

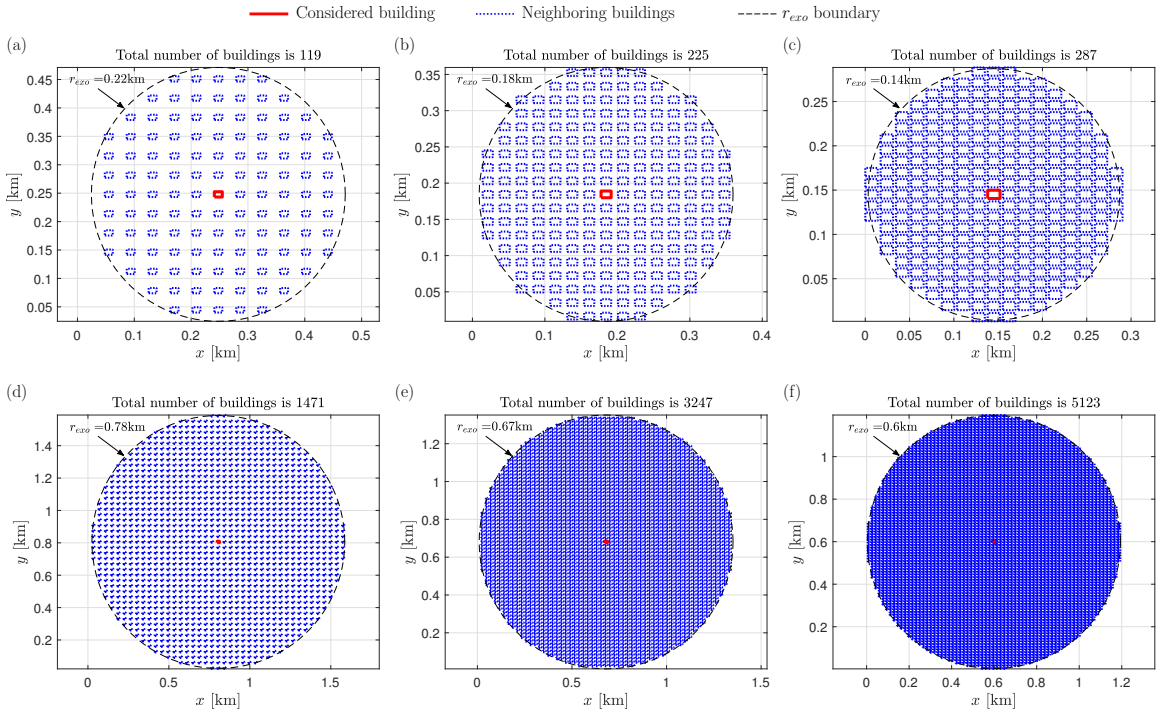

Figure 3.4: Plan of the generated geometric model for construction cases 3-10: (a) $V_{max} = 65$ m/s and $FAR = 0.1$; (b) $V_{max} = 65$ m/s and $FAR = 0.3$; (c) $V_{max} = 65$ m/s and $FAR = 0.6$; (d) $V_{max} = 85$ m/s and $FAR = 0.1$; (e) $V_{max} = 85$ m/s and $FAR = 0.3$; and (f) $V_{max} = 85$ m/s and $FAR = 0.6$.

3.4.2 Performance assessment

To quantify the significance of the damage from windborne debris on the building performance, the damage estimation for the building components is carried out for two cases: (1) including damage from windborne debris impact, and (2) excluding damage from windborne debris. Tables 3.4 to 3.7 summarize the building fragility curves of all studied cases for damage states 1, 2, 3, and 4, respectively. It should be noted that some cases show a zero probability to be in the damage state 4 over the considered range of V_{max}. These cases are construction case 10 at $FAR = 0.3$ & 0.6,

construction case 9 at $FAR = 0.6$, and construction case 8 at $FAR = 0.6$.

Figure 3.5 shows the building fragility curves for 3 construction cases (3, 5 and 7) which are chosen to represent weak, moderate, and strong construction cases, respectively. Fragility curves for DS_1 and DS_2 are identical in construction case 3, and almost identical for construction case 5 because of the condition of no roof/wall sheathing failure in DS_1 (table 3.1). In other words, roof/wall cover are attached to roof/wall sheathing, this attachment leads to a higher wind pressure acting on the sheathing than the covering because of the internal pressure. Knowing that the pressure resistance for the sheathing is lower than the covering in construction case 3, it is almost impossible to have a case where the covering is damaged without the sheathing is also damaged. As the pressure resistance of the sheathing becomes higher than the covering (as in construction case 5 and 7), the gap between DS_1 and DS_2 fragility curves starts to increase.

The effect of FAR on the considered building performance is shown in fig. 3.5; as FAR increases, building resistance increases. For example, in construction case 3, a hurricane of category 3-4 will most probably cause destruction (DS_4) to the building when the FAR equals to 0.1. Increasing FAR to 0.6 will upgrade the building's resistance that a hurricane of category 4-5 is required to cause the same impact (i.e. destruction). This apparent increase in resistance is actually due to the reduction of wind pressure caused by the shielding effect of the neighboring buildings (see e.g. *Ahmad and Kumar*, 2001; *Gavanski et al.*, 2013; *Surry and Lin*, 1995; *Tokyo Polytechnic University*, 2007). However, increasing FAR leads to increasing the number of windborne debris which causes more damage from windborne debris. This increase in the damage from windborne debris can be observed in fig. 3.5.

Table 3.4: Building fragility curves for damage state 1.

Construction case	DS_1 - $FAR = 0.1$				DS_1 - $FAR = 0.3$				DS_1 - $FAR = 0.6$			
	Debris		No debris		Debris		No debris		Debris		No debris	
	λ_1	ζ_1	λ_1	ζ_1	λ_1	ζ_1	λ_1	ζ_1	λ_1	ζ_1	λ_1	ζ_1
1	3.13	0.09	3.13	0.09	3.21	0.09	3.21	0.10	3.31	0.10	3.31	0.10
2	3.38	0.12	3.38	0.12	3.49	0.13	3.49	0.13	3.63	0.10	3.63	0.10
3	3.57	0.11	3.57	0.11	3.68	0.12	3.68	0.12	3.82	0.09	3.82	0.09
4	3.70	0.13	3.70	0.13	3.81	0.10	3.81	0.10	3.94	0.11	3.94	0.11
5	3.80	0.11	3.80	0.11	3.89	0.12	3.90	0.13	4.05	0.10	4.05	0.10
6	3.88	0.12	3.88	0.12	4.00	0.12	4.00	0.12	4.11	0.09	4.12	0.09
7	3.94	0.14	3.95	0.14	4.06	0.11	4.07	0.11	4.18	0.09	4.19	0.09
8	4.02	0.10	4.02	0.10	4.11	0.11	4.12	0.11	4.23	0.09	4.25	0.09
9	4.06	0.10	4.07	0.10	4.16	0.10	4.17	0.10	4.28	0.10	4.30	0.10
10	4.11	0.10	4.11	0.10	4.20	0.10	4.21	0.10	4.33	0.09	4.36	0.09

Note: v is in m/s

Table 3.5: Building fragility curves for damage state 2.

Construction case	DS_2 - $FAR = 0.1$				DS_2 - $FAR = 0.3$				DS_2 - $FAR = 0.6$			
	Debris		No debris		Debris		No debris		Debris		No debris	
	λ_2	ζ_2	λ_2	ζ_2	λ_2	ζ_2	λ_2	ζ_2	λ_2	ζ_2	λ_2	ζ_2
1	3.13	0.09	3.13	0.09	3.21	0.10	3.21	0.10	3.31	0.10	3.31	0.10
2	3.38	0.12	3.38	0.12	3.49	0.13	3.49	0.13	3.63	0.10	3.63	0.10
3	3.57	0.11	3.57	0.11	3.68	0.12	3.68	0.12	3.82	0.09	3.82	0.09
4	3.70	0.13	3.70	0.13	3.81	0.11	3.81	0.11	3.94	0.11	3.94	0.11
5	3.80	0.12	3.80	0.12	3.90	0.13	3.90	0.13	4.05	0.10	4.06	0.10
6	3.89	0.13	3.89	0.13	4.00	0.12	4.01	0.12	4.12	0.09	4.12	0.10
7	3.96	0.15	3.96	0.15	4.07	0.12	4.08	0.12	4.18	0.10	4.19	0.10
8	4.04	0.12	4.05	0.12	4.12	0.12	4.13	0.12	4.24	0.10	4.25	0.10
9	4.09	0.11	4.09	0.11	4.18	0.11	4.18	0.11	4.29	0.11	4.31	0.11
10	4.14	0.11	4.14	0.11	4.22	0.11	4.23	0.11	4.34	0.10	4.37	0.10

Note: v is in m/s

3.4.3 Risk assessment

As previously discussed, hurricane-imposed risks are quantified using P_{fi}. To estimate P_{fi}, the Weibull distribution parameters, eq. (3.4), α and β are determined for Miami, FL. α equals 1.769, and β equals 27.298 m/s. The fitted cumulative distribution function is shown in fig. 3.6. Equation (3.3) is solved using the Monte Carlo method, the resulting values of P_{fi} are summarized in fig. 3.7. The annual probability of failure increases (i.e. risk increases) as the building components re-

Table 3.6: Building fragility curves for damage state 3.

Construction case	DS_3 - $FAR = 0.1$				DS_3 - $FAR = 0.3$				DS_3 - $FAR = 0.6$			
	Debris		No debris		Debris		No debris		Debris		No debris	
	λ_3	ζ_3	λ_3	ζ_3	λ_3	ζ_3	λ_3	ζ_3	λ_3	ζ_3	λ_3	ζ_3
1	3.45	0.05	3.45	0.05	3.51	0.08	3.51	0.08	3.62	0.05	3.62	0.05
2	3.72	0.07	3.72	0.07	3.82	0.05	3.82	0.05	3.91	0.06	3.93	0.06
3	3.89	0.07	3.91	0.07	3.98	0.07	4.00	0.07	4.06	0.07	4.11	0.07
4	4.01	0.05	4.02	0.04	4.10	0.07	4.13	0.07	4.22	0.06	4.24	0.06
5	4.11	0.08	4.13	0.08	4.21	0.06	4.24	0.06	4.31	0.06	4.35	0.06
6	4.21	0.05	4.22	0.05	4.29	0.07	4.31	0.07	4.39	0.06	4.43	0.07
7	4.27	0.06	4.29	0.06	4.36	0.07	4.39	0.07	4.46	0.06	4.51	0.07
8	4.33	0.07	4.36	0.08	4.41	0.07	4.45	0.08	4.52	0.07	4.58	0.06
9	4.39	0.07	4.41	0.07	4.47	0.07	4.52	0.07	4.57	0.07	4.63	0.07
10	4.44	0.06	4.46	0.07	4.52	0.07	4.56	0.07	4.61	0.06	4.68	0.07

Note: v is in m/s

Table 3.7: Building fragility curves for damage state 4.

Construction case	DS_4 - $FAR = 0.1$				DS_4 - $FAR = 0.3$				DS_4 - $FAR = 0.6$			
	Debris		No debris		Debris		No debris		Debris		No debris	
	λ_4	ζ_4	λ_4	ζ_4	λ_4	ζ_4	λ_4	ζ_4	λ_4	ζ_4	λ_4	ζ_4
1	3.72	0.04	3.72	0.04	3.81	0.06	3.81	0.06	3.92	0.03	3.93	0.03
2	3.95	0.04	4.00	0.05	4.06	0.05	4.10	0.05	4.17	0.04	4.20	0.03
3	4.14	0.05	4.17	0.04	4.24	0.05	4.25	0.06	4.34	0.04	4.36	0.04
4	4.26	0.06	4.28	0.06	4.36	0.06	4.37	0.06	4.46	0.05	4.48	0.05
5	4.37	0.06	4.38	0.06	4.46	0.06	4.48	0.06	4.57	0.06	4.59	0.06
6	4.46	0.05	4.47	0.05	4.54	0.07	4.56	0.08	4.65	0.08	4.68	0.08
7	4.52	0.07	4.53	0.07	4.61	0.08	4.63	0.08	4.72	0.07	4.73	0.07
8	4.58	0.07	4.59	0.07	4.67	0.09	4.70	0.09	–	–	–	–
9	4.63	0.08	4.64	0.08	4.72	0.08	4.73	0.08	–	–	–	–
10	4.68	0.08	4.69	0.08	–	–	–	–	–	–	–	–

Note: v is in m/s

sistance decrease. For the same construction case, the annual probability of failure decrease as FAR increases due to the shielding effect, discussed earlier.

The significance of damage from windborne debris impact is illustrated in fig. 3.8. It is clear that including the impact of windborne debris is critical for estimating the risk from hurricanes as this risk can be increased by $0 - 310\%$ when accounting for windborne debris. This wide range can be explained as following:

1. Floor-area ratio (FAR): increasing FAR means increasing the number of build-

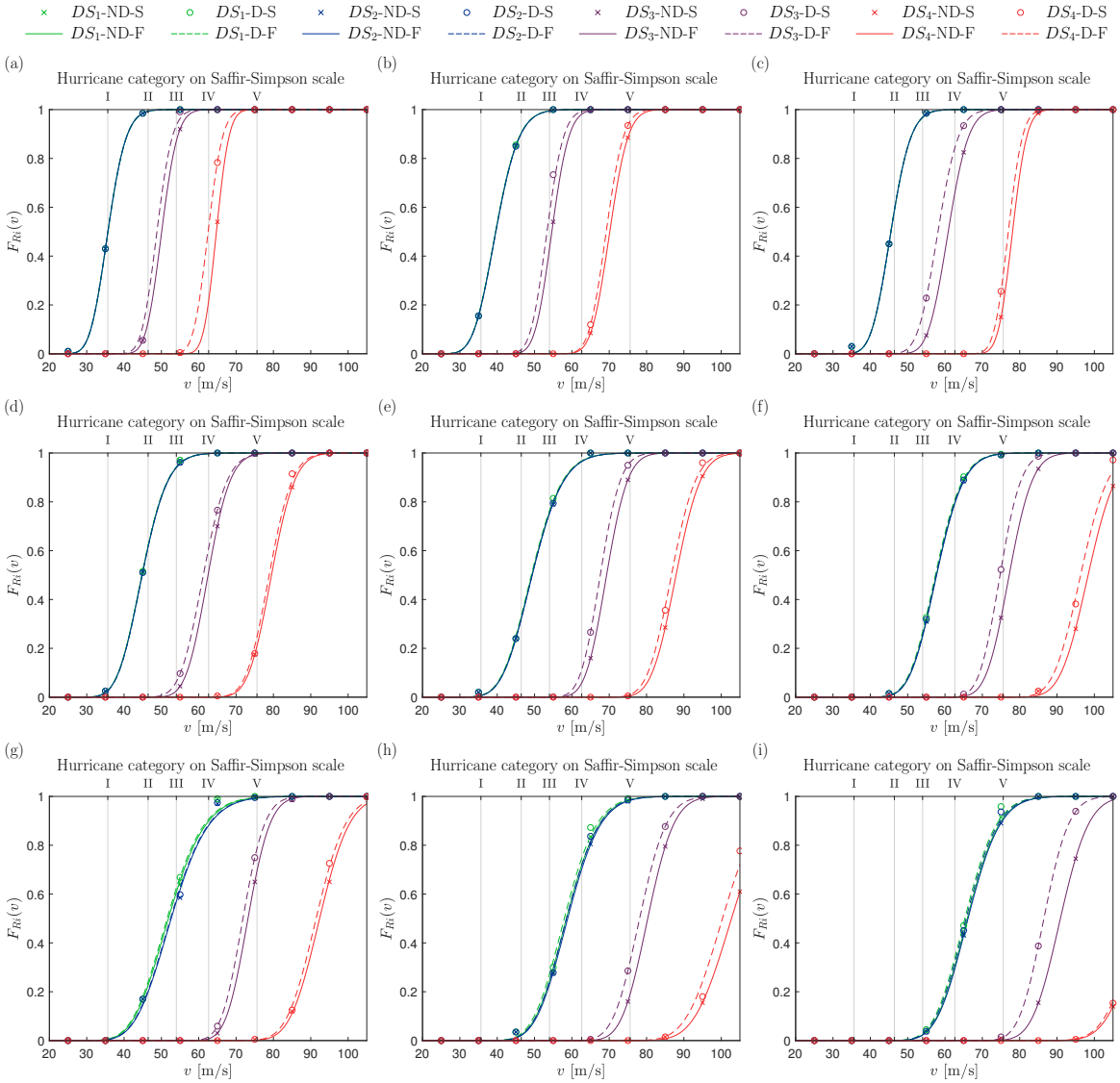

Figure 3.5: Building fragility curves: (a) construction case = 3 and $FAR = 0.1$; (b) construction case = 3 and $FAR = 0.3$; (c) construction case = 3 and $FAR = 0.6$; (d) construction case = 5 and $FAR = 0.1$; (e) construction case = 5 and $FAR = 0.3$; (f) construction case = 5 and $FAR = 0.6$; (g) construction case = 7 and $FAR = 0.1$; (h) construction case = 7 and $FAR = 0.3$; and (i) construction case = 7 and $FAR = 0.6$. Nomenclature: no debris (ND); debris (D); simulation results (S); and fitted log-normal CDF (F).

ings in the same area which will lead to an increase in the number of windborne debris which will increase its damage. So, the variation of FAR influence the contribution from windborne debris damage to the total risk.

2. Building strength: as building strength increases the significance of windborne debris increases. This increase is due to the increase in the required wind speed

to cause damage to the buildings. Once building components are damaged, they will experience these higher wind speeds which will lead to longer flying distance and higher impact energy or momentum.

The effect of the building strength on the significance of windborne debris is shown in fig. 3.9. The chart is divided into two zones: (1) zone I ($e^{\lambda_i} < 50$ m/s): buildings in this zone have low strength. Windborne debris does not increase the annual probability of failure in this zone as the damaged components does not experience wind speed high enough to impact other buildings; and (2) zone II ($e^{\lambda_i} \geq 50$ m/s): buildings in this zone have higher strength than zone I. As e^{λ_i} (i.e. building strength) increases the effect of windborne debris on the annual probability of failure increases.

It should be noted that damage state 3 and 4 exhibit the highest and lowest rate of increase in the annual probability of failure due to windborne debris, respectively. The highest rate of DS_3 is because it is higher than DS_1 and DS_2 so it requires higher wind speeds to occurs. Moreover, DS_3 requires a larger number of damaged windows and doors (most vulnerable components to windborne debris damage) than DS_1 and DS_2 and a wider range (> 3 and ≤ 8). The lowest rate of DS_4 is because roof-wall connection failure is one of the conditions for the building to enter this damage state. Although impact from windborne debris can induce internal pressurization which will increase the wind pressure on the roof-wall connection, windborne debris impact does not directly cause roof-wall connection failure. Moreover, if the building is destructed (in DS_4) just by the wind pressure, adding windborne debris impact will not add much to the damage in this case.

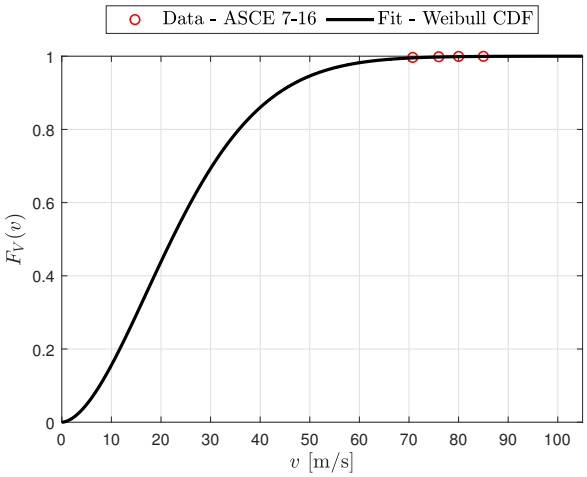

Figure 3.6: Cumulative distribution function for the annual maximum hurricane wind speed in Miami, FL.

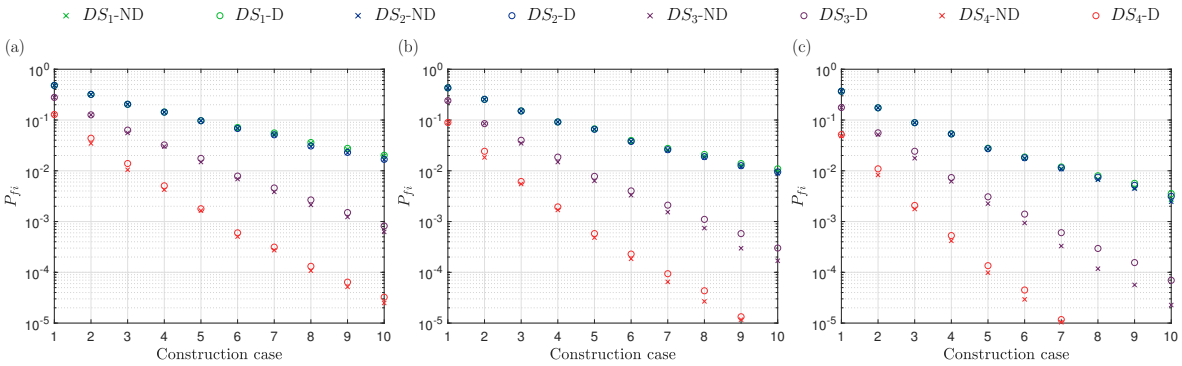

Figure 3.7: Annual probability of failure P_{fi}: (a) $FAR = 0.1$; (b) $FAR = 0.3$; and (c) $FAR = 0.6$. Nomenclature: no debris (ND); debris (D).

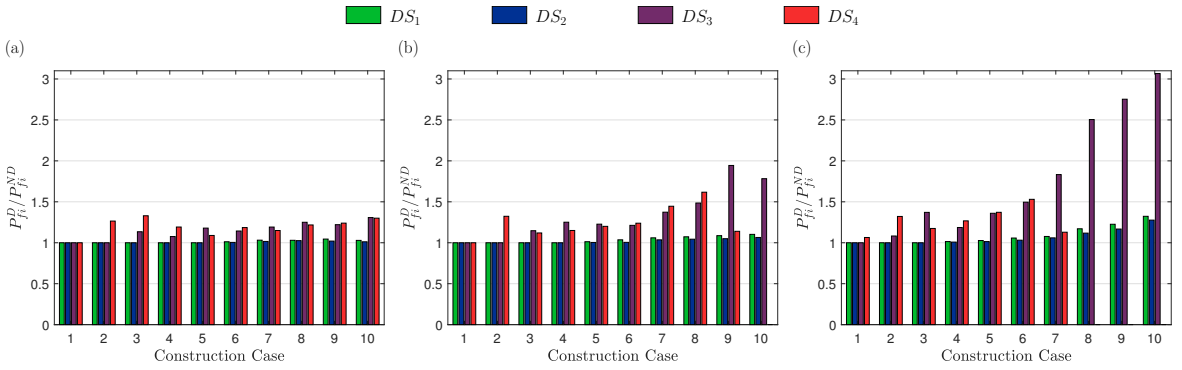

Figure 3.8: Ratio between the annual probability of failure for the debris case P_{fi}^D and the no debris case P_{fi}^{ND}: (a)$FAR = 0.1$; (b) $FAR = 0.3$; and (c) $FAR = 0.6$.

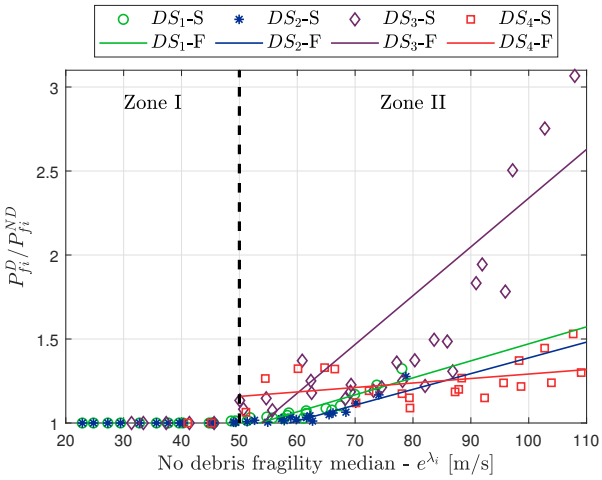

Figure 3.9: Zones for the significance of windborne debris damage on hurricane-imposed risks. Nomenclature: simulation results (S); and fitted linear function (F).

3.5 Conclusions

Hurricane-imposed risks to residential wooden buildings, as well as their performance against hurricanes, are the main focus of this work. Building performance is estimated probabilistically using a fragility analysis approach. The proposed fragility modeling methodology uses the Monte Carlo simulation method to estimate the building fragility for discreet values of the maximum hurricane wind speed. Building fragility is, then, represented using the log-normal CDF. The proposed methodology accounts for two damage mechanisms to develop the building fragility curves, (1) excessive dynamic wind pressure; and (2) impact from windborne debris. An application to the gable-roof archetype is presented. Ten construction cases are studied as well as three floor-area ratios. The resulting fragility curves show the significance of the shielding effect caused by the high floor-area ratio on the building performance and the hurricane-imposed risk. The influence of windborne debris on the hurricane-imposed risk is categorized into two zones, zone I (low-strength buildings) where windborne debris does not contribute to the damage; and zone II (high-strength

buildings) where the contribution of the windborne debris increases as the building strength increases.

CHAPTER IV

A Framework for the Probabilistic Quantification of the Resilience of Communities to Hurricane Winds[1]

Abstract

Enhancing community resilience against hurricanes, one of the costliest natural hazards to impact the United States over the past four decades, is an essential requirement for the nation's security and welfare. A fundamental step in this direction is to provide computational frameworks that are able to quantify the response of the community to the hazard immediately after its impact and during its recovery process. Existing frameworks focus on estimating damage and losses immediately subsequent to the hurricane impact through vulnerability models. This paper provides a framework that integrates damage estimated from vulnerability models with a probabilistic recovery model for quantifying community resilience against hurricanes. The framework is based on five resilience limit states that identify the required recovery activities for each building based on the amount of damage. A building-level recovery model, based on discrete functionality states, translates these limit states to a building-level recovery function. By aggregating building recovery functions, a community recovery function and resilience measure are obtained. The framework is embedded in a Monte Carlo simulation strategy for uncertainty propagation therefore

[1] Abdelhady, A.U., Spence, S.M.J. and McCormick, J. (2021). "A framework for the probabilistic quantification of the resilience of communities to hurricane winds," *Journal of Wind Engineering & Industrial Aerodynamics*, 206, 104376.

enabling a fully probabilistic quantification of community resilience. The framework is illustrated with a case study consisting of a typical residential neighborhood in Miami, FL.

4.1 Introduction

The risks to the built environment from natural hazards has been increasing over time with predictions agreeing that this trend will continue in the future (*Jain et al.*, 2005). In this respect, hurricanes are the costliest natural hazard to which the United States is subject (*sigma*, 2017). Over the past five decades, an increasing number of hurricanes have reached categories 4 and 5 (*Webster et al.*, 2005), while their potential destructiveness, defined in terms of the total dissipation of power over the lifetime of the hurricane, has shown a marked increase since the mid-1970s (*Emanuel*, 2005). Hurricane prone areas have also, in many cases, experienced significant population growth and increased wealth concentration (*NOAA*, 2013), all of which contribute to increased vulnerability. While recent improvements in forecasting and early warning systems have resulted in a decrease in fatalities resulting from hurricanes, the impact on the mental health of survivors, the environment, as well as the economy cannot be fully mitigated through the aforementioned strategies. A more comprehensive and robust approach to hurricane risk mitigation (in terms of risk reduction, transfer of risk, and better preparedness and response effectiveness) can be achieved through implementing strategies that increase community resilience (*Mitchell and Harris*, 2012 (accessed April 30, 2018): a concept that has recently been used to mitigate risks from various other natural hazards (e.g. earthquakes and tornadoes) (*Bruneau et al.*, 2003; *Burton et al.*, 2016; *Cimellaro et al.*, 2010; *Masoomi and van de Lindt*, 2018). Over the past two decades research has focused on developing an understanding of

the concept of resilience by introducing definitions as well as identifying measures, properties and dimensions (*Aven*, 2011; *Bhamra et al.*, 2011; *Haimes*, 2009; *Hosseini et al.*, 2016a; *Sharma et al.*, 2017; *Woods*, 2015). In particular, the following definition is provided by the National Academy of Science "*Community resilience is the ability to prepare and plan for, absorb, recover from, and more successfully adapt to actual or potential adverse events*" (NAS, 2012).

Quantifying community resilience against hurricanes, in light of the previous definition, requires the development of computational frameworks that can capture the response of the community during and after a hurricane event by: (1) estimating the amount of damage and losses immediately subsequent to the hurricane and (2) modeling the community recovery process. A community, which is viewed as an interdependent socio-technical system, is composed of various interdependent systems (e.g. buildings, electrical power grid, water pipelines, gas pipelines, people, etc.). The buildings of a community constitute a critical system within the community and quantifying its response and performance under hurricanes is a fundamental step towards quantifying and enhancing the resilience of the community. The damage caused by hurricanes to the built environment is typically due to: (1) strong winds: which results in excessive dynamic wind pressure on the building envelope as well as impacts from windborne debris captured by the wind; (2) storm surge: which causes coastal flooding; and (4) heavy precipitation: the leakage of the rainwater into the building causes significant damage to its internal contents, moreover if the rainfall is persistent over longer period of time this can overwhelm the drainage system which leads to inland flooding. Quantifying the performance of the built environment against strong winds associated with hurricanes is the focus of this work. Previous research efforts have been focused on estimating the amount of damage and losses

due to hurricane winds immediately subsequent to the event either at the building level or the community level through vulnerability models. A comprehensive literature review can be found in *He et al.* (2017); *Pita et al.* (2015); *Walker* (2011). This paper is therefore focused on proposing a novel framework that integrates damage estimated immediately subsequent to a hurricane through vulnerability models with a probabilistic community recovery model. The recovery model is based on defining a set of building resilience limit states that relate the amount of damage suffered by each building during the hurricane to the required recovery activities. Building recovery models are then introduced for relating the building resilience limit states to appropriate building recovery functions that can be used to estimate the community recovery function. By embedding the framework in a Monte Carlo simulation scheme, a fully probabilistic quantification of community resilience against hurricanes is achieved. A case study for a typical residential neighborhood in Miami, FL is presented to show the framework's capabilities.

4.2 Proposed framework

4.2.1 Overview

An overview of the proposed framework is illustrated in fig. 4.1. The basic idea underpinning the framework is to use building-level damage, estimated through vulnerability models, as input to a new building-level recovery model. By aggregating the resulting building-level recovery functions, community-level recovery functions are derived. By subsequently embedding the framework in a Monte Carlo simulation scheme, a novel framework is defined that is capable of providing a probabilistic quantification of both the community-level recovery function as well as any community resilience metric of interest.

In the proposed framework, the hurricane hazard is modeled through the site-

specific probabilistic hurricane hazard model introduced by *Vickery and Twisdale* (1995b). Damage resulting from the hurricane winds is estimated for each building using the engineering-based vulnerability model presented in *Grayson et al.* (2013) with the following enhancements: (1) external pressure coefficients estimated directly from the *Tokyo Polytechnic University* (2007) wind tunnel database for non-isolated low-rise buildings; (2) internal pressure coefficients calculated using Holmes' internal pressure model (*Holmes*, 2017); and (3) inclusion of wind-borne debris coming from outside the considered community. The outcome from the damage estimation stage is unlike traditional vulnerability models, as damage for each building is directly related to recovery activities through resilience limit states. In particular, the following five resilience limit states for residential wooden buildings are defined in this work: (1) very minor damage triggering minor inspections, (2) minor occupiable damage, (3) moderate unoccupiable damage, (4) severe irreparable damage, and (5) complete collapse. The building-level recovery model then translates the limit states into a building-level recovery function. Since residential communities are the focus of this work, the number of housed people (housed population) is the considered resilience metric of the building-level recovery model. This resilience metric reflects the ability of the building to maintain functionality through ensuring occupancy while providing occupants with essential services (i.e. electricity, water, etc.). The community-level recovery function is then estimated by aggregating the building-level recovery functions.

To quantify the effects of uncertainty, a Monte Carlo simulation scheme is proposed in which uncertainties in the hurricane intensity, debris field, building capacities, and building-level recovery curves are considered. This enables a fully probabilistic description of of both the community-level recovery function as well as the

associated resilience metrics.

4.2.2 Community resilience measure

One of the main goals of the proposed framework is to quantify the resilience of communities against hurricanes through the following measure:

$$R = \frac{1}{T_R} \int_{t_E}^{t_E+T_R} H(t)dt \tag{4.1}$$

where t_E is the time of event occurrence (i.e. hurricane impact); T_R is the community recovery time; and $H(t)$ is a normalized community recovery function at time t. The measure of eq. (4.1) has been widely adopted to quantify community resilience for other types of natural hazards (*Burton et al.*, 2016; *Cimellaro et al.*, 2010; *Sharma et al.*, 2017) and is therefore adopted in this work. The first step in quantifying R is the definition of an appropriate community recovery function $H(t)$.

4.2.3 Community recovery function

As proposed by *Burton et al.* (2016), in this work the community recovery function is estimated through the aggregation of an appropriate set of building-level recovery functions, and therefore as:

$$Q(t) = \sum_{i=1}^{N_b} p_i h_i(t) \tag{4.2}$$

where N_b is the number of buildings in the community; p_i is the number of people residing in the building prior to the hurricane event; and $h_i(t)$ is the recovery function of the ith building at time t. In particular, the modeling of $h_i(t)$ requires the definition of an appropriate building-level recovery model. To obtain the normalized community recovery function used in eq. (4.1), $Q(t)$ is normalized as follows:

$$H(t) = \frac{Q(t)}{P} \tag{4.3}$$

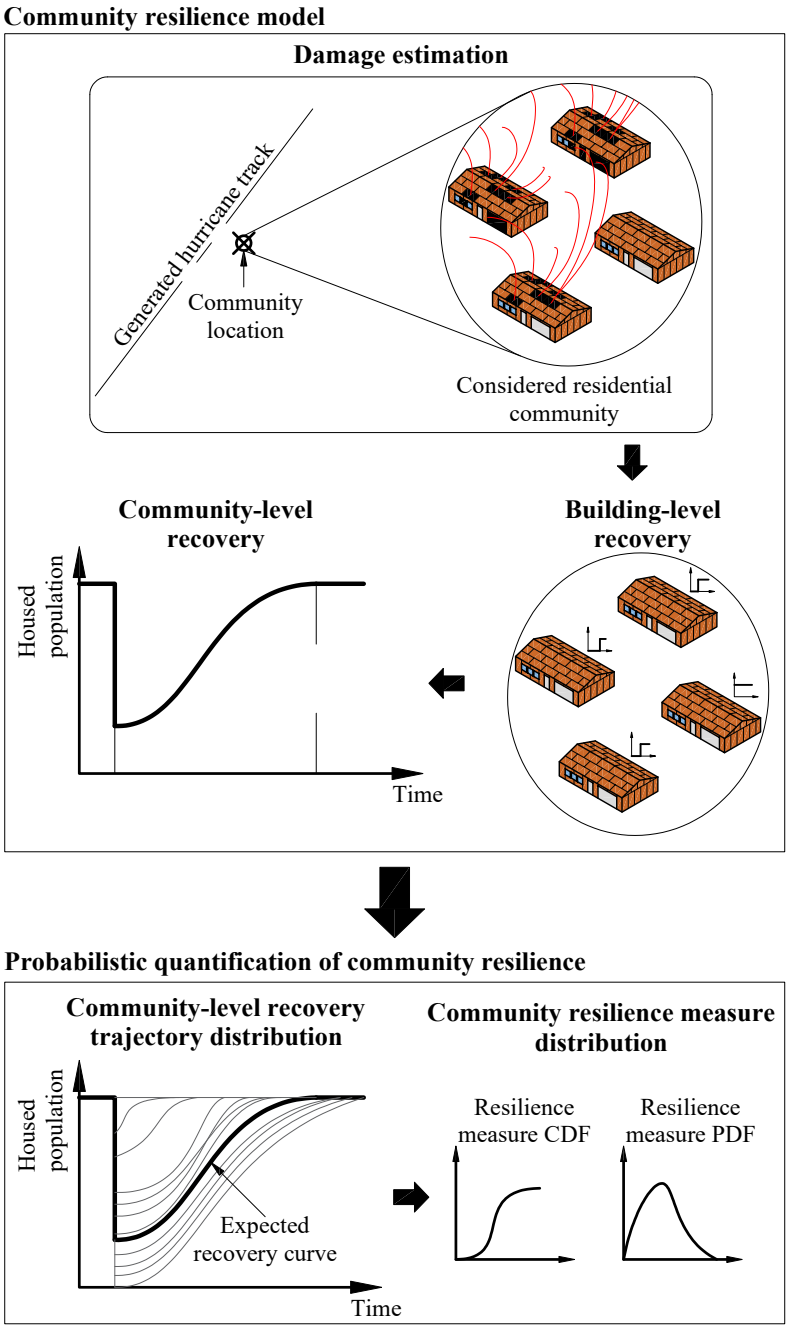

Figure 4.1: Schematic of the proposed framework.

where P is the total population of the considered community, which is equal to $\sum_{i=1}^{N_b} p_i$.

4.2.4 Building-Level recovery model

4.2.4.1 Vulnerability model

A necessary first step in estimating the building recovery, and therefore resilience through the measure of eq. (4.1), is the estimation of the damage to each building of the community immediately subsequent to the hurricane. This estimation can be achieved through an appropriate vulnerability model. While numerous models have been proposed (e.g. *He et al.*, 2017; *Pita et al.*, 2015; *Walker*, 2011), the engineering-based vulnerability model presented by *Grayson et al.* (2013) is adopted as it provides a relatively high-fidelity apprach in which the resistance of each building is modeled at the level of individual component capacities while the effects of debris are included through a mechanics-based three-dimensional probabilistic trajectory model. It also does not restrict the model used to describe the hurricane wind speed field which in this work is described through the site-specific probabilistic model outlined in *Vickery and Twisdale* (1995b).

In applying this vulnerability model, the following enhancements are implemented: 1) the pressure coefficients used to model the external pressure field on each building are based on wind tunnel data obtained from the *Tokyo Polytechnic University* (2007) for non-isolated, low-rise buildings as opposed to the semi-empirical approach of the Florida Public Hurricane Loss Projection Model (*Gurley et al.*, 2005); 2) the internal pressure coefficients are calculated through Holmes' internal pressure model (*Holmes*, 2017) as opposed to the enclosure classifications of ASCE 7 (*ASCE/SEI 7-16*, 2017); and 3) wind-borne debris coming from not only inside the study community, but also outside the study community, were considered in estimating debris damage.

4.2.4.2 Resilience limit states

In order to quantify the building-level recovery function of eq. (4.2), the damage estimated from the vulnerability model for each building must first be translated into specific recovery activities required for the restoration of building functionality. To this end, five resilience limit states (RLS) are introduced. In particular, each RLS consists of a unique combination of the following activities required for building recovery: (1) inspection, evaluation and planning activities; (2) repair activities for building envelope components as well as internal components (for cases of repairable buildings); and (3) demolition and building replacement activities (for cases of non-repairable buildings). The five RLS are defined as follows:

RLS_1: Minimal damage. The building is considered intact and the required recovery activity is limited to inspection.

RLS_2: Minor occupiable damage. The building is still occupiable with only limited inspections and repairs necessary to fully recover after the hurricane event.

RLS_3: Moderate unoccupiable damage. Damage is enough to render the building uninhabitable. Inspection, evaluation and planning activities are required to decide the type of repair actions that will lead to full recovery.

RLS_4: Severe irreparable damage. The amount of damage that occurs to the building makes repairs unfeasible. The only way to restore building functionality is full demolition and replacement. Inspection, evaluation and planning activities are required to provide detailed plans about how the demolition and the replacement activities will be carried out.

RLS_5: Complete collapse. The building experiences almost complete damage. Recovery activities consist of inspection and planning, followed by removal and replacement of the damaged building.

The methodology used to assess whether a building is in one of the RLS outlined above should be based on a combination of indicators that reflect the amount of damage to the building envelope as well as building internal contents. For simplicity, the approach used to assign the RLS after a hurricane event is based on assuming a one-to-one mapping between the RLS and the building damage states defined in HAZUS-MH (*Vickery et al.*, 2006b). Therefore, once the damage to each building is assessed through the vulnerability model, the appropriate RLS can be assigned once the HAZUS-MH damage state is determined.

4.2.4.3 Recovery function

The resilience of residential communities is of interest to this work. Therefore the metric, $h(t)$, that is chosen to model the recovery of each building in the community is related to the capacity of the building to house its occupants at time t. This metric is well suited for this problem as it provides a measure of the ability of each building composing the community to maintain functionality through ensuring occupancy, while providing occupants with essential services (i.e. electricity, water, etc.).

To assign an analytical form to $h(t)$, three functionality states are proposed that directly link $h(t)$ to the RLS. These functionality states are: (1) safe and full service (SFS), (2) safe with some services off (SSO), and (3) not safe (NS). The work progress for the recovery activities typically advances continuously over time while the functionality state changes only at completion of a group of activities (*Burton et al.*, 2016; *Miles and Chang*, 2006; *Sharma et al.*, 2017). As a result, a step recovery function is proposed to model this behavior, as shown in fig. 4.2, where 1.0 indicates full functionality (i.e. residents can live in the building) while 0.0 indicates no functionality (i.e. residents must evacuate the building). Within the context outlined

above, the building recovery function can be written in the following form:

$$\begin{aligned} h(t) =& h_{SFS} - (h_{SFS} - h_{NS})\,\theta(t - t_E) + (h_{SSO} - h_{NS})\,\theta(t - (t_E + T_{NS})) \\ &+ (h_{SFS} - h_{SSO})\,\theta(t - (t_E + T_{NS} + T_{SSO})) \end{aligned} \tag{4.4}$$

where h_{SFS}, h_{SSO} and h_{NS} are the functionality levels associated with the functionality states SFS, SSO and NS respectively; T_{NS} and T_{SSO} are the times spent by the building in the states of NS and SSO; t_E is the arrival time of the hurricane event; and $\theta()$ is the Heaviside step function.

The level of functionality associated with SFS is full therefore $h_{SFS} = 1.0$ while for NS the building is unsafe leading to $h_{NS} = 0.0$. For the functionality state of SSO, the decision of the residents to evacuate or return back once their residence is in the state of SSO will dictate whether $h_{SFS} = 1.0$ or $h_{SFS} = 0.0$. This decision is affected by the amount of damage suffered by the building itself and the surrounding buildings in the neighborhood. It is also affected by residents' social and economic conditions (e.g. income, education, tenure, available opportunities outside the neighborhood, etc.). Household decision-making models presented in *Masoomi et al.* (2018) and *Burton et al.* (2018, 2019) account for most of these factors in predicting the decision of the residents. Integrating similar models in the presented framework to predict the level of functionality of the SSO state is a straight-forward process. However, for simplicity, the functionality level associated with SSO will be modeled probabilistically in terms of the resilience limit state, as will be outlined at the end of this section.

The time spent by the building in the functionality states of NS or SSO depends on which operations have to be carried out for recovery. Therefore, the time lengths T_{NS} and T_{SSO} can be defined in terms of duration of specific tasks, such as: (1) inspection time, T_{INSP}, defined as time required for building inspection as well

as damage evaluation and decisions about consequent repair actions; (2) mobilization time, T_{MOB}, defined as the time required to mobilize construction crews and equipment; (3) building envelope repair or replacement time, T_{REP}; and (4) building internal contents repair time, T_{INT}, defined as time to restore lost services inside the building. The values of T_{INSP}, T_{MOB}, T_{REP} and T_{INT}, as well as the relationships between these time intervals and T_{NS} and T_{SSO}, characterize the recovery function for a given building and depend on the resilience limit state of the building after the hazard event.

The relationship between the resilience limit states and the functionality states is illustrated in fig. 4.2 and described as follows:

- **RLS**$_1$: the building is in SFS throughout the passage of the hurricane with full functionality.
- **RLS**$_2$: the building is safe to occupy but limited inspection and repairs are required which will lead to a functionality state of SSO before the building is deemed fully functional and therefore in the state SFS. In this case $T_{SOS} = T_{INSP} + T_{MOB} + T_{REP}$. Residents can decide to evacuate and return back after these minor repairs are done or continue living in the building.
- **RLS**$_3$: the recovery path in this case will involve all three functionality states. The building is initially not safe to occupy and will therefore start in the NS state until inspection and required safety repairs are completed. The time spent in NS will be $T_{NS} = T_{INSP} + T_{MOB} + T_{REP}$. The building then enters the SSO state until all services are reestablished leading to the state of SFS ($T_{SSO} = T_{INT}$). Residents may decide to return back to the building once the SSO state has been declared.
- **RLS**$_4$: the building will initially be in the NS state until inspection, planning,

demolition and replacement activities are completed ($T_{NS} = T_{INSP} + T_{MOB} + T_{REP}$). Once the main structural system is complete and the building is safe to occupy the SSO state will be declared. Once the installation of all internal components and services are complete, the building will enter the SFS state ($T_{SSO} = T_{INT}$). Unlike RLS_2 and RLS_3, the declaration of SSO does not lead to residents returning, as the building is missing internal components and services.

- **RLS_5**: since the building in this limit state suffers complete damage, the recovery path will follow the same steps associated with RLS_4.

In this work, the decision that residents will either evacuate and not return, evacuate and return or not evacuate once the functionality state of SSO has occurred is modeled through introducing the probability of functionality loss, $P(FuncLoss|SSO, \text{RLS})$, given SSO and the resilience limit state. The value assumed by $P(FuncLoss|SSO, \text{RLS})$ for each resilience limit state is reported in table 4.1. From table 4.1, it can be observed that as the resilience limit state increases, i.e. the building requires more repair actions to regain functionality, the value of $P(FuncLoss|SSO, \text{RLS})$ increases indicating how people are more likely to evacuate or not return once the building is safe to occupy. In particular, for RLS_4 and RLS_5, $P(FuncLoss|SSO) = 1$ as for both these resilience limit states the building is replaced and reaching SSO essentially coincides with the completion of the main structural system (i.e. the building is safe), however, no services are available.

The previous discussion is focused on the recovery on the building-level which treats each building as an isolated entity from the surrounding community. In fact, there are many factors outside the building that can impact its recovery process like (1) community resourcefulness: the availability of funds, materials, equipment and labor required for the repairs and replacement of damaged buildings will affect the

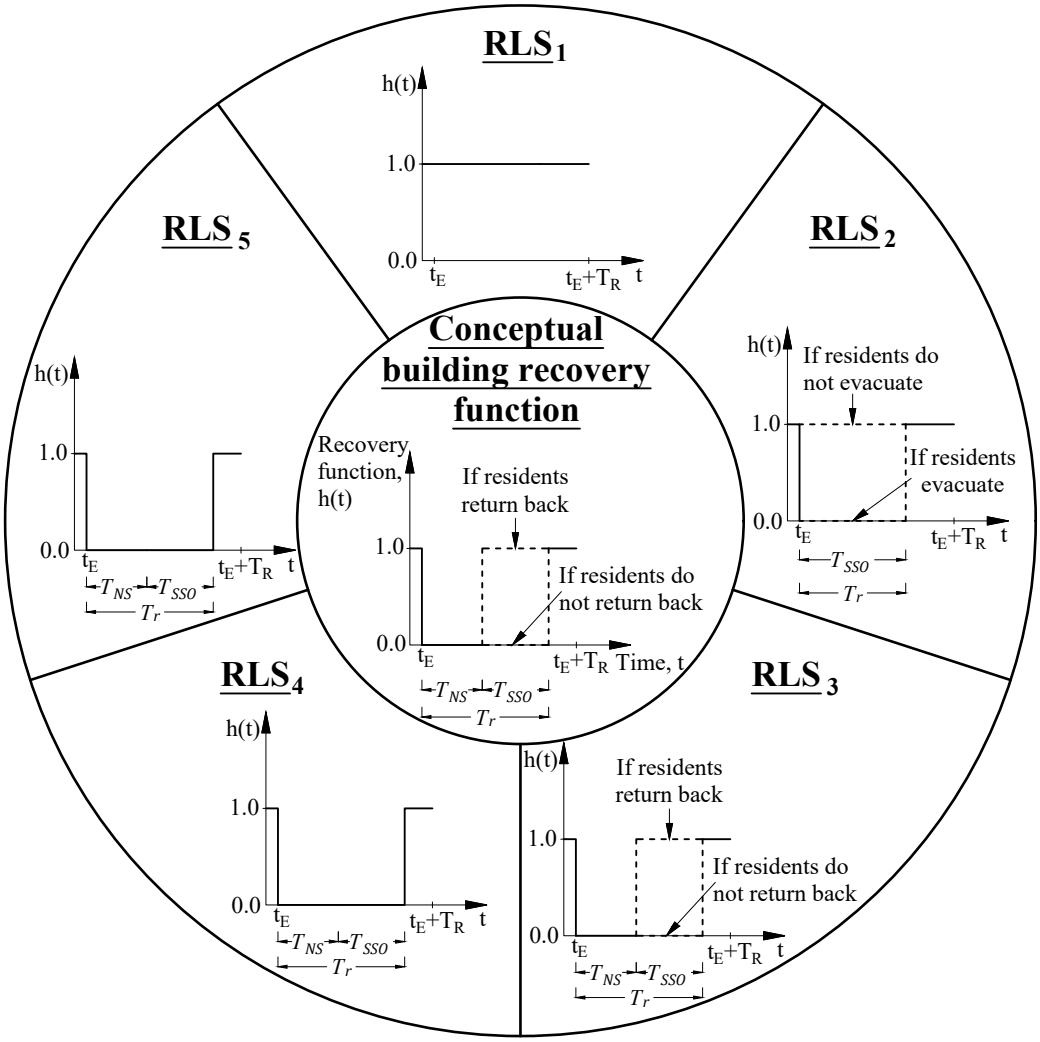

Figure 4.2: Building recovery function.

speed of the recovery process; (2) community infrastructure damage: for example damage in the electric power network may lead to power outage to all buildings, damage to transportation network may affect building accessibility; and (3) damage of the surrounding buildings: this can affect building accessibility and hinders its recovery process. These factors can be considered in the presented framework, in a similar fashion to the seismic hazard *Burton et al.* (2016), by introducing amplification factors to the times required for various recovery activities (T_{INSP} , T_{MOB}, T_{REP}, and T_{INT}).

Table 4.1: Probability of functionality loss given the functionality state SSO and resilience limit state.

Resilience Limit State	$\mathbf{RLS}_1$	$\mathbf{RLS}_2$	$\mathbf{RLS}_3$	$\mathbf{RLS}_4$	$\mathbf{RLS}_5$
$P(FuncLoss\|SSO, \text{RLS})$	0	0.1	0.5	1.0	1.0

4.2.5 Probabilistic quantification of resilience

A key aspect to understanding community resilience is accounting for all relevant uncertainties. To account for these uncertainties, the models of the previous sections are embedded in a Monte Carlo framework. Because of the generality of Monte Carlo methods, any parameter of the models can be taken as uncertain. In particular, in this version of the proposed framework, the following major uncertainties are considered:

- **Hazard uncertainty**: to account for the inhenert randomness that inevitably affect the track of the hurricane as well as its intensity, the site-specific probabilistic hurricane model developed by *Vickery and Twisdale* (1995b) is adopted.
- **Damage uncertainty**: randomness in the spatial variation of hurricane gust wind speed and debris flight trajectories are considered as outlined in *Grayson et al.* (2012a, 2013), while uncertainties associated with the capacities of the building components are considered by assigning each component an appropriate probability distribution.
- **Recovery uncertainty:** randomness in the recovery process is modeled by assigning probability distributions to the recovery times appearing in eq. (4.4).

From the samples generated during the Monte Carlo simulation, various probabilistic measures of resilience can be directly estimated. Of particular interest is the expected level of functionality at a given time $t = \hat{t}$ for hurricanes of category greater

than or equal to *cat*, based on Saffir-Simpson scale, that can be estimated as:

$$E\left[H(t=\hat{t})|CAT \geqslant cat\right] = \frac{\sum_{i=1}^{N_{CAT\geqslant cat}} \hat{H}_i(t=\hat{t}|CAT \geqslant cat)}{N_{CAT\geqslant cat}} \tag{4.5}$$

where $N_{CAT\geqslant cat}$ is the number of hurricanes of category greater than or equal to *cat* in the Monte Carlo simulation; and $\hat{H}_i$ is the community recovery function for the ith realization. Another measure of interest is the probability of reaching or exceeding a target level of functionality ($H_{\hat{t}}$) at time $t = \hat{t}$ for hurricanes of category greater than or equal to *cat* that can be directly estimated as:

$$P\left[H(t=\hat{t}) \geqslant H_{\hat{t}}|CAT \geqslant cat\right] = \frac{1}{N_{CAT\geqslant cat}} \sum_{i=1}^{N_{CAT\geqslant cat}} \mathbb{1}_{H(t=\hat{t})\geqslant H_{\hat{t}}|CAT\geqslant cat} \tag{4.6}$$

where $\mathbb{1}$ is the indicator function. Similar expressions to eqs. (4.5) and (4.6) can be used for estimating quantities such as the expected level of resilience, $E[R|CAT \geqslant cat]$, or the probability of community resilience reaching or exceeding a target level of resilience, $P\left[R \geqslant R_{\hat{t}}|CAT \geqslant cat\right]$, for hurricanes of category greater than or equal to *cat*.

4.3 Case study

4.3.1 Description

4.3.1.1 Community layout

The proposed framework is used to asses the hurricane resilience of a residential community consisting of 513 buildings in Miami-Dade county, FL (fig. 4.3). As illustrated in fig. 4.4, the buildings surrounding the community were also modeled to ensure an accurate estimate of windborne debris damage. Indeed, a considerable portion of debris damage can be attributed to windborne missiles originating from damaged buildings located outside the considered community. The size of the surrounding area considered was determined through the distance l_{out}, as illustrated

Figure 4.3: Location of the considered community (inside the solid rectangle) and the surrounding buildings (inside the dotted rectangle).

in fig. 4.3. In particular, l_{out} = 850 m was chosen as it represents the maximum distance a typical plywood sheathing can travel when subjected to a wind speed of 152 m/s (the maximum wind speed generated from the hurricane hazard analysis). The chosen l_{out} is assumed to be adequately large to account for all debris coming from outside the community.

4.3.1.2 Building archetype and construction cases

The archetype one-story residential wooden building shown in fig. 4.5 is considered to be representative of all buildings in the community. To illustrate the capability of the proposed framework in assessing the effects on resiliency of applying upgrades to various building components as a mitigation plan, two construction cases are considered: (1) as-built case: which is considered representative of the current residential built environment in Florida (*Gurley et al.*, 2005); and (2) enhanced case: in which

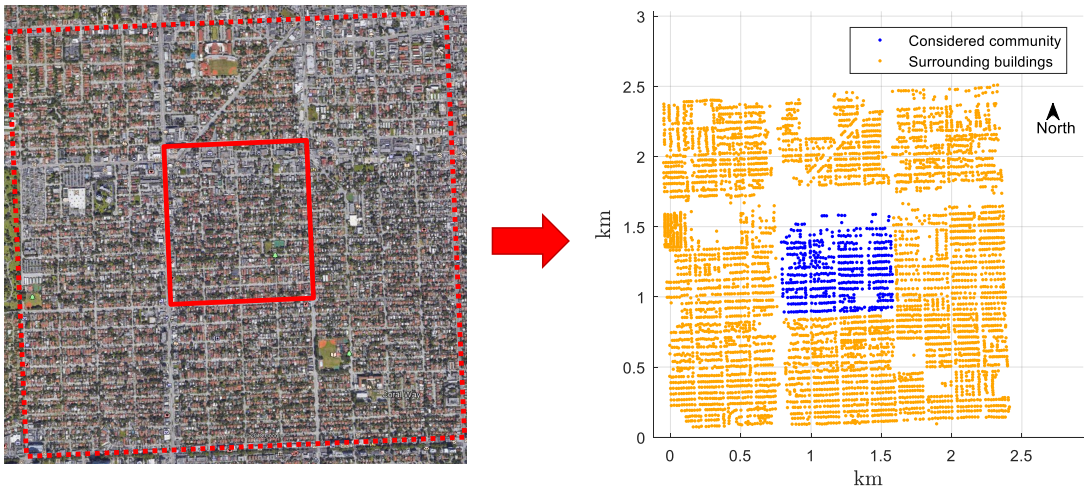

Figure 4.4: Layout of the modeled community and its surrounding buildings.

enhancements have been applied to the building components capacities. In particular, the component capacities for both cases are based on those outlined in (*Datin et al.*, 2011; *Gurley et al.*, 2005; *Vickery et al.*, 2006b) and are summarized in Table 5.1. In applying the Monte Carlo scheme, the normal distribution is truncated at two standard deviations from the mean.

To estimate damage from wind-borne debris impact, roof cover, roof sheathing and gable-end sheathing are considered as possible debris sources; while windows, doors and garage doors are assumed vulnerable to debris impact (*Lin et al.*, 2010b). The resistance of windows and doors to impact, in terms of kinetic energy, is taken as deterministic and equal to 68 Nm for the as-built case (*Vickery et al.*, 2006b). Installation of window and door protection (shutters) is added to the enhanced case which upgrades the impact resistance to 475 Nm (*Vickery et al.*, 2006b).

4.3.1.3 Community population

In calibrating the housed population of the community, census report data for Miami-Dade County is used (*Census Reporter*, 2017). This data led to the probability distribution for number of residents reported in fig. 4.6. By sampling from this

Table 4.2: Resistance to wind pressure of the building components for the as-built and enhanced construction cases.

Building component	Mean resistance		COV	Distribution
	As-built case	Enhanced case		
Glass window	2.5 kPa	2.5 kPa	0.20	Normal
Door	4.8 kPa	4.8 kPa	0.20	Normal
Garage door	2.5 kPa	2.5 kPa	0.20	Normal
Wall sheathing	6 kPa	8.7 kPa	0.4	Normal
Roof sheathing	7.2 kPa	8.7 kPa	0.4	Normal
Wall cover	3.2 kPa	6.2 kPa	0.20	Normal
Roof cover	3.35 kPa	6.2 kPa	0.40	Normal
Roof-wall connection	16.5 kN	20 kN	0.20	Normal

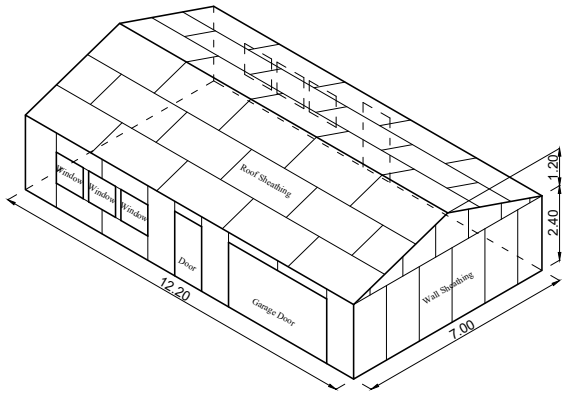

Figure 4.5: Typical residential building adapted from *Yau* (2011).

distribution, the number of occupied buildings in the community is determined to be 436 (85%) while the number of vacant buildings is estimated to be 77 (15%). The location of occupied vs vacant buildings for the community is shown in fig. 4.7. In total 1351 people are considered to reside in the 436 buildings resulting in an average occupancy of 3.1 people per building.

4.3.1.4 Hurricane hazard

As mentioned, the hurricane hazard is simulated through the probabilistic model outlined in *Vickery and Twisdale* (1995b). In this model, each event is defined by five parameters that control the hurricane track and intensity. These parameters

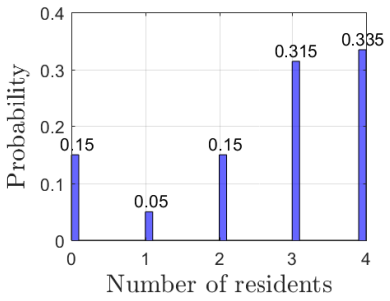

Figure 4.6: Calibrated probability mass function governing number of residents per building for the community.

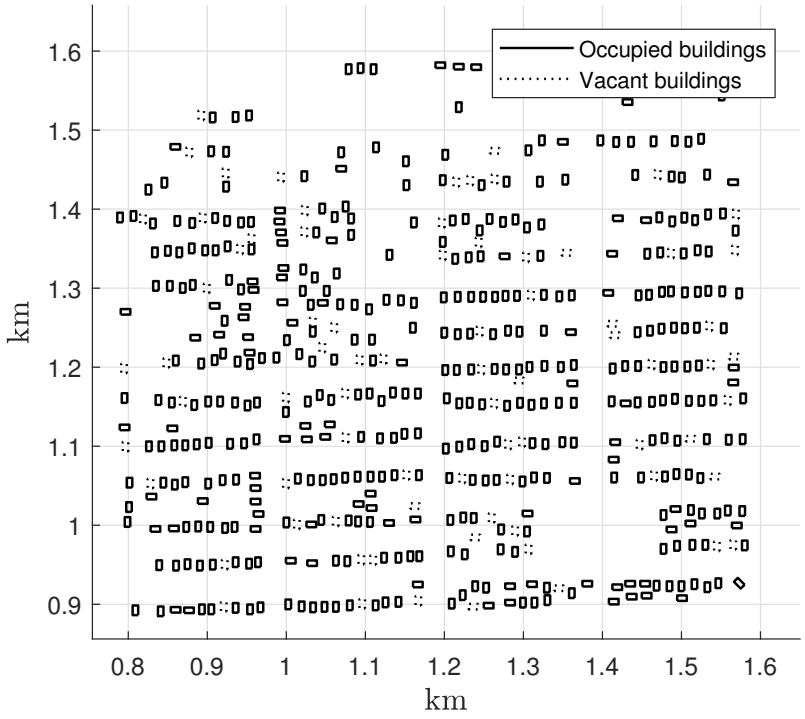

Figure 4.7: Occupied vs vacant buildings.

are central pressure difference (Δp), radius to the maximum wind speed (R_{max}), hurricane translational speed ($\mathbf{V}_{tr}$), hurricane heading (θ), and the minimum distance (d_{min}) between the hurricane track and the community of interest. Appropriate probability distributions for each parameter can be found in *Vickery and Twisdale* (1995b).

4.3.1.5 Recovery times

Uncertainty in the recovery model is accounted for through assigning appropriate probability distributions to the recovery times of eq. (4.4). In this respect, T_{INSP}, T_{MOB}, T_{REP} and T_{INT} were modeled as lognormal random variables. Values of dispersion for T_{REP} and T_{INT} are 0.4, while for T_{INSP} and T_{MOB}, a value of 0.8 is assumed. These values are commonly used in modeling the community recovery from earthquakes (*Burton et al.*, 2016) and are assumed reasonable for hurricanes. Based on the median repair and recovery times for residential wooden buildings available in *HAZUS-MH 2.1* (2003), the following medians are assumed for the recovery times:

- The median values for T_{INSP} are dependent on the resilience limit states. These values are equal to 0, 1, 5, 10 and 20 days for RLS_1, RLS_2, RLS_3, RLS_4 and RLS_5, respectively;
- Median values for T_{MOB} are also assumed dependent on the resilience limit states and are taken equal to 0, 0.5, 2, 4 and 6 days for RLS_1, RLS_2, RLS_3, RLS_4 and RLS_5, respectively;
- Calculation of T_{REP} and T_{INT} require specifying values for repair/replacement times of each building component. Median values for the repair/replacement times are specified as follows:
  - 1 day for a window.

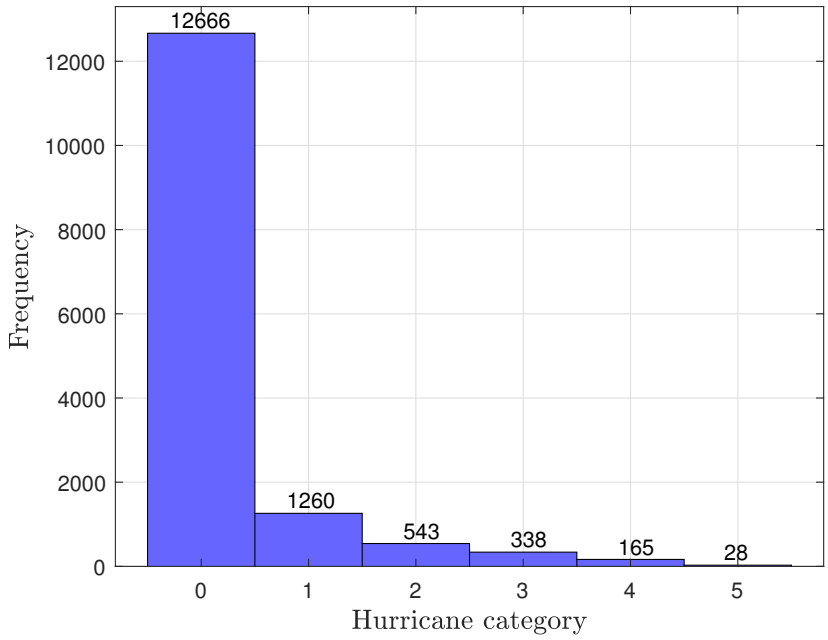

Figure 4.8: Frequency distribution of the hurricanes considered in the Monte Carlo scheme.

- 1 day for a door.
- 2 days for a garage door.
- 50 days for the roof-wall connection.
- 0.5 day/m^2 for wall and roof sheathing, and wall and roof cover.

4.3.2 Community resilience results and discussion

4.3.2.1 Preamble

In applying the Monte Carlo scheme of section 4.2.5, 15000 samples, and therefore hurricanes, were considered. Following the probability distributions suggested in *Vickery and Twisdale* (1995b) for Miami, this resulted in the distribution of hurricane category, based on Saffir-Simpson wind scale, shown in fig. 4.8. In particular, category zero hurricanes are defined as those hurricanes that have a 1-minute maximum sustained wind speed of less than 33 m/s.

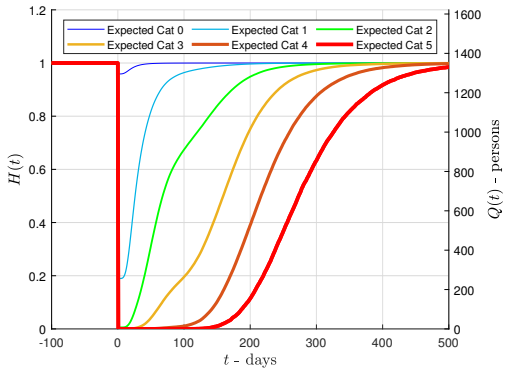

Figure 4.9: Expected community recovery functions for the as-built case.

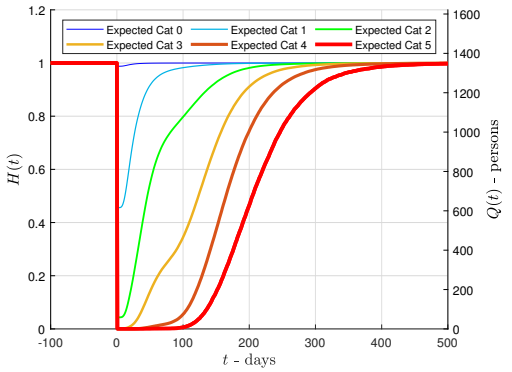

Figure 4.10: Expected community recovery functions for the enhanced case.

4.3.2.2 Community recovery curve

Figures 4.9 and 4.10 show the expected community recovery curves obtained from the proposed framework conditioned on hurricane category. The proposed framework captured the improvement in the performance of the enhanced case over the as-built case which can be deduced by comparing expected community recovery curves for both cases. The need for carrying out probabilistic analysis is demonstrated in figs. 4.11 and 4.12 where the standard deviation as well as the expected recovery curves are shown. The significant standard deviations seen imply that modeling the community recovery using a deterministic approach will generally not be sufficient. This result is consistent for all hurricane categories for both cases as it can be noticed that the standard deviation is equal to or higher the expected value, especially in the early stage of recovery. Another advantage of a probabilistic quantification lies in how it can be used to inform decision makers through estimation of the probability of reaching a specific level of functionality at any given time during the recovery process. By assuming, for example, that the community target level of functionality ($H_{\hat{t}}$) is 98%, the probability of reaching or exceeding this level of functionality can be directly estimated as illustrated in fig. 4.13.

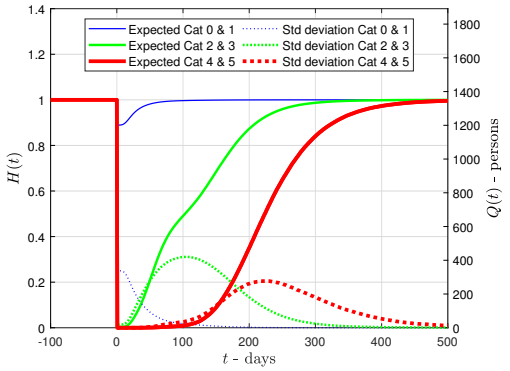

Figure 4.11: Standard deviation and expected community recovery curves for the as-built case.

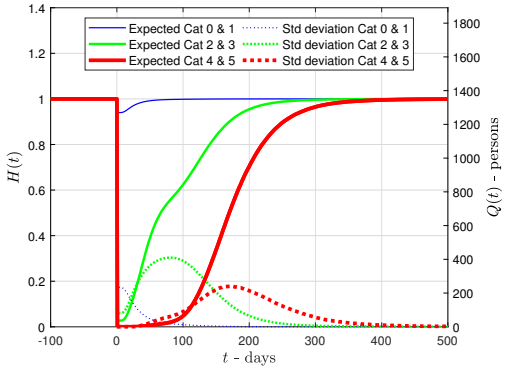

Figure 4.12: Standard deviation and expected community recovery cures for the enhanced case.

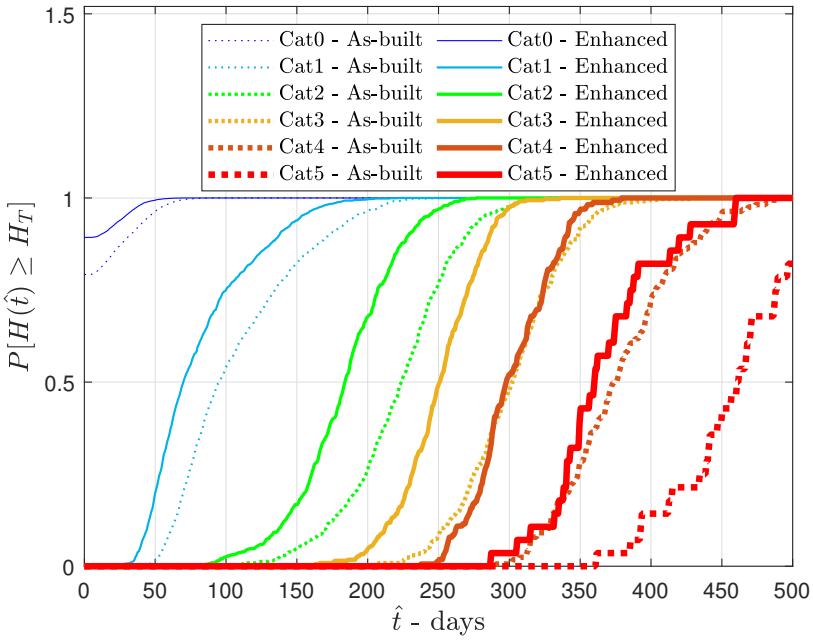

Figure 4.13: Probability of reaching or exceeding a target 98% functionality for the as-built and enhanced cases.

As discussed in section 4.3.1.1, buildings both inside as well as outside the community are considered in estimating damage induced by debris. To show the influence of debris originating from buildings that are outside the community, windborne debris is categorized according to its source as follows: (1) internal debris: debris generated from buildings inside the considered community; (2) external debris: debris generated from buildings outside the considered community. The landing locations of both types of debris are shown in fig. 4.14 for the as-built and enhanced cases. It can be noticed that most of the internal debris lands around the buildings as it is generated from them, while external debris is concentrated at the south and east parts of the considered community. The landing locations of the external debris can be explained by fig. 4.15 which shows that most hurricanes are coming from the south. Table 4.3 summarizes the expected number of debris objects of each type and their ratios for each construction case. The expected number of debris objects that land inside the considered community in the as-built case is significantly greater than in the enhanced case. This result can be traced back to how buildings in the as-built case suffer more damage than the enhanced case. However, the ratio of the external to internal debris in the enhanced case (0.22) is notably more than the as-built case (0.17). This result is due to the greater capacities of the wall and roof sheathing, and the wall and roof cover (debris sources) in the enhanced case as compared to the as-built case. In other words, higher wind speeds are required to release (cause damage) components in the enhanced case compared to the as-built case. Once any of these components are released (damaged) in the enhanced case, they will experience higher wind speeds that will lead to longer flight distances. The low value of the expected number of internal debris in the enhanced case reflects this phenomenon which leads to a higher ratio of the external to internal debris in the enhanced case. These results

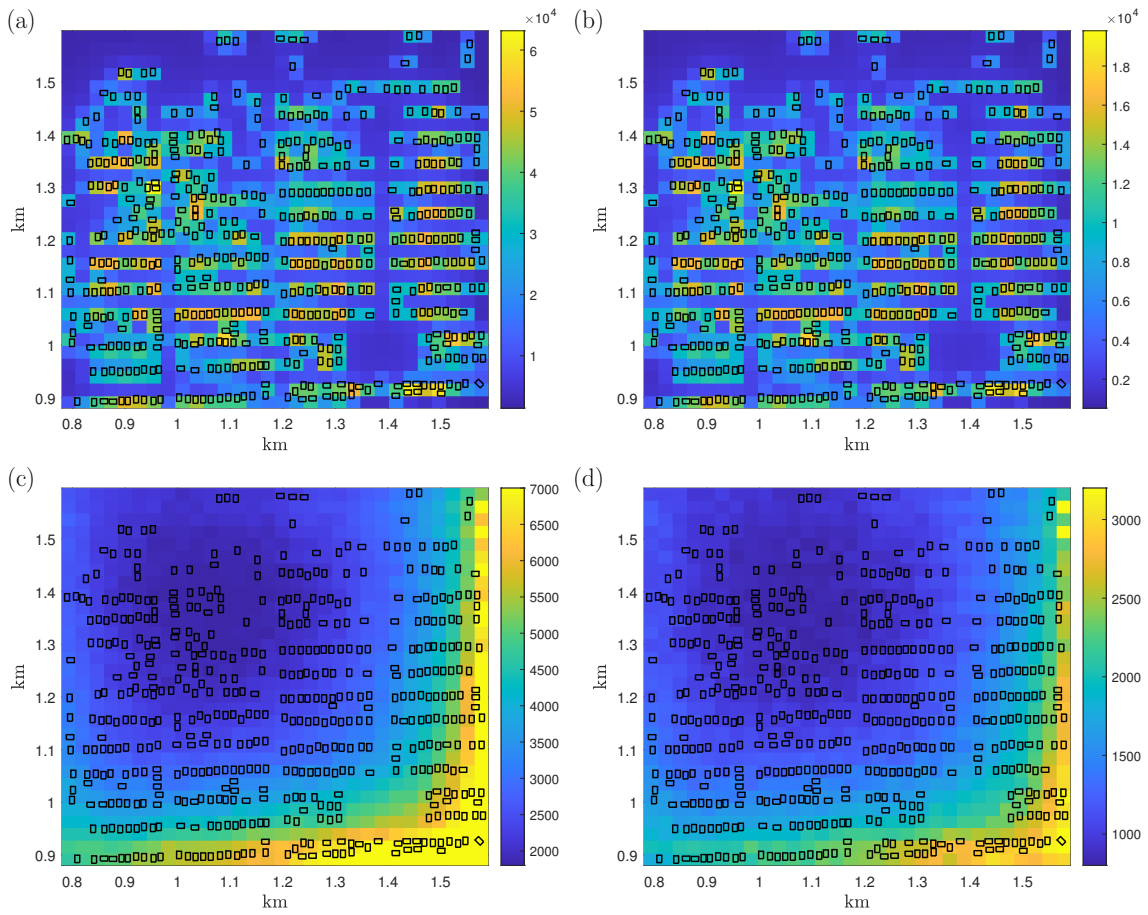

Figure 4.14: Heat map for the debris landing locations for the 15000 generated hurricanes: a) internal debris for the as-built case; b) internal debris for the enhanced case; c) external debris for the as-built case; and d) external debris for the enhanced case.

shows how ignoring the effect of debris originating from outside the community will lead to an underestimation of damage which in general will lead to underestimation of the community recovery time and functionality loss. This finding is illustrated by comparing the recovery curves estimated by ignoring the effects of debris external to the community, figs. 4.16 and 4.17, with those estimated considering both internal and external debris, figs. 4.9 and 4.10. Significant underestimation of the recovery times and functionality loss are seen, especially in the case of enhanced building component capacities.

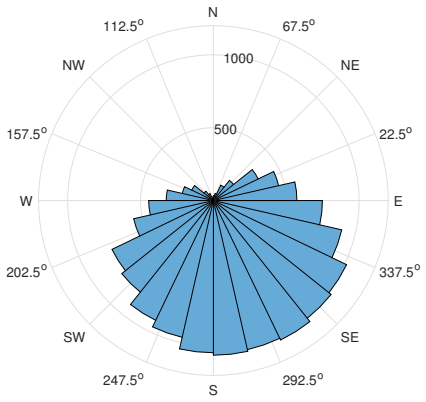

Figure 4.15: Histogram of the hurricane-genesis location with respect to Miami, FL.

Table 4.3: Expected number of the internal and external debris objects for each construction case.

Construction case	As-built case	Enhanced case
Expected number of internal debris	1215	387
Expected number of external debris	207	86
Ratio of external to internal debris	0.17	0.22

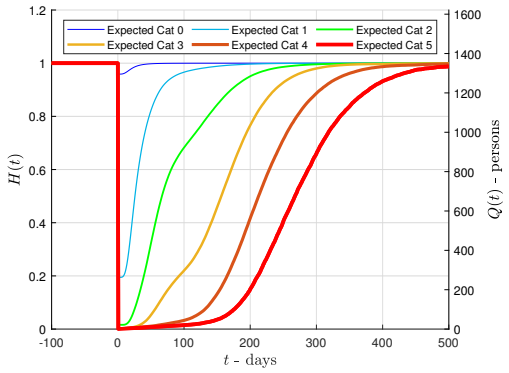

Figure 4.16: Community recovery functions for the as-built case considering damage from inside debris only.

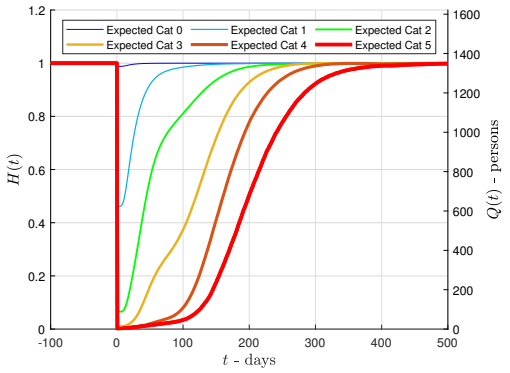

Figure 4.17: Community recovery functions for the enhanced case considering damage from inside debris only.

4.3.2.3 Community resilience

From the recovery curves of the Monte Carlo simulation, the resilience measure of eq. (4.1) can be directly estimated. In this respect, fig. 4.18 reports the expected value for R conditional on hurricane category, construction case, and inclusion/exclusion of debris originating outside the community. From fig. 4.18, the effect of ignoring

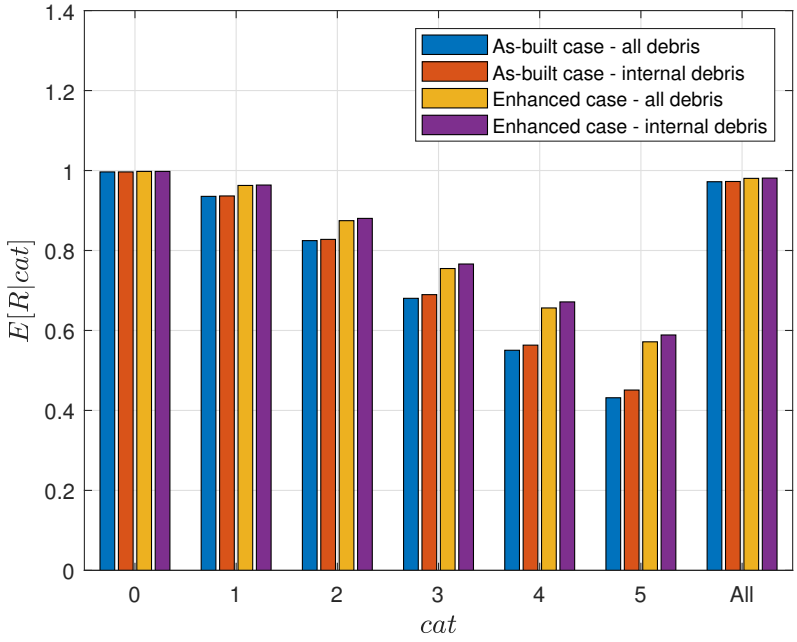

Figure 4.18: Expected value of the Resilience measure (R) for both construction cases.

outside debris becomes more significant as the hurricane category increases due to how this increases the amount of debris objects entering the community and therefore causing damage.

With the aim of quantifying the resilience measure probabilistically, figs. 4.19 and 4.20 show the cumulative distribution functions of R conditioned on hurricane category for the as-built and enhanced case, respectively. The improvement in the performance of the enhanced case over the as-built is reflected on the right-shift of the cumulative distribution function of R for the earlier with respect to the later. The dispersion of the values of the resilience measure becomes more noticeable for hurricanes of higher category for both construction cases. This dispersion of R once again emphasizes the importance of a probabilistic quantification of community resilience in the case of hurricanes.

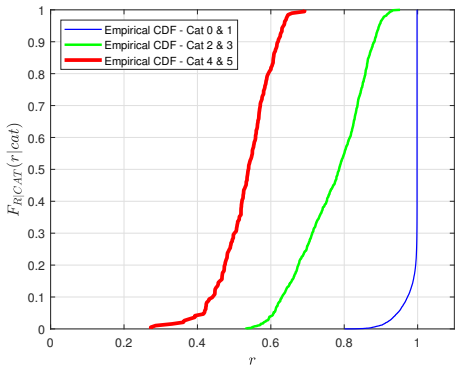

Figure 4.19: Conditional cumulative distribution functions of the resilience metric R for the as-built case considering damage from all debris.

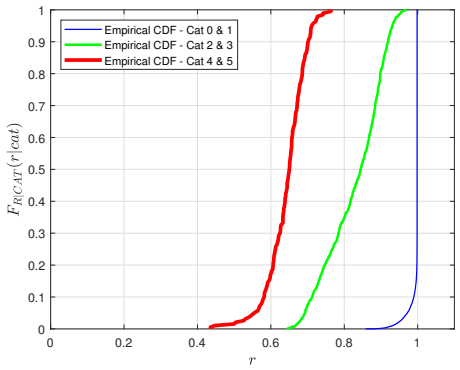

Figure 4.20: Cumulative distribution functions of the resilience metric R for the enhanced case considering damage from all debris.

4.4 Conclusions

A framework to probabilistically quantify community resilience against hurricanes is presented. The modeling of the community response to hurricane winds is achieved by integrating an engineering-based vulnerability model with a novel community recovery model that enables the estimation of the community recovery curve and subsequently community resilience. By embedding the model in a Monte Carlo simulation scheme, probabilistic representations of both the recovery curves as well as the resilience measure are obtained. To illustrate the proposed framework, a case study consisting of a typical residential community in Miami, FL is presented. In particular, two construction cases are considered, an as-built case and an enhanced case, in order to show how the effects of mitigation strategies can be measured in terms of changes in resilience through the proposed framework. Two main conclusions from the case study are as follows: (1) the modeling of debris originating from outside the community is essential for accurate estimation of community damage and therefore accurate estimation of the community recovery function and any subsequent community resilience measure; (2) probabilistic analysis is essential for community

resilience quantification as significant uncertainty exists in the recovery curves even when the analysis is conditioned on hurricane category. These findings can be used by designers and developers to account more accurately for the damage caused by windborne debris, and by planners and decision makers to help identify strategies to mitigate the risks and consequences of hurricanes.

CHAPTER V

A Framework for Estimating Water Ingress Due to Hurricane Rainfall[1]

Abstract

Hurricane rainfall can have adverse effects on residential communities and pose a significant risk to the community's economic prosperity and quality of life. These adverse effects are mainly caused by the ingress of rainfall water into the buildings due to wind-driven rain (WDR) and inland flooding. Existing frameworks focus on estimating the amount of water ingress due to WDR and inland flooding separately. This paper provides a comprehensive framework that considers both WDR and inland flooding in estimating the amount of water ingress into residential buildings due to hurricane rainfall. The framework estimates the water ingress due to WDR by combining the WDR intensity with the perforated area (i.e., damaged area) of the building envelope. The intensity of the WDR is quantified using an Eulerian Multi-phase Model (EMM) which characterizes the wind field by solving the Reynolds-Averaged Navier-Stokes (RANS) equations with a realizable $k-\epsilon$ turbulence model. The buildings' envelope is considered susceptible to damage from the impact of windborne debris and excessive dynamic wind pressure. For inland flooding, the framework uses a coupled hydrologic-hydrodynamic model (tRIBS-OFM)

[1] Abdelhady, A.U., Xu, D., Ouyang, Z., Spence, S.M.J., McCormick, J. and Ivanov, V.Y. (2021). "A framework for the estimate of water ingress due to hurricane rainfall," *Building and Environment*, Under Preparation.

to estimate the inundation depth at each building. The framework is illustrated by a case study consisting of a residential community in Houston, TX which is subject to Hurricane Harvey. The main conclusion of the case study is the importance of considering both WDR and inland flooding to estimate losses due to hurricane rainfall.

5.1 Introduction

Hurricanes typically produce severe and widespread rainfall. This rainfall can cause significant damage to the built environment and its supporting infrastructure. In particular, the damage caused by rainfall to buildings happens progressively over two stages. In the first stage, rainwater seeps into the building, under the influence of the wind (wind-driven rain), through perforations in the building envelope leading to potential damage to the internal contents and, in extreme cases, to the structural system. The second stage starts when the rainfall persists over a longer period, this saturates the ground and overwhelms surrounding drainage systems leading to inland flooding. Thus, a fundamental step to accurately estimating the damage caused by hurricane rainfall to residential communities is to quantify the amount of water ingress to buildings over both stages.

Estimating water ingress due to wind-driven rain (WDR) is a highly complex problem that is governed by many factors (e.g. rainfall intensity, raindrop size and distribution, wind speed and direction, buildings geometry and arrangement, etc.). Research efforts in this area can be categorized into experimental methods (e.g. *Ge et al.*, 2017; *Raji et al.*, 2020; *Vutukuru et al.*, 2020), semi-empirical methods (e.g. *ISO*, 1997; *Straube*, 1997), and numerical methods (e.g. *Choi*, 1993, 1994; *Dao and Van De Lindt*, 2010; *Ouyang and Spence*, 2019, 2020; *Wang et al.*, 2019). The

experimental and semi-empirical methods have an important role in understanding the inherent complexity of the problem. This understanding provides the basis to develop numerical methods that are based on Computational Fluid Dynamics (CFD) which are essential to investigate the impact of various scenarios of hurricane rainfall on the built environment. A comprehensive review of these methods can be found in (*Blocken and Carmeliet*, 2004, 2010).

The estimation of water ingress due to inland flooding hinges on the quantification of flood inundation depth at each building in the community. Methods used for flood inundation modeling have been categorized by *Teng et al.* (2017) into empirical methods, simplified-conceptual methods, and hydrodynamic methods (one-, two-, and three-dimensional models). The empirical and simplified-conceptual methods are generally suitable for flood monitoring, crude flood risk assessment, calibration, and validation of more sophisticated methods, etc. However, the two-dimensional (2D) hydrodynamic models that are based on the 2D Saint-Venant (shallow-water) equations are more appropriate for simulation of overland flow over complex topography (*Akanbi and Katopodes*, 1988; *Begnudelli and Sanders*, 2006; *Di Giammarco et al.*, 1996; *Gottardi and Venutelli*, 2008; *Horritt*, 2002; *Nofal and Van De Lindt*, 2020; *Nofal and van de Lindt*, 2020).

In contrast to the large amount of research that has treated WDR and the inland flooding separately, to knowledge of the authors, there is a significant lack of published studies that focus on the integrated quantification of the impacts of WDR and inland flooding on the built environment. Even though WDR and inland flooding are both consequences of hurricane rainfall, each one is different in nature and requires diverse mitigation actions. For example, while mitigation measures like dams, levees, floodwalls, and crawl-space foundations can be efficient in mitigating

the damage from flooding, these measures do not mitigate damage from wind-driven rain. Within this context, this paper provides an initial framework for estimating the amount of water ingress into residential buildings through both stages of hurricane rainfall.

5.2 The framework

5.2.1 Overview

For a given residential community subject to a hurricane with significant rainfall, the basic idea is to simultaneously estimate the temporal evolution of water ingress into the buildings due to both WDR and inland flooding using a time-stepping approach. The framework is schematically represented in fig. 5.1. The approach steps through the hurricane event incrementally using a predefined time step (Δt). For each time step, the hurricane wind speed (v) and direction (α) are estimated at the considered community using a hurricane wind field model (e.g., *Guo and van de Lindt*, 2019; *Holland*, 1980; *Jakobsen and Madsen*, 2004; *Vickery et al.*, 2000).

The volume of the water ingress due to WDR is then obtained by combining the WDR intensity with the perforated area (i.e., damaged area) of the building envelope. The spatial distribution of the WDR intensity over the envelope of the buildings is estimated through an Eulerian multiphase model (EMM) (*Huang and Li*, 2010; *Kubilay et al.*, 2013, 2014; *Ouyang and Spence*, 2019, 2020) while the perforated area of the building envelope is estimated using an engineering-based vulnerability model (e.g. *Grayson et al.*, 2013; *Yau et al.*, 2011). The vulnerability model estimates damage due to dynamic wind pressure and the impact of windborne debris.

The water ingress due to inland flooding is quantified for each time step by estimating the flood inundation depth at each building using a coupled hydrologic-hydrodynamic model. In particular, the hydrologic processes over the land surface

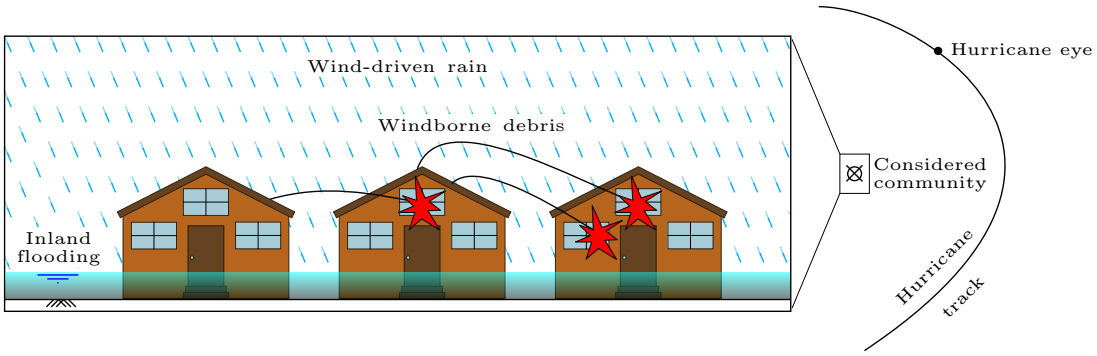

Figure 5.1: Conceptual representation of the proposed framework.

and subsurface are modeled using the TIN (Triangulated Irregular Network)-Based Real-time Integrated Basin Simulator (tRIBS) (*Ivanov et al.*, 2004). The flow of the runoff, resulting from the hydrologic processes, over the ground can be regarded as the propagation of shallow water waves. The shallow water waves are described mathematically using the 2D Saint-Venant (shallow-water) equations which are solved using the hydrodynamic model, overland flow model (OFM), to estimate the flood inundation depth at each building in the community (*Kim et al.*, 2012).

5.2.2 Vulnerability model

The engineering-based vulnerability model outlined in (*Abdelhady et al.*, 2020; *Grayson et al.*, 2013; **?**) is adopted due to its high-fidelity in modeling damage due to dynamic wind pressure and the impact of windborne debris. The main features of the vulnerability model are summarized as follows:

1. Hurricane wind speed (v) and direction (α) are evaluated at each building in the community using the parametric hurricane wind field model provided by *Jakobsen and Madsen* (2004) based on the location of the hurricane eye (defined by the hurricane track), the hurricane translational velocity, the radius to the maximum wind speed (R_{max}), and the central pressure difference (Δp).

2. Dynamic wind pressure is evaluated using external pressure coefficients ex-

tracted from the wind tunnel database provided by *Tokyo Polytechnic University* (2007) and internal pressure coefficients obtained from the internal pressure model provided by *Holmes* (2017).

3. Pressure damage is evaluated by comparing the calculated dynamic wind pressure of each building component with its pressure resistance.
4. If pressure damage occurs to any of the building envelope components (e.g., roof coverings, roof sheathing, etc.), the damaged component is traced using a six-degree-of-freedom debris trajectory model (*Grayson et al.*, 2012a; *Richards et al.*, 2008b). If the damaged component impacts any downwind building component, the impact energy is compared to the impact resistance to determine if further damage occurs.
5. Both pressure and debris damage to the envelope of the buildings trigger internal pressurization which can cause more damage to the buildings.

These features allow for the explicit modeling of the interdependencies between pressure and debris damage. The total damage of the building envelope components at each time step is then estimated as follows:

$$D_C^{iq}(t_j) = \mathbb{1}_{\max_{j=1}^{j} P^{iq}(t_j) > R_P^{iq} \ \vee \ \max_{j=1}^{j} I^{iq}(t_j) > R_I^{iq}} \tag{5.1}$$

where $i = 1, \cdots, n_B$ with n_B the number of buildings in the considered community; $q = 1, \cdots, n_C$ with n_C the number of components in the building; $j = 1, \cdots, n_T$ with n_T the total number of simulation time steps; t is the simulation time; $\mathbb{1}$ is the indicator function; P is the dynamic wind pressure; I is the impact energy of the windborne debris; and R_P and R_I are the pressure and impact resistances.

The perforated area of the i^{th} building envelope is then estimated as follows:

$$A_P^i(t_j) = \sum_{q=1}^{n_C} D_C^{iq}(t_j) A_C^{iq} \tag{5.2}$$

where A_C is the area of the building envelope component.

5.2.3 Wind-driven rain

The volume of the water ingress due to WDR (V_{WDR}) into the i^{th} building can be written as follows:

$$V^i_{WDR}\left(t_j\right) = V^i_{WDR}\left(t_{j-1}\right) + \int_{A^i_P(t_j)} R^i_{WDR}\left(t_j\right) \Delta t \, \mathrm{d}A \tag{5.3}$$

where R^i_{WDR} is the spatial distribution of the WDR intensity over the envelop of the i^{th} building. The quantification of R_{WDR} is carried out using the Eulerian multiphase framework outlined in (*Kubilay et al.*, 2013, 2014; *Ouyang and Spence*, 2019, 2020).

The framework can be summarized into two main steps. In the first step, the time-averaged wind speed, $\mathbf{v}_w$, is estimated around the buildings by solving the Reynolds-averaged Navier–Stokes (RANS) equations with the realizable $k-\epsilon$ turbulence model (*Shih et al.*, 1995).

$$\mathbf{v}_w\left(\mathbf{x}, t_j\right) = \mathcal{RANS}_{k-\epsilon}\left(v\left(t_j\right), \alpha\left(t_j\right), z_o\right) \tag{5.4}$$

where z_o is the site roughness length.

In the second step, the Eulerian multiphase model (EMM) uses the simulated $\mathbf{v}_w$ to model the WDR field. In this model, the rain field is divided into n_{WDR} phases based on the raindrop diameter sizes d_m for $m = 1, \cdots, n_{WDR}$. The velocity ($\mathbf{v}_m$) and the volume fraction (a_m) of the m^{th} rain phase at the envelope of the i^{th} building can be estimated as follows:

$$\left[\mathbf{v}^i_m\left(t_j\right), a^i_m\left(t_j\right)\right] = \mathcal{EMM}\left(\mathbf{v}_w\left(\mathbf{x}, t_j\right)\right) \tag{5.5}$$

Based on $\mathbf{v}_m$ and a_m, the specific catch ratios (η_m) for each rain phase are defined as:

$$\eta^i_m\left(t_j\right) = a^i_m\left(t_j\right) \frac{\left|\mathbf{v}^i_m\left(t_j\right) \cdot \mathbf{n}^i\right|}{u_m} \tag{5.6}$$

where $\mathbf{n}^i$ is the unit normal vector to the i^{th} building envelope and u_m is the terminal velocity of the raindrops of diameter d_m. Using η_m, R_{WDR} can be estimated as follows:

$$R^i_{WDR}(t_j) = R_h(t_j) \cdot \sum_{m=1}^{n_{WDR}} \int_{d_m - \frac{\Delta d_m}{2}}^{d_m + \frac{\Delta d_m}{2}} f_h(d_m|R_h)\, \eta^i_m(t_j)\, \mathrm{d}d \tag{5.7}$$

where R_h is the horizontal rainfall intensity; Δd_m is the diameter range associated with the m^{th} rain phase; and $f_h(d_m|R_h)$ is the horizontal raindrop size distribution that can be obtained from *Best* (1950).

It should be noted that, for a given residential community, η_m depends only on v and α. Therefore, based on eq. (5.7), R_{WDR} can be rapidly updated based on the value of R_h if v and α are held constant. Since v and α are continuously varying as the hurricane approaches the community, η_m needs to be estimated for each time step (t_j). This approach will require solving the RANS and the EMM each time step which is computationally expensive. Alternatively, the evaluation of η_m can be carried out using interpolation between limiting values of v and α. Such an interpolation approach has been validated in literature (e.g., *Kubilay et al.*, 2013, 2014, 2017).

5.2.4 Inland flooding

The input data for the tRIBS model are community layout (L), land use (U), topography (T), vegetation (V), soil characteristics (S), and meteorological data (M); e.g. temperature, humidity, radiation, horizontal rainfall, etc. The tRIBS uses these data to model each relevant hydrologic processes, such as evapotranspiration, infiltration, rainfall interception, etc., to estimate the temporal variation of the surface runoff:

$$R(t) = \mathcal{TRIBS}(M(t), T, L, S, U, V) \tag{5.8}$$

The OFM propagates the surface runoff in the residential community using shallow-water equations to estimate the inundation depth (h) at each building:

$$h^i\left(t_j\right) = \mathcal{OFM}\left(R\left(t\right), T, L, S, U, V\right) \tag{5.9}$$

The shallow-water equations are solved using the finite-volume method which uses Roe's approximate Riemann solver to calculate fluxes (*Begnudelli and Sanders*, 2006; *Kim et al.*, 2012). Additionally, the flow boundaries in urban environments affecting surface flows is represented in tRIBS-OFM, for example, the buildings are included in the model explicitly. This will provide a certain blockage to the flow path therefore intensifying local inundation. Those capabilities guarantee the good performance of tRIBS-OFM in simulating the flow depth and velocity around buildings.

It should be noted that, generally, the time step used in tRIBS is not the same as that used in the OFM and both are different from Δt. The time step used in OFM is constrained by the Courant-Friedrichs-Lewy (CFL) condition while tRIBS typically operates using much larger time step *Sanders* (2008). Consequently, R produced from eq. (5.8) is assumed to be constant over the tRIBS's time step when communicating with the OFM. The OFM then solves for h and the output is exported every Δt to be consistent with the output from the WDR model.

5.2.5 Simulation strategy

Figure 6.4 illustrates the simulation strategy of the proposed framework. The WDR and the inland flooding simulations advance in parallel. For the WDR, the simulation starts by evaluating the R_{WDR} for chosen values of v and α. These chosen values will be used later to obtain the required R_{WDR} using interpolation as described in section 5.2.3.

The simulation then proceeds by time-stepping through the hurricane event. For

each t_j, hurricane wind speed (v) and direction (α) are estimated and used in the building damage estimation. After estimating the damage of each building component according to eq. (5.1), the perforated area of the building envelope is estimated using eq. (5.2). A_P is then combined with the interpolated value of R_{WDR} using eq. (5.3) to estimate the volume of water ingress into each building due to WDR.

For the inland flooding, the tRIBS models the appropriate hydrologic processes and estimates the spatial and temporal variation of the surface runoff. The OFM then propagates the surface runoff through the considered community to estimate h at each building. After the last time step, the simulation exports the time histories of V_{WDR} and h for each building.

5.3 Case Study

5.3.1 Description

5.3.1.1 Community location and layout

The framework is used to estimate the water ingress for residential wooden buildings in Houston due to the rainfall that occurred during Hurricane Harvey. Figure 5.3 shows the location of the storm track with respect to Houston as well as the evolution of Harvey from a tropical storm to category four then its decay to a tropical storm as reported in *NOAA Satellite Imagery of Hurricane Harvey* (2017). The beginning and end portions of the storm track are excluded in the model as they do not have any impact on the results. The modeled part of the storm track is shown in fig. 5.3. A residential community of 580 buildings in Houston is modeled using the proposed framework, the location and orientation of the buildings are shown in fig. 5.4.

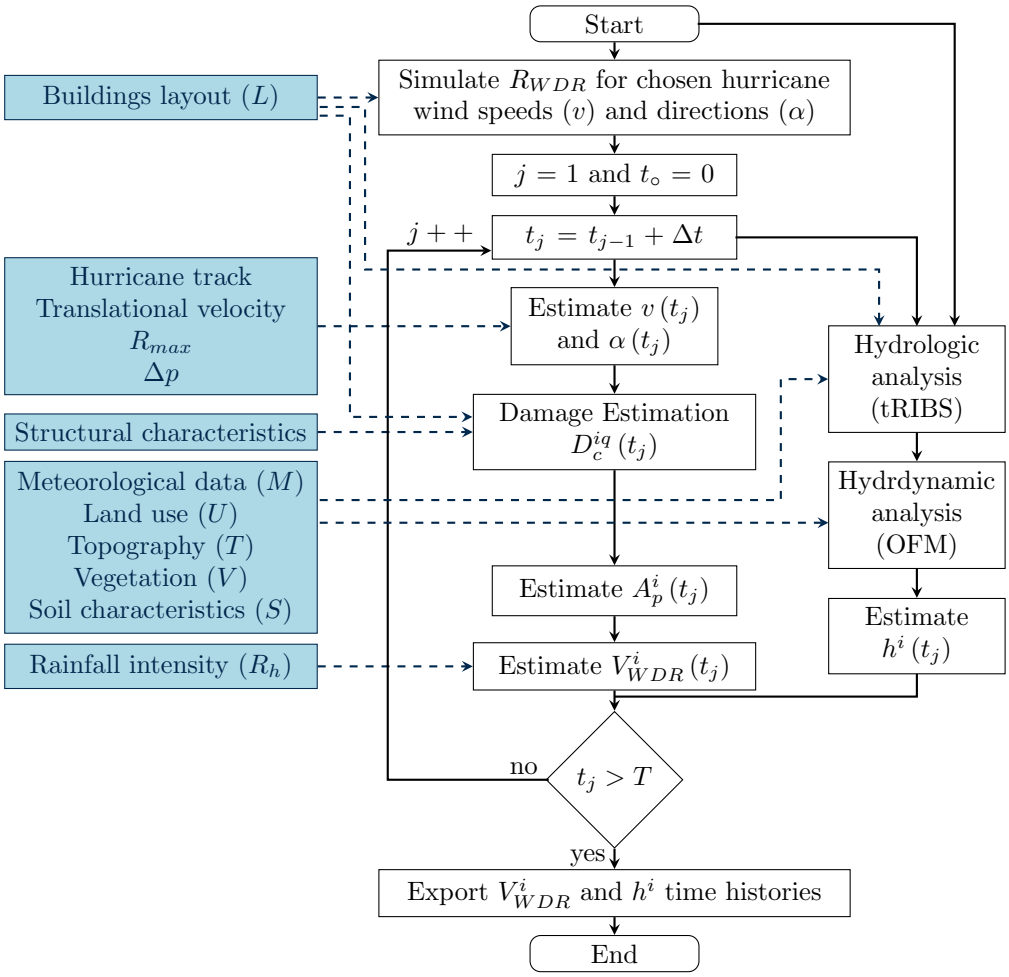

Figure 5.2: Flowchart of the proposed framework.

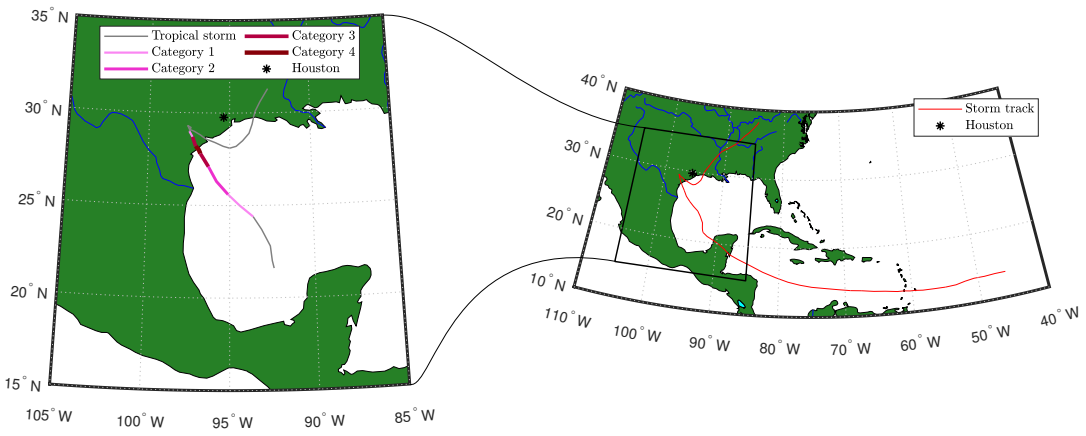

Figure 5.3: Hurricane Harvey storm track: the full track is shown on the right; the modeled portion of the track is shown on the left.

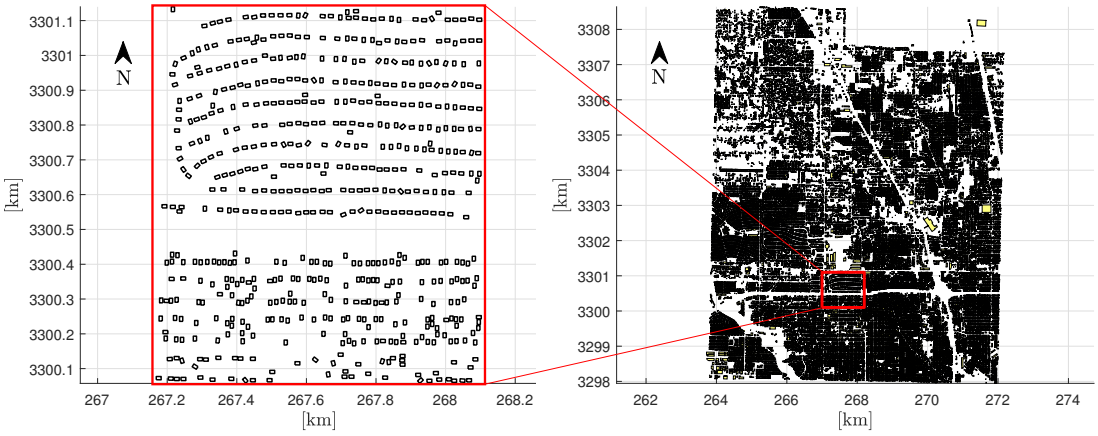

Figure 5.4: Location and orientation of the residential buildings composing the community.

5.3.1.2 Building archetype and construction cases

The residential buildings in the considered community are modeled using the gable-roof archetype shown in fig. 5.5. The resistance of the building envelope components to both wind pressure and windborne debris impact is categorized, using values suggested in the literature (e.g. *Datin et al.*, 2011; *Grayson et al.*, 2013; *Gurley et al.*, 2005; *Vickery et al.*, 2006b), into weak, moderate, and strong, The chosen values for the resistances are summarized in table 5.1.

Table 5.1: Resistance to wind pressure and windborne debris impact of the building components for the weak, moderate, and strong construction cases.

Building component	Wind pressure			Windborne debris impact		
	Weak	Moderate	Strong	Weak	Moderate	Strong
Wall sheathing	3.21 kPa	4.16 kPa	5.51 kPa	0.25 kJ	1.04 kJ	2.13 kJ
Roof sheathing	3.21 kPa	4.16 kPa	5.51 kPa	0.25 kJ	1.04 kJ	2.13 kJ
Wall cover	3.20 kPa	3.20 kPa	3.20 kPa	0.25 kJ	0.25 kJ	0.25 kJ
Roof cover	2.90 kPa	3.35 kPa	5.25 kPa	0.25 kJ	1.04 kJ	2.13 kJ
Glass window	3.33 kPa	3.33 kPa	3.33 kPa	0.10 kJ	0.10 kJ	0.10 kJ
Door	4.79 kPa	4.79 kPa	4.79 kPa	0.10 kJ	0.10 kJ	0.10 kJ
Garage door	2.49 kPa	2.49 kPa	2.49 kPa	0.20 kJ	0.20 kJ	0.20 kJ
Roof-wall connection	11.68 kN	11.68 kN	11.68 kN	N/A	N/A	N/A

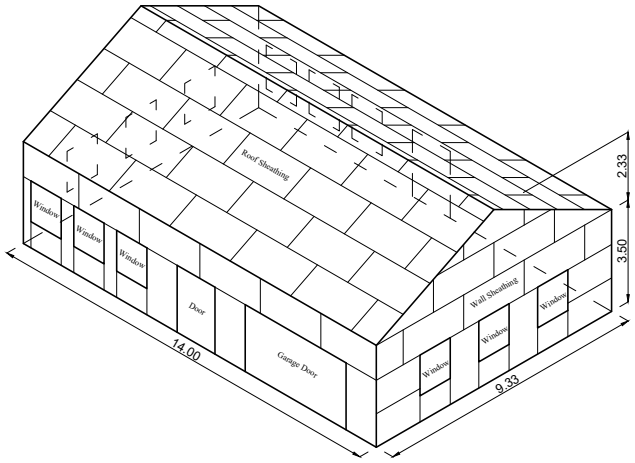

Figure 5.5: Typical residential building archetype adapted from **?**.

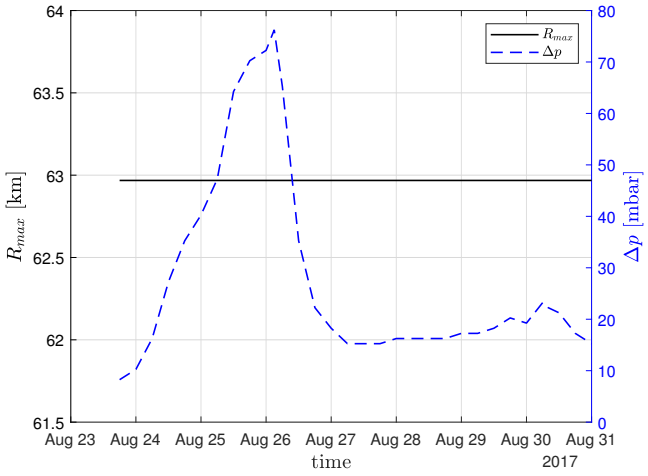

Figure 5.6: Hurricane Harvey input parameters as reported in *National Oceanic and Atmospheric Admenstiration (NOAA)* (2017).

5.3.1.3 Wind field modeling

Input data required to model the wind field associated with Hurricane Harvey is obtained from *National Oceanic and Atmospheric Admenstiration (NOAA)* (2017). The time history of the storm eye location is defined by the storm track, shown in fig. 5.3, and is used to obtain the translational velocity of the storm eye. The size of the hurricane, defined by the radius to maximum wind speeds (R_{max}) and the pressure difference (Δp) at the center of the storm, are shown in fig. 5.6.

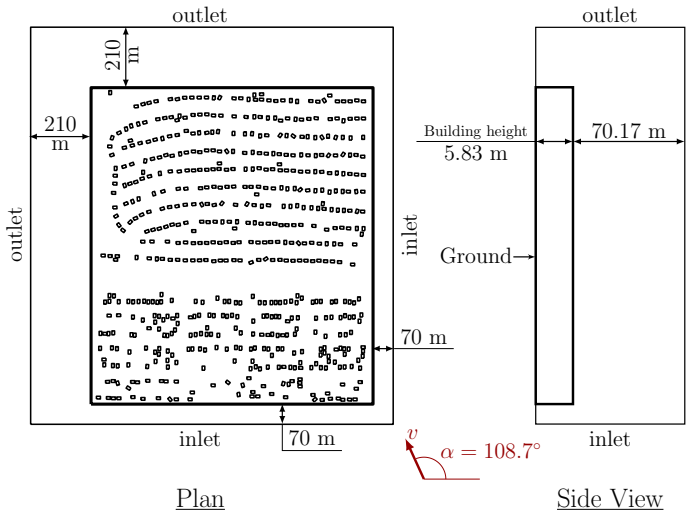

Figure 5.7: Schematic of the computational domain used to estimate the wind-driven rain.

5.3.1.4 Wind-driven rain modeling

A computational domain of size $1362 \times 1215 \times 76$ m^3 is discretized into 30 million cells to model the WDR within the considered residential community, as shown in figs. 5.7 and 5.8. The discretization is carried out using the snappyHexMesh algorithm in OpenFOAM (*Weller et al.*, 1998). The wind flow is simulated for $\alpha = 108.7°$ (as illustrated infigs. 5.7 and 5.8), as this represents the average wind direction during the rainfall event. A logarithmic inlet profile with $z_o = 0.07$ m was calibrated to a reference wind speed of 10 m/s at the building top. Horizontal rainfall intensity (R_h) associated with Hurricane Harvey was obtained from *NCEI* (2017) and modeled using 17 rain phases (i.e., $n_{WDR} = 17$) with representative raindrop diameters ranging from 3-60 mm. After the initial R_{WDR} value is calculated through eq. (5.7), an empirical linear scaling method for flows around shaped-edged bluff bodies is used to scale R_{WDR} to be consistent with the target hurricane wind speed (v) *Kubilay et al.* (2013).

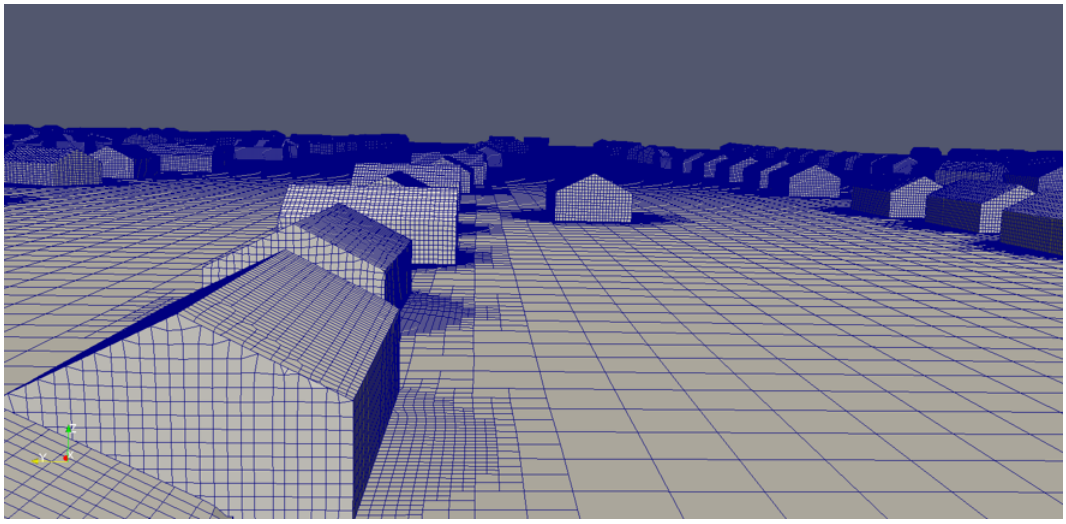

Figure 5.8: Illustration of the computational domain of $1362 \times 1215 \times 76\text{m}^3$ size with 30 millions cells.

5.3.1.5 Flood modeling

The whole Houston area (i.e., not just the considered community) is modeled using tRIBS-OFM to accurately estimate the inundation depth at each building in the considered community. The total watershed area is 46.9 km^2, the number of buildings is 76,609 and the ratio between the area of buildings to the watershed area is 0.3 (i.e., urbanized watershed). For an urbanized watershed that is simulated over a short period of time, the losses from rainfall due to the hydrologic processes, such as soil infiltration and evapotranspiration, can be neglected and all rainfall can be converted directly to surface runoff. The validation of this assumption can be found in *Ivanov et al.* (2021).

The finite volume mesh used to solve the shallow water equations consists of 271,215 triangular cells. The mesh is constructed with river channel network and Digital Elevation Model (DEM) at 3 m resolution obtained from *USGS* (2021). Building footprint data are obtained from *Koordinates* (2021) then merged into the mesh such that the buildings' cells are eliminated and wall boundary conditions are applied at the edges (i.e., the flow velocity normal to the building edge is zero). The Manning

coefficient, which is assumed to be spatially uniform, is calibrated to be 0.015 $m^{1/3}/s$ (*Ivanov et al.*, 2021).

5.3.2 Results and discussion

5.3.2.1 Preamble

The wind speeds generated from the hurricane wind field model are compared against the best track estimate reported in *National Oceanic and Atmospheric Admenstiration (NOAA)* (2017). Figure 5.9 shows that the simulated maximum sustained surface wind speeds are in agreement with the best track estimate. Daily snapshots of Harvey's wind speeds generated from the wind field model are shown in fig. 5.10, and the time history of the hurricane wind speed and direction impacting Houston is shown in fig. 5.11. It should be noticed from fig. 5.11 that Hurricane Harvey impacted Houston as a Tropical Storm with a maximum surface 1-min wind speed of 22 m/s which matches the data from *National Oceanic and Atmospheric Admenstiration (NOAA)* (2017). The wind speeds at Houston are amplified so that Hurricane Harvey impacts Houston as Category two and three hurricanes. This amplification is to study more what-if scenarios to provide more understanding of the role of WDR and inland flooding on the amount of water ingress due to hurricane rainfall.

5.3.2.2 Water ingress

The amount of water ingress is measured using the volume of water entering the building (V_{WDR}) and the inundation depth (h) for the WDR and inland flooding, respectively. To make the comparison between both the WDR and inland flooding possible, a nominal inundation depth for the WDR is defined by dividing the V_{WDR} by the plan area (14 m $\times$ 9.33 m) of the building.

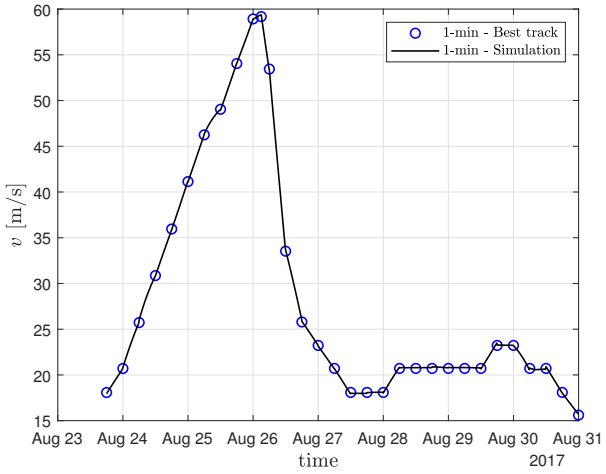

Figure 5.9: Simulated maximum sustained surface wind speed for Hurricane Harvey and the best track estimate as reported in *National Oceanic and Atmospheric Admenstiration (NOAA)* (2017).

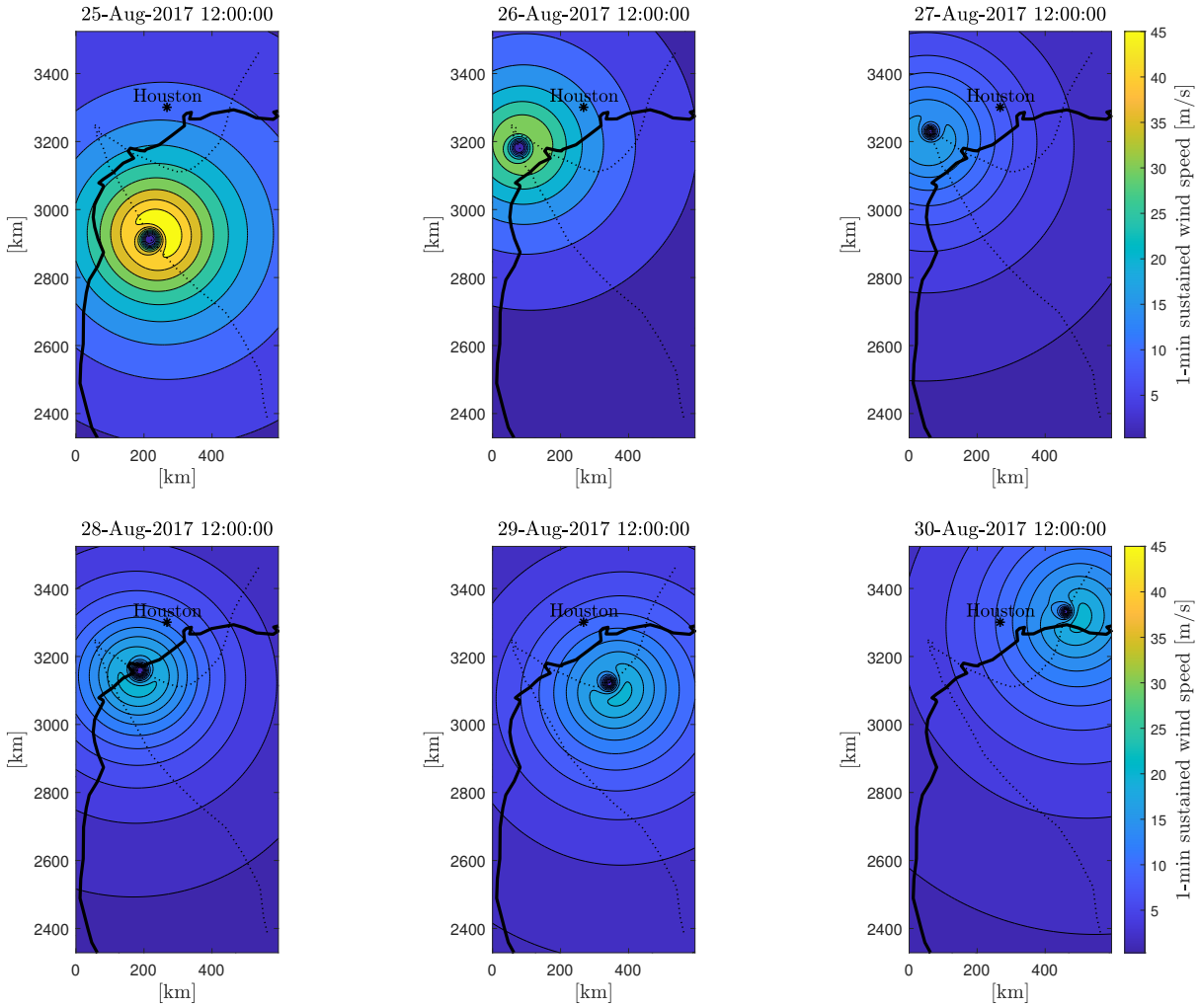

Figure 5.10: Daily snapshots for the simulated wind speeds of hurricane Harvey.

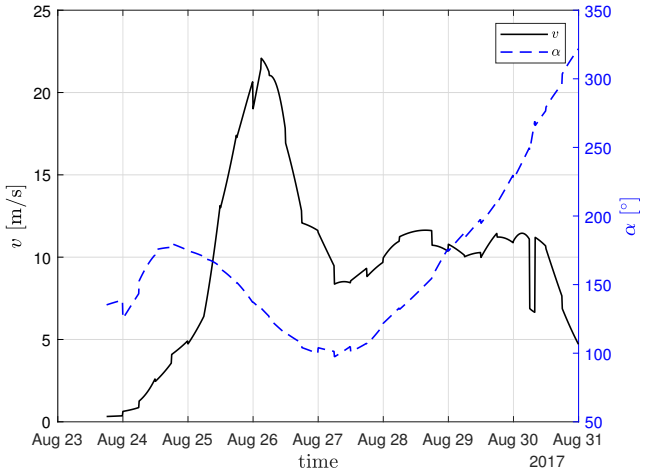

Figure 5.11: Simulated surface 1-min wind speed and direction for Houston.

Figure 5.12 compares the resulting discharge from the tRIBS-OFM model at the location of the USGS 08074540 gauge with the measured discharge during Harvey obtained from *USGS* (2017). The agreement between tRIBS-OFM and the measured data validates the approach.

The complexity of the spatial distribution of the WDR intensity (R_{WDR}) over the buildings' envelope is highly dependent on the surrounding environment. This dependency is considered explicitly using the presented framework by modeling the entire community, rather than a single building, as illustrated by the spatial distribution of η_3 shown in fig. 5.13.

Figures 5.14 and 5.15 shows that no damage was caused by the tropical storm winds in any of the three construction cases. This leads to the ratio A_p/A_t equaling zero for all buildings, where $A_t = 331$ m^2 and is the total area of the building envelopes. In this case, the water ingress due to WDR is zero as there is no water seepage into the building envelope and all the water ingress is due to inundation from the inland flooding shown in figs. 5.12 and 5.16.

For the case of a category two hurricane, the amount of water ingress due to

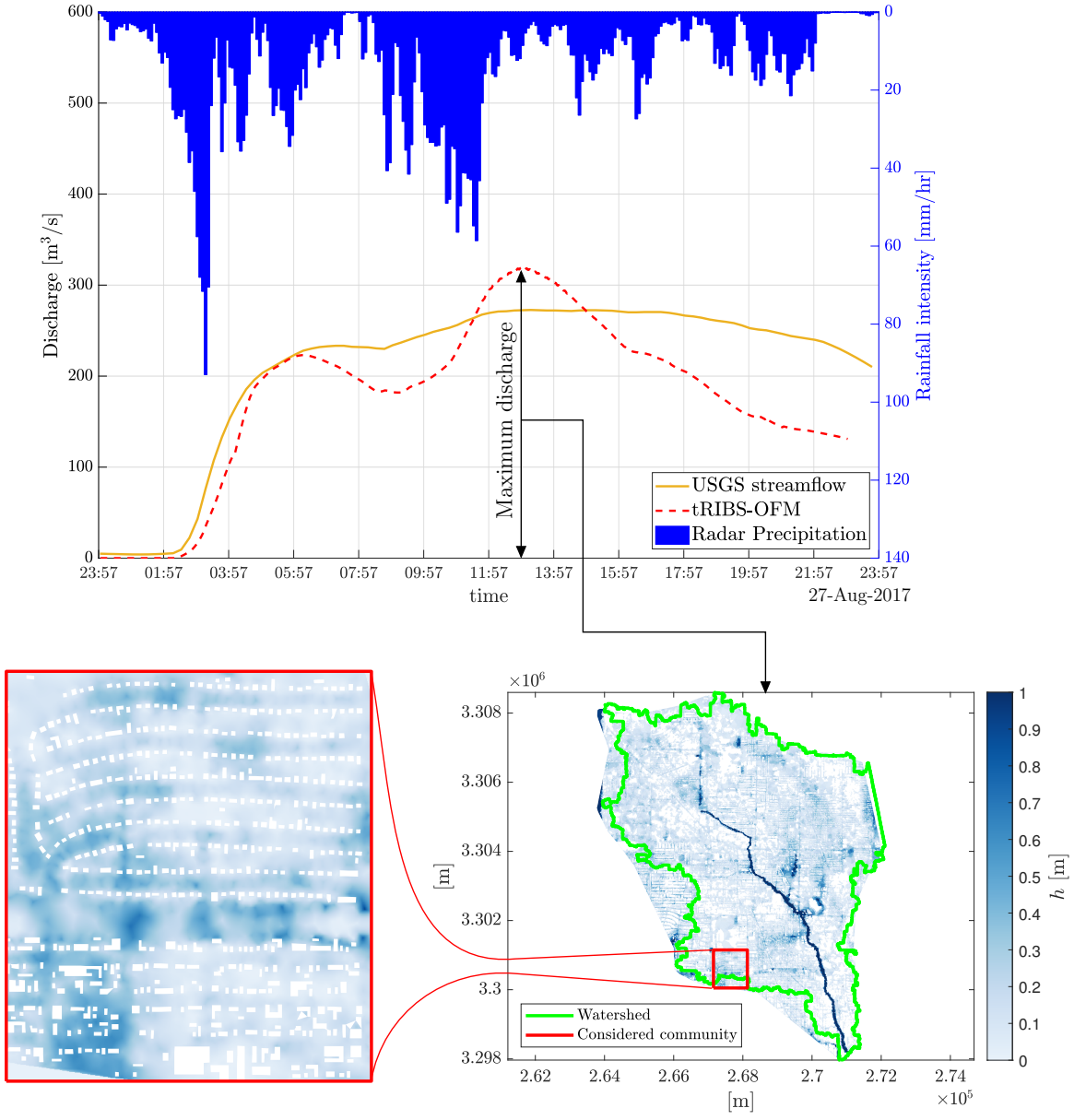

Figure 5.12: Validation of the tRIBS-OFM model is shown in the top panel by comparing the resulting discharge with data from the USGS 08074540 gauge. A snapshot of the inland flooding inundation depth at the time of maximum discharge is shown in the bottom panel.

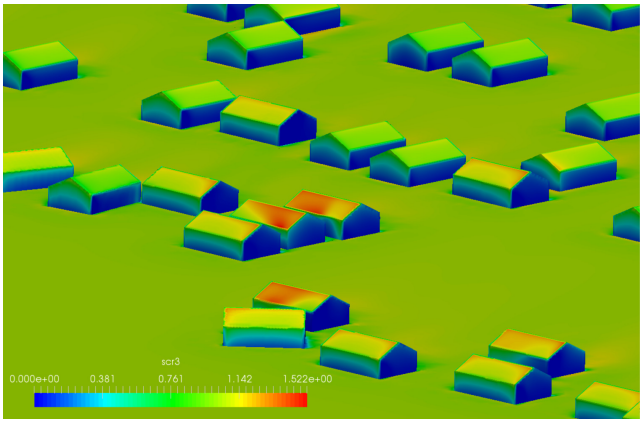

Figure 5.13: Spatial distribution of the specific catch ratio, η_3, of the 3$^{\text{rd}}$ rain phase with d_3 in the range of [7.5,10.5] mm.

WDR is: of no significance in the strong construction case; almost equal to half the water ingress due to flooding in the moderate case; around 1.25 times the water ingress due to flooding in the weak case. In the case of a category four hurricane, the water ingress due to WDR dominates the amount of water ingress for the moderate and weak construction cases, as shown in fig. 5.16. The results of the water ingress due to both wind-driven rain and flooding emphasizes the importance of considering both these mechanisms when estimating the losses for residential communities due to hurricane rainfall.

5.4 Conclusions

This paper presents a framework for the estimate of water ingress due to hurricane rainfall in residential communities. Water ingress due to hurricane rainfall occurs as a result of WDR and inland flooding. To estimate the amount of water ingress due to WDR, the framework combines the WDR intensity over the buildings' envelope with the perforated area caused by the hurricane wind damage to the building envelope. WDR intensity is estimated using a RANS-EMM framework while the building envelope damage is estimated due to dynamic wind pressure and

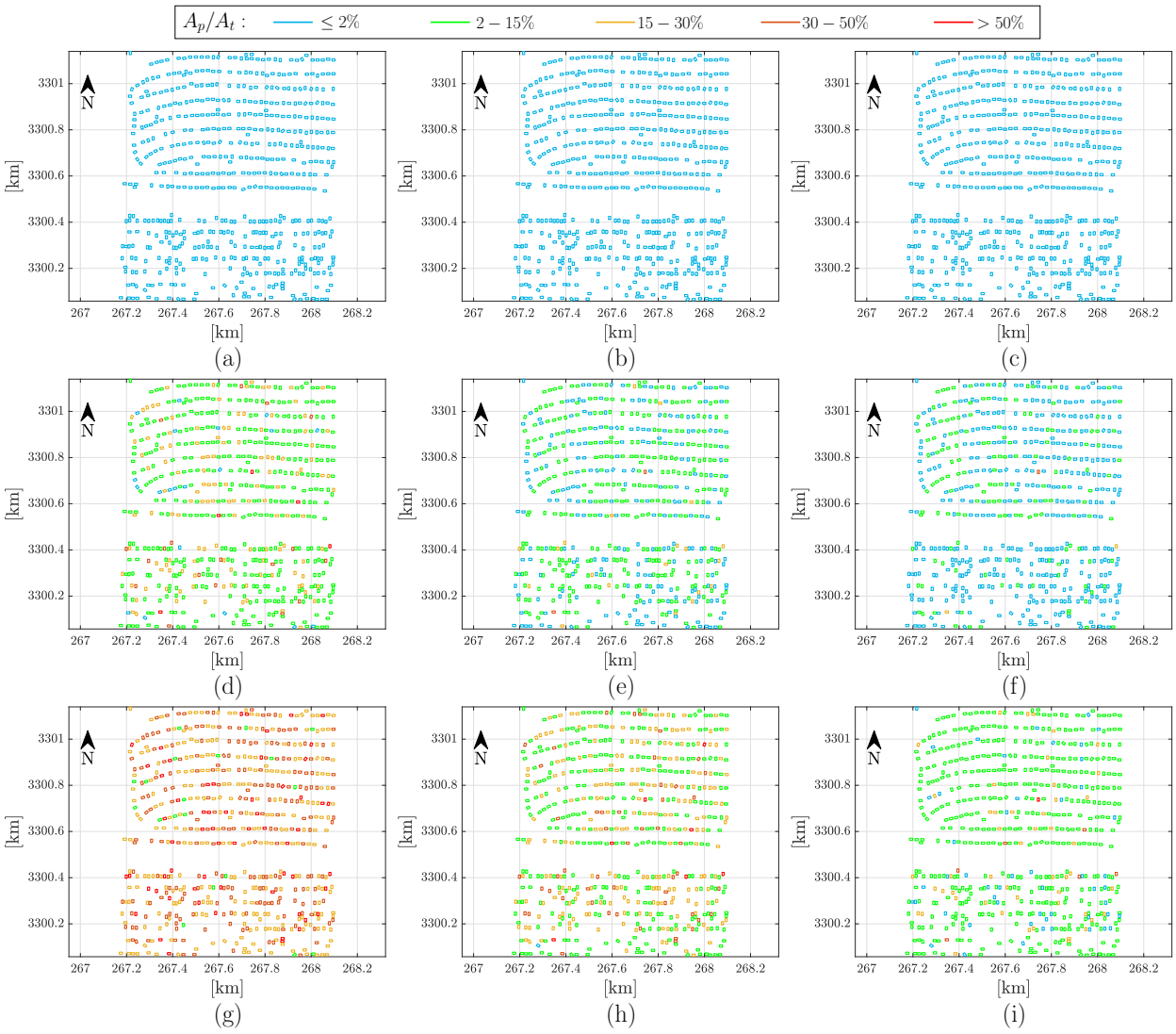

Figure 5.14: Perforated area of the buildings' envelope: (a) weak construction case subject to Harvey; (b) moderate construction case subject to Harvey; (c) strong construction case subject to Harvey; (d) weak construction case subject to Category 2 amplified Harvey; (e) moderate construction case subject to Category 2 amplified Harvey; (f) strong construction case subject to Category 2 amplified Harvey; (g) weak construction case subject to Category 3 amplified Harvey; (h) moderate construction case subject to Category 3 amplified Harvey; and (i) strong construction case subject to Category 3 amplified Harvey.

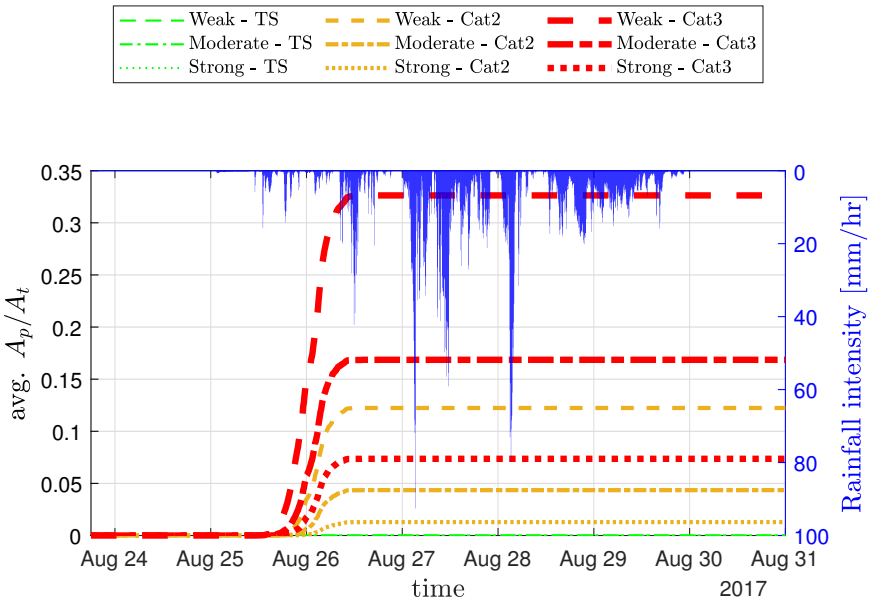

Figure 5.15: Time history of the rainfall intensity and the evolution of the average area of perforation of the envelope of all buildings in the considered neighborhood.

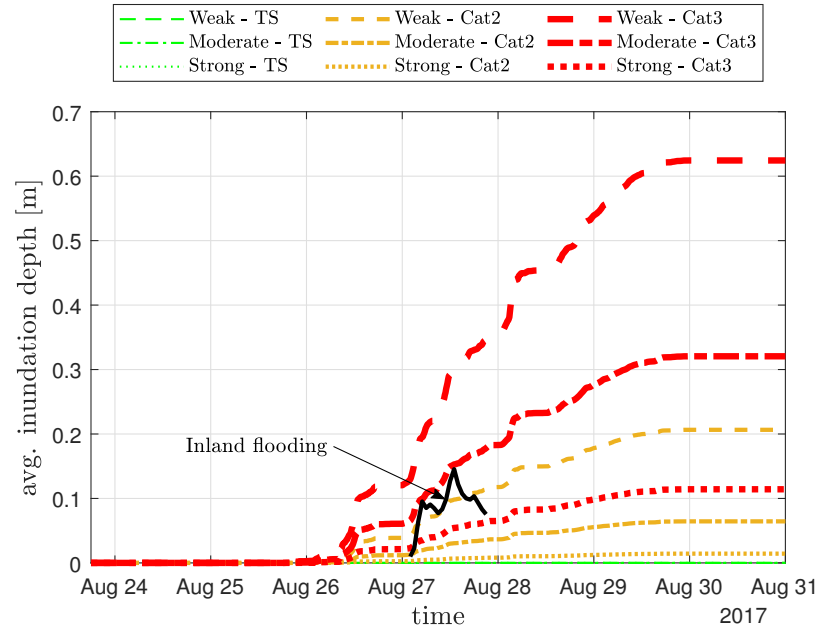

Figure 5.16: Average inundation due to wind-driven rains and flooding for all buildings in the considered neighborhood.

windborne debris impact using a hurricane damage estimation model. The water ingress due to inland flooding is estimated using a coupled hydrologic-hydrodynamic model (tRIBS-OFM) which estimates the inundation depth at each building in the considered community. The framework is applied to a case study consisting of a residential community in Houston, TX, that is subject to Hurricane Harvey. Three construction cases are considered (weak, moderate, and strong). The results of the case study show that the amount of water ingress due to hurricane rainfall can be dominated by either WDR or inland flooding depending on the construction case and the hurricane wind speeds. These results emphasize the importance of considering both WDR and inland flooding while estimating losses due to hurricane rainfall.

CHAPTER VI

A Six-Degree-of-Freedom Windborne Debris Trajectory Model for Tornadoes[1]

Abstract

Windborne debris is a major cause of damage to the built environment during tornadoes. A fundamental step for quantifying this damage is to provide models that are able to describe the trajectory of the flying debris and thereby determine their impact location and associated momentum/energy. This goal can be achieved through the adoption of an appropriate three-dimensional (3D) six-degrees-of-freedom (6DOF) debris trajectory model. However, existing 3D 6DOF debris trajectory models are focused on describing the debris flight in straight line winds and therefore cannot be applied to tornado winds that are characterized by relatively small but rapidly rotating vortices. This paper presents a 3D 6DOF debris trajectory model for describing the flight of windborne debris in tornadoes. The proposed solution strategy is based on a predictor-corrector time-marching scheme which solves the equations of motion for each time step while updating the wind field from an appropriate tornado wind field model. A convergence analysis is carried out to determine the suitable time step that balances the accuracy of the numerical scheme with the computational run-time. The proposed model is then used to show the significant difference in modeling the

[1] Abdelhady, A.U., Spence, S.M.J. and McCormick, J. (2021). "Three-dimensional six-degree-of-freedom windborne debris trajectory model for tornadoes," *Journal of Wind Engineering & Industrial Aerodynamics*, Submitted.

debris trajectories in tornado wind fields as compared to straight line winds.

6.1 Introduction

Damage surveys and field studies after past tornadoes have shown that a significant amount of damage to buildings is caused by debris impact (*Marshall*, 2002; *McDonald*, 1990; *Tanner*, 2002). Moreover, when flying debris penetrates the building envelope, increases in the internal pressure can occur leading to additional damage to the building envelope (i.e. release of additional windborne debris) and a cascading or progressive failure mechanism. To quantify the damage caused by windborne debris in tornadoes, four main quantities should be identified: (1) the nature of the debris object (i.e. mass and shape); (2) the number of debris objects flying in the wind field; (3) the landing location; and (4) the impact energy or momentum. Field studies from past tornadoes have shown that, while large tornado-generated missiles such as pipes, utility poles and cars attract media attention, their occurrence is very rare (*McDonald*, 1990). Most common missiles are medium size pieces of timber planks from damaged residences and other timber structures (*Marshall*, 2002; *McDonald*, 1990; *Tanner*, 2002). The shape of these missiles can be classified geometrically into plate-like, rod-like and compact-like objects (*Wills et al.*, 2002). Hence, the number of debris objects is a function of the amount of damage occurring to buildings and can be initially determined using a pressure damage model. Landing location and impact momentum or energy require the identification of an appropriate debris flight trajectory model.

Debris flight trajectory models can be divided into two-dimensional (2D) and three-dimensional (3D) models. The 2D models are primarily based on the pioneering research of *Tachikawa* (1983) who studied the trajectory of plate-like debris

objects. This work was extended in (*Tachikawa*, 1988) for estimating the probability distribution of debris trajectories through randomizing the lift coefficient. In *Holmes et al.* (2006), numerical calculations using 2D models based on the work of Tachikawa for plate like debris objects were validated using the wind tunnel and full-scale test results presented in (*Lin et al.*, 2006; *Tachikawa*, 1983, 1988). In *Lin and Vanmarcke* (2010a), a debris risk analysis methodology was introduced, based on the 2D model presented in (*Tachikawa*, 1983), and subsequently adopted in a vulnerability model (*Lin et al.*, 2010a).

Although 2D models are easier to implement as compared to 3D models, *Baker* (2007) highlighted the need of having 3D models to describe the flight of plate-and rod-like debris objects. Sebsequently, *Richards et al.* (2008a) derived the deterministic solution to the 3D motion of plate-and rod-like debris objects using a 6 degree of freedom (DOF) trajectory model. Force and moment coefficients were calculated based on wind tunnel tests. To account for uncertainties in the debris flight, *Grayson et al.* (2012b) extended this deterministic 3D 6-DOF trajectory model to a probabilistic setting capable of reproducing debris landing patterns similar to those obtained from wind tunnel tests. The aforementioned debris trajectory models were all developed under the assumption of straight line wind fields. This assumption is reasonable for modeling the flight of debris in hurricanes since they are generally characterized by a relatively slow rate of change in wind direction. This behavior is not the case for tornadoes that are transitory in nature and will generally produce rapid changes in wind direction. Due to the lack of wind tunnel data on the aerodynamic forces and moments acting on general debris objects that are required for developing 3D 6-DOF trajectory models, *Simiu and Cordes* (1976) estimated the debris flight trajectory for only compact objects flying in a Rankine-vortex tornado-like wind field.

To account for the effects of turbulence on the flight of compact debris, *Maruyama* (2011) generated the unsteady wind field of tornadoes through Large Eddy Simulation. Recently, *Baker and Sterling* (2017) derived a simple and realistic tornado wind field model that can be used in structural engineering applications, *Baker and Sterling* (2018). This model was subsequently used for computing the trajectory of compact debris in tordardoes. Both *Maruyama* (2011) and *Baker and Sterling* (2017) highlighted the need for the development of trajectory models that are able to account for the effects of the configuration and aerodynamic characteristics of the debris object, and therefore adequately model the flight of, for example, rod- and plate-like debris objects.

This paper presents a 3D 6DOF debris trajectory model for describing the debris trajectories of non-compact objects in tornadoes. The wind field model is based on that presented in *Baker and Sterling* (2017), while the aerodynamic force and moment coefficients are compiled from the wind tunnel data presented in *Richards et al.* (2008a). The proposed solution strategy is based on a predictor-corrector time-marching scheme. The presented model is used to trace the trajectory of a typical plywood roof sheathing panel where the size of the time step is determined using convergence analysis that is carried out for a wide range of possible initial conditions for the debris object. Results of the panel trajectory in the tornado wind field show significant difference from trajectories generated using straight line winds.

6.2 Debris flight

6.2.1 Equations of motion: flying debris

A flying debris object can be assumed as a rigid body in space, therefore six degrees of freedom are required to describe its motion. This assumption has been adopted by several studies in the literature (e.g. *Grayson et al.*, 2012b; *Redmann*

et al., 1978; *Richards et al.*, 2008a) and is the basis of the presented trajectory model. Based on the geometric classification provided by *Wills et al.* (2002), the rectangular hexahedron in fig. 6.1 is used to model the geometry of the debris objects of interest.

As illustrated in fig. 6.1, the following reference systems are considered in describing the motion of the debris object: (1) a global reference system, $OX_1X_2X_3$; and (2) a local reference system, $D\xi_1\xi_2\xi_3$, with origin fixed at the center of mass of the object (D). The axes $D\xi_1\xi_2\xi_3$ correspond to the debris object's principal axes of inertia that translate and rotate during the flight of the object. For a debris object with dimensions l_{ξ_1}, l_{ξ_2} and l_{ξ_3}, as shown in fig. 6.1, the axes of the local reference system are chosen such that $l_{\xi_1} \leq l_{\xi_2} \leq l_{\xi_3}$. The orientation of the local principal axes with respect to the global axes is defined by the *roll* (θ_1), *yaw* (θ_2) and *pitch* (θ_3) convention of Euler angles, as illustrated in fig. 6.2.

The position of the debris object is defined by the position of D with respect to $OX_1X_2X_3$, and therefore by the vector $\mathbf{X}_D = [X_{D1}, X_{D2}, X_{D3}]^T$ which is shown in fig. 6.1. The orientation is given by $\boldsymbol{\theta} = [\theta_1, \theta_2, \theta_3]^T$, as shown in fig. 6.2. As a consequence, the linear velocity of D is $\mathbf{V}_D = \dot{\mathbf{X}}_D = \left[\dot{X}_{D1}, \dot{X}_{D2}, \dot{X}_{D3}\right]^T$, while the angular velocity is given by:

$$\boldsymbol{\omega} = \left\{ \begin{array}{c} \omega_1 \\ \omega_2 \\ \omega_3 \end{array} \right\} = \left\{ \begin{array}{c} \dot{\theta}_1 + \dot{\theta}_2 \sin(\theta_3) \\ \dot{\theta}_3 \sin(\theta_1) + \dot{\theta}_2 \cos(\theta_1)\cos(\theta_3) \\ \dot{\theta}_3 \cos(\theta_1) - \dot{\theta}_2 \sin(\theta_1)\cos(\theta_3) \end{array} \right\} \tag{6.1}$$

The object is subjected to aerodynamic forces and gravity. Under these loads, the equations of motion can be written as:

$$m\dot{\mathbf{V}}_D = \mathbf{F}_{aer} - mg\hat{\mathbf{i}}_2 \tag{6.2}$$

$$\dot{\mathbf{L}}_P = \mathbf{M}_{aer} + \mathbf{M}_D - \boldsymbol{\omega} \times \mathbf{L}_P \tag{6.3}$$

where $\mathbf{F}_{aer}$ is the aerodynamic force; m is the mass of the debris object; g is the magnitude of the gravitational acceleration; $\hat{\boldsymbol{\imath}}_2$ is the unit vector of axis X_2; $\mathbf{L}_P = [I_{\xi_1\xi_1} \cdot \omega_1, I_{\xi_2\xi_2} \cdot \omega_2, I_{\xi_3\xi_3} \cdot \omega_3]^T$ is the angular momentum vector of the debris object; $\mathbf{M}_{aer}$ is the aerodynamic moment; and $\mathbf{M}_D$ is a damping moment necessary to prevent unbounded rotation of the debris object.

The aerodynamic forces and moments depend on the relative velocity of the debris ($\mathbf{V}_{DW}$) with respect to the velocity of the surrounding wind field ($\mathbf{V}_W$), and can be written as:

$$\mathbf{V}_{DW} = \mathbf{V}_D - \mathbf{V}_W \tag{6.4}$$

In particular, the aerodynamic forces are expressed as a function of force coefficient C_F which can be extracted from the wind tunnel database compiled in *Richards et al.* (2008a). Analogously, the aerodynamic and damping moments depend on the moment and damping coefficients C_M and C_D, respectively. In particular, from the results of wind tunnel tests, it has been shown that the force and moment coefficients are functions of the angle of attack (ε) and angle of tilt (γ) of the object at a given instant. These angles give the orientation of the relative velocity vector ($\mathbf{V}_{DW}$) with respect to the local principal axes and are defined as:

$$\varepsilon = \sin^{-1}\left(\frac{V_{DW_{\xi_1}}}{V_{DW}}\right) \tag{6.5}$$

$$\gamma = \tan^{-1}\left(\frac{V_{DW_{\xi_2}}}{V_{DW_{\xi_3}}}\right) \tag{6.6}$$

where $V_{DW} = |\mathbf{V}_{DW}|$; and $V_{DW_{\xi_1}}$, $V_{DW_{\xi_2}}$ and $V_{DW_{\xi_3}}$ are the components of the vector $\mathbf{V}_{DW}$ in the local reference system, $D\xi_1\xi_2\xi_3$.

For straight line winds, solutions to Equations (6.2) and (6.3) can be found in the literature, (*Grayson et al.*, 2012b; *Richards et al.*, 2008a). This assumption is considered reasonable for modeling the debris flight in hurricanes as the change

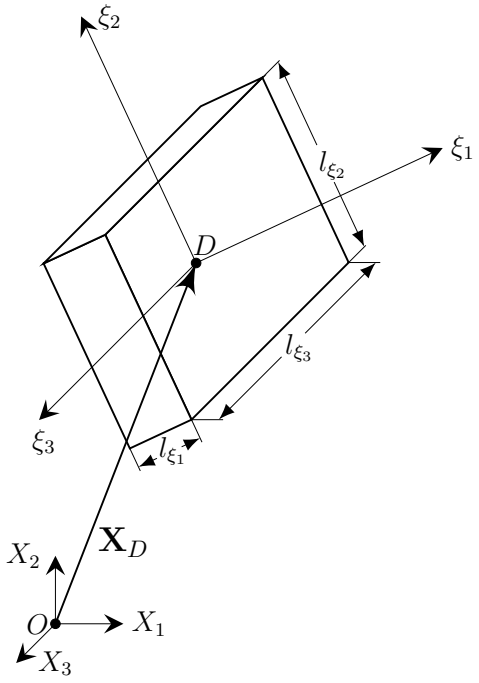

Figure 6.1: Reference systems used for describing the debris trajectory.

of wind speed and direction over the debris flight time and distance is negligible. However, in the case of tornadoes, the high rate of change of wind speed and direction requires solving eqs. (6.2) and (6.3) for non-straight line winds. Consequently, a tornado wind field model is required to obtain $\mathbf{V}_W$.

6.2.2 Tornado wind field model

Tornadoes represent complex meteorological phenomenon that generate wind fields of a sophisticated nature. To model the translating vortex structure of the tornado wind field, the wind velocity generated by the tornado can be simplified into four main components: (1) translational velocity ($\mathbf{V}_{tr}$); (2) radial velocity ($\mathbf{V}_r$); (3) circumferential velocity ($\mathbf{V}_c$); and (4) vertical velocity ($\mathbf{V}_v$). At any given time instant (t), ignoring the dynamic and nonlinear translational effects, the tornado wind field velocity at the location of the debris center of mass (D) can be described mathematically as the vector sum of the previously defined velocities (also as illustrated in

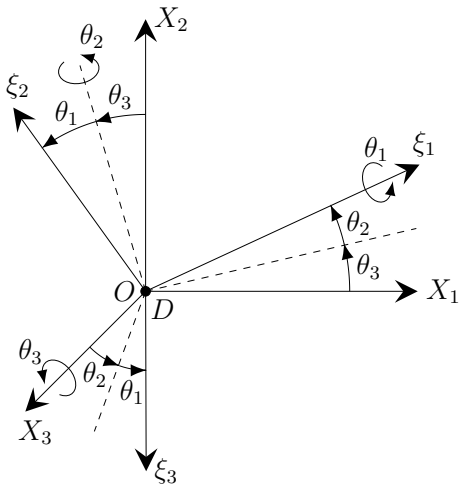

Figure 6.2: Angles defining the orientation of the debris.

fig. 6.3):

$$\mathbf{V}_W = \mathbf{V}_{tr} + \mathbf{V}_r + \mathbf{V}_c + \mathbf{V}_v \tag{6.7}$$

The translational velocity ($\mathbf{V}_{tr}$) of eq. (6.7) can be estimated directly from available tornado wind field data (e.g. *Baker and Sterling*, 2019). The other three velocity components ($\mathbf{V}_r$, $\mathbf{V}_c$ and $\mathbf{V}_v$) can be estimated from available tornado wind field models (e.g. *Gillmeier et al.*, 2018). The single-celled tornado model developed by *Baker and Sterling* (2017) is used in this study.

Given that the location of the center of the tornado is described by $\mathbf{X}_T = [X_{T1}, X_{T2}, X_{T3}]^T$, the radial, circumferential and vertical components of the tornado wind field velocity can be written as follows:

$$\mathbf{V}_r = \frac{-4V_{rm}RHX_{DT3}}{(R^2 + X_{DT}^2)(H^2 + X_{DT3}^2)} \cdot \begin{Bmatrix} X_{DT1} \\ X_{DT2} \\ 0 \end{Bmatrix} \tag{6.8}$$

$$\mathbf{V}_c = \frac{2.88V_{cm}R\left[\ln\left(H^2 + X_{DT3}^2\right) - \ln\left(H^2\right)\right]}{(R^2 + X_{DT}^2)} \cdot \begin{Bmatrix} -X_{DT2} \\ X_{DT1} \\ 0 \end{Bmatrix} \tag{6.9}$$

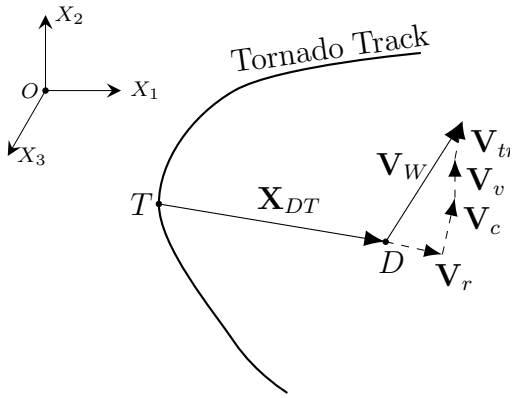

Figure 6.3: Schematic of the velocity components of the tornado wind field.

$$\mathbf{V}_v = \frac{4V_{rm}R^3H\left[\ln\left(H^2+X_{DT3}^2\right)-\ln\left(H^2\right)\right]}{\left(R^2+X_{DT}^2\right)^2}\cdot\left\{\begin{array}{c}0\\0\\1\end{array}\right\} \tag{6.10}$$

where $\mathbf{X}_{DT} = \mathbf{X}_D - \mathbf{X}_T = [X_{DT1}, X_{DT2}, X_{DT3}]^T$ is the relative position of D with respect to T; $X_{DT} = |\mathbf{X}_{DT}|$; V_{rm} and V_{cm} are the maximum radial and circumferential wind speeds, respectively; R is the radius of maximum radial and circumferential wind speeds; and H is the height of maximum radial wind speeds. To enable modeling over the life-time of the tornado, i.e. from genesis until decay, the parameters defining the tornado's track ($\mathbf{X}_T$), size (R and H), and intensity (V_{rm}, V_{cm} and $\mathbf{V}_{tr}$) are treated as time dependent quantities.

6.3 Proposed solution strategy

6.3.1 Overview

The solution strategy developed in this study is based on a predictor-corrector time-marching scheme which continues to update the parameters defining the wind-borne debris trajectory for each time step until the debris object impacts the ground (i.e. $X_{D2_{i+1}} \leq 0$). The required input data for the time-marching scheme are (1) the debris initial conditions: debris initial location, orientation, and linear and angular

velocity; (2) tornado wind field parameters: time histories of parameters defining tornado track, size, and intensity; and (3) wind tunnel data: aerodynamic forces and moment coefficients as well as moment damping coefficients. Figure 6.4 shows a flowchart of the solution strategy proposed to solve eqs. (6.2) and (6.3) using the tornado wind field model of eq. (6.7).

6.3.2 Predictor time-marching step

The predictor time-marching step starts from the current value ($\bullet_i$), then calculates an initial guess ($\tilde{\bullet}_{i+1}$) for the next time step via the Euler method. In particular, the debris location, orientation, linear velocity and angular velocity are updated as follows:

$$\tilde{\mathbf{X}}_{D_{i+1}} = \mathbf{X}_{D_i} + \Delta t \mathbf{V}_{D_i} \tag{6.11}$$

$$\tilde{\boldsymbol{\theta}}_{i+1} = \boldsymbol{\theta}_i + \Delta t \dot{\boldsymbol{\theta}}_i \tag{6.12}$$

$$\tilde{\mathbf{V}}_{D_{i+1}} = \mathbf{V}_{D_i} + \Delta t \dot{\mathbf{V}}_{D_i} \tag{6.13}$$

$$\tilde{\boldsymbol{\omega}}_{i+1} = \boldsymbol{\omega}_i + \Delta t \dot{\boldsymbol{\omega}}_i \tag{6.14}$$

where Δt is the time step and $\tilde{\dot{\boldsymbol{\theta}}}_{i+1}$ can be estimated using eqs. (6.1) and (6.14). The tornado wind field will then be updated according to the new location ($\tilde{\mathbf{X}}_{D_{i+1}}$) of the debris as follows:

$$\tilde{\mathbf{X}}_{DT_{i+1}} = \tilde{\mathbf{X}}_{D_{i+1}} - \mathbf{X}_{T_{i+1}} \tag{6.15}$$

$$\tilde{\mathbf{V}}_{W_{i+1}} = \tilde{\mathbf{V}}_{tr_{i+1}} + \tilde{\mathbf{V}}_{r_{i+1}} + \tilde{\mathbf{V}}_{c_{i+1}} + \tilde{\mathbf{V}}_{v_{i+1}} \tag{6.16}$$

where $\tilde{\mathbf{V}}_{r_{i+1}}$, $\tilde{\mathbf{V}}_{c_{i+1}}$, and $\tilde{\mathbf{V}}_{v_{i+1}}$ are estimated from eqs. (6.8) to (6.10) and (6.15).

The initial guess of the debris relative velocity is estimated as $\tilde{\mathbf{V}}_{DW_{i+1}} = \tilde{\mathbf{V}}_{D_{i+1}} - \tilde{\mathbf{V}}_{W_{i+1}}$, from which $\tilde{\varepsilon}_{i+1}$ and $\tilde{\gamma}_{i+1}$ are calculated through eqs. (6.5) and (6.6). Subsequently, $\tilde{\varepsilon}_{i+1}$ and $\tilde{\gamma}_{i+1}$, together with the wind tunnel data provided in *Richards*

et al. (2008a), are used to obtain $\tilde{C}_{F_{i+1}}$, $\tilde{C}_{M_{i+1}}$ and $\tilde{C}_{D_{i+1}}$. This approach enables the evaluation of the initial guess of the aerodynamic force ($\tilde{\mathbf{F}}_{aer_{i+1}}$), the aerodynamic moment ($\tilde{\mathbf{M}}_{aer_{i+1}}$), and the damping moment ($\tilde{\mathbf{M}}_{D_{i+1}}$). Finally, $\tilde{\dot{\boldsymbol{\theta}}}_{i+1}$, $\tilde{\dot{\mathbf{V}}}_{D_{i+1}}$ and $\tilde{\dot{\boldsymbol{\omega}}}_{i+1}$ are obtained from eqs. (6.1) to (6.3).

6.3.3 Corrector time-marching step

The corrector time-marching step improves the initial guess ($\tilde{\bullet}_{i+1}$) using the trapezoidal rule to obtain the value at the next time step ($\bullet_{i+1}$). It follows the same sequence in updating variables as in the predictor step which is summarized as follows:

$$\mathbf{X}_{D_{i+1}} = \mathbf{X}_{D_i} + \frac{\Delta t}{2}\left(\mathbf{V}_{D_i} + \tilde{\mathbf{V}}_{D_{i+1}}\right) \tag{6.17}$$

$$\boldsymbol{\theta}_{i+1} = \boldsymbol{\theta}_i + \frac{\Delta t}{2}\left(\dot{\boldsymbol{\theta}}_i + \tilde{\dot{\boldsymbol{\theta}}}_{i+1}\right) \tag{6.18}$$

$$\mathbf{V}_{D_{i+1}} = \mathbf{V}_{D_i} + \frac{\Delta t}{2}\left(\dot{\mathbf{V}}_{D_i} + \tilde{\dot{\mathbf{V}}}_{D_{i+1}}\right) \tag{6.19}$$

$$\boldsymbol{\omega}_{i+1} = \boldsymbol{\omega}_i + \frac{\Delta t}{2}\left(\dot{\boldsymbol{\omega}}_i + \tilde{\dot{\boldsymbol{\omega}}}_{i+1}\right) \tag{6.20}$$

The rest of the variables are updated in the same fashion as in the predictor step using the improved guess ($\bullet_{i+1}$) rather than the initial guess ($\tilde{\bullet}_{i+1}$).

6.4 Application for roof sheathing

6.4.1 Description

In this section, the proposed solution strategy is applied to estimate the trajectory of a typical plywood roof sheathing panel subject to tornado winds. The solutions are subsequently compared against those obtained from straight line winds. The dimensions of the roof sheathing panel are 2.44 m $\times$ 1.22 m $\times$ 1.19 cm, with a density of 517 kg/m^3. Figure 6.5 shows the location of the tornado track with respect to the roof sheathing panel. The initial elevation of the panel is chosen to be 5 m, which is within the range of roof heights for residential timber

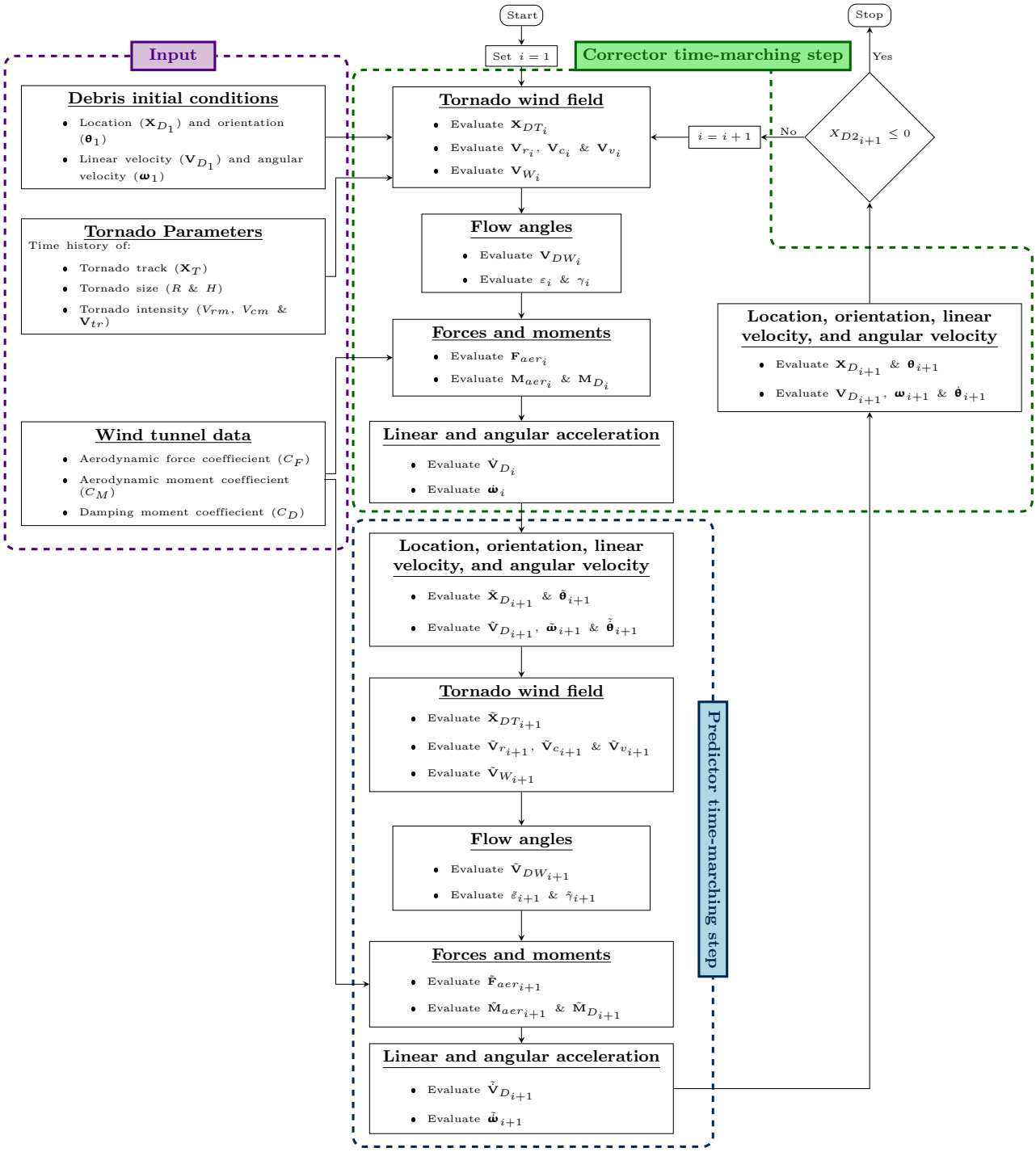

Figure 6.4: Flowchart of the proposed solution strategy.

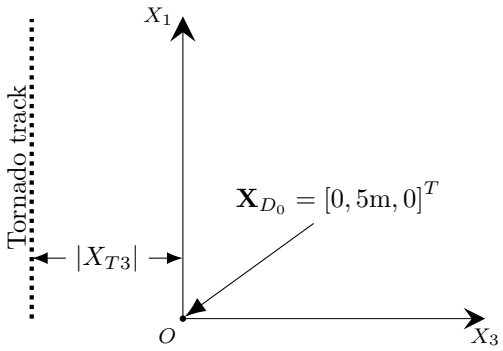

Figure 6.5: Layout of the application problem.

Table 6.1: Characteristics of the simulated tornadoes .

Tornado size	R (m)	V_{cm} (m/s)	V_{rm} (m/s)	$\lvert\boldsymbol{V}_{tr}\rvert$ (m/s)
Small	50	40	7.27	5
Medium	200	50	5.88	10
Large	500	60	5	12

houses. The initial position vector of the debris object is therefore defined as $\mathbf{X}_{D_0} = [0, 5\text{m}, 0]^T$. The initial orientation of the panel is $\boldsymbol{\theta}_0 = [0, \theta_{2_0}, 65°]^T$, where $\theta_{2_0} = \{-60°, -45°, -30°, -15°, 0°, 15°, 30°, 45°, 60°\}$ and is chosen to cover possible orientations of the building with respect to the tornado track.

Tornadoes can vary significantly in their size and intensity *Edwards et al.* (2013); *Kosiba and Wurman* (2010); *Tanamachi et al.* (2007). In *Baker and Sterling* (2019), full-scale tornado data were collected and analyzed. As a result, standard tornadoes were defined that cover a wide range of possible tornado sizes and intensities. These standard tornadoes are used here to define the tornado wind field, as summarized in table 6.1. The tornado track, shown in fig. 6.5, is located such that $|X_{T3}|/R = \{0.5, 1, 1.5, 2\}$. In total, 108 cases are defined through the parameter variations of this section (i.e. 3 tornadoes $\times$ 9 values of θ_{2_0} $\times$ 4 locations defined by $|X_{T3}|$).

6.4.2 Time step

The use of the predictor-corrector numerical method as the basis of the proposed solution strategy requires the identification of a suitable time step (Δt) that balances the accuracy of the numerical approximations with the computational run-time. A convergence analysis is carried out over the 108 cases defined in section 6.4.1 to determine a suitable Δt. The numerical error, required for the convergence analysis, of any given parameter ($\bullet$) is defined as follows:

$$\epsilon_{\bullet_{j+1}} = \frac{\bullet_{j+1} - \bullet_j}{\bullet_{j+1}} \tag{6.21}$$

where $\bullet_j$ is the estimated value of the parameter of interest at the j^{th} time step.

The parameters of interest in the debris trajectory problem are those related to the debris landing location and impact momentum or energy upon landing. These parameters are the flight time (FT), the flight distance (FD), and the landing velocity (LV). Figure 6.6 shows the convergence of the numerical error for each of these parameters. In generating the results of fig. 6.6, the analysis commenced with $\Delta t = 0.1$ sec and proceeded by reducing Δt by half until $\Delta t = 7.8125 \times 10^{-4}$ sec.

The total error in the three parameters, at the j^{th} time step, is defined as follows:

$$\epsilon_{total_j} = \sqrt{\epsilon^2_{FT_j} + \epsilon^2_{FD_j} + \epsilon^2_{LV_j}} \tag{6.22}$$

Figure 6.7 shows that the solution achieves a total error of less than 2% at $\Delta t = 7.8125 \times 10^{-4}$ sec, fig. 6.7(a), with an average computational run-time of 548 seconds, fig. 6.7(b). This time step was therefore chosen for all subsequent analyses.

6.4.3 Results

Figures 6.8 to 6.10 show the trajectory of the roof sheathing panel for the case of small, medium and large tornadoes. As would be expected, due to higher wind speed,

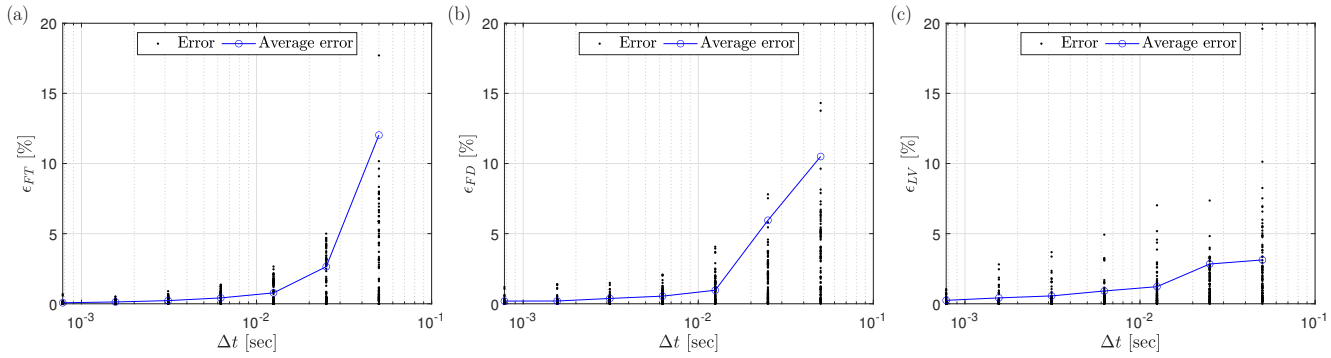

Figure 6.6: Error convergence: (a) flight time error, (b) flight distance error, and (c) landing velocity error.

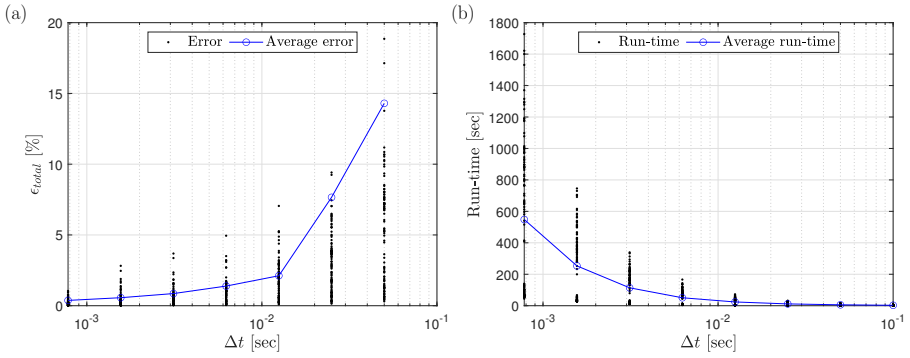

Figure 6.7: Numerical accuracy vs. computational efficiency: (a) convergence of the total error (ϵ_{total}), and (b) computational run-time.

it can be observed that the flight distance for the large tornado is greater than that for the medium tornado which is in turn greater than the small tornado. The tornado track location influences the wind speeds experienced by the panel, which alters the panel trajectory. The highest wind speeds are observed when $|X_{T3}/R| = 1$ which leads to the longest flight distance. The case with $|X_{T3}/R| = 0.5$ and $|X_{T3}/R| = 2$ typically have the smallest initial wind speed. In particular, the case $|X_{T3}/R| = 0.5$ has debris trajectories with the shortest flight distance as the radial inflow tornado velocity component drives the panel towards the center of the tornado, therefore leading to higher wind speeds for $|X_{T3}/R| = 2$ as compared to $|X_{T3}/R| = 0.5$. These variations in the panel trajectory are not observed in the case of straight line winds as the wind field does not vary spatially or temporally. The effect of house orientation (i.e. θ_{2_0}) can be summarized as the more perpendicular (i.e. close to $\theta_{2_0} = 0°$) the house is with respect to the initial tornado wind field velocity, the longer the flight distance will be. As the house orientation moves away from perpendicular to the initial wind velocity, e.g. fig. 6.9(a)-(d) for $\theta_{2_0} = \{-30°, 30°\}$, the initial aerodynamic forces are inadequate for propelling the panel long distances. Figures 6.8 to 6.10 also show the comparison of the trajectories of the panel when subject to non-straight tornado winds versus straight line winds. There are clear differences in the trajectories for each wind type. This difference is smaller in the case of small tornadoes, fig. 6.8, as the wind speeds are not high enough to keep the panel windborne for long distances. This comparison clearly emphasizes the importance of considering the non-straight nature of tornado winds when modeling the flight of wind borne debris.

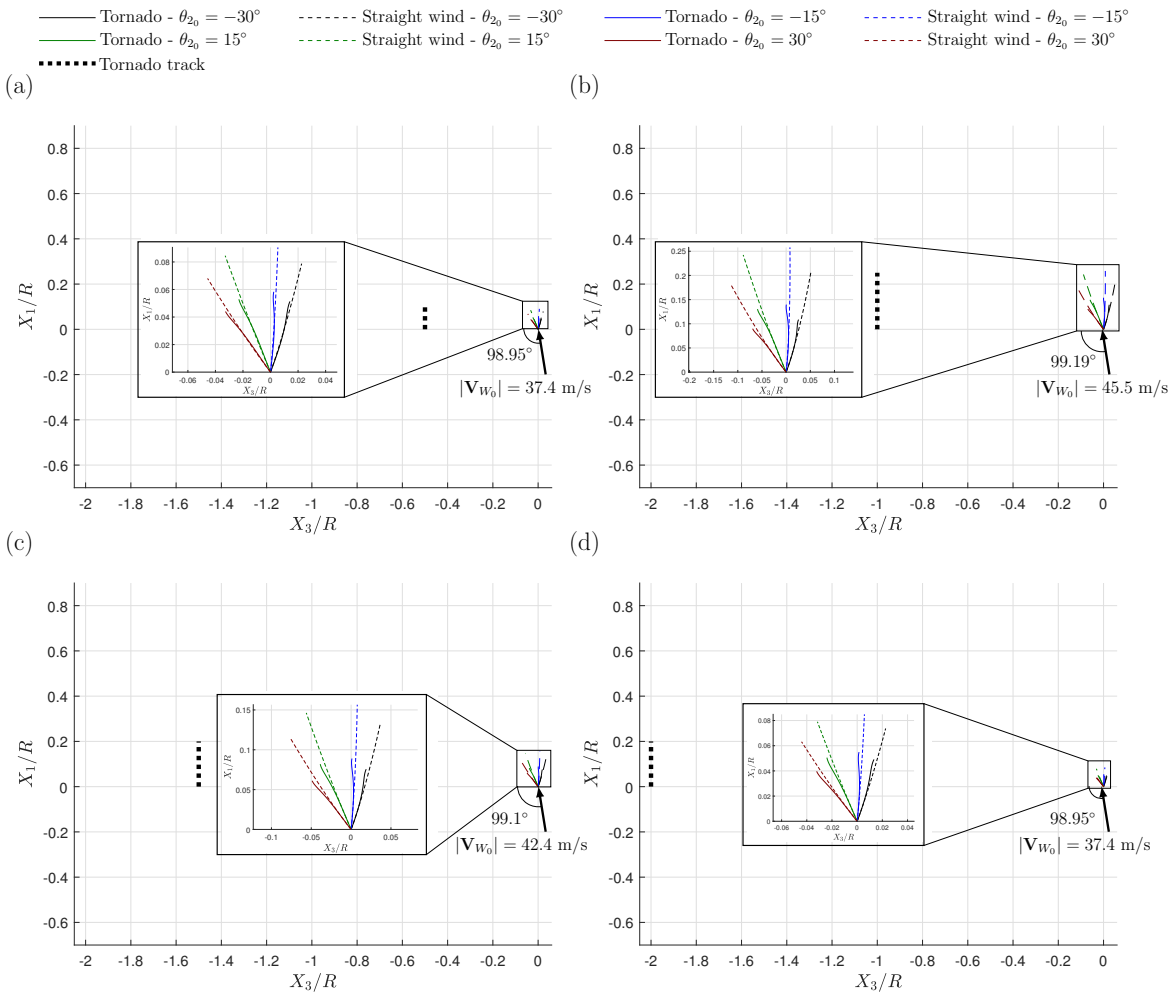

Figure 6.8: Windborne debris trajectory for the small tornado case and the corresponding straight wind case: (a) $|X_{T3}/R| = 0.5$, (b) $|X_{T3}/R| = 1$, (c) $|X_{T3}/R| = 1.5$, and (d) $|X_{T3}/R| = 2$.

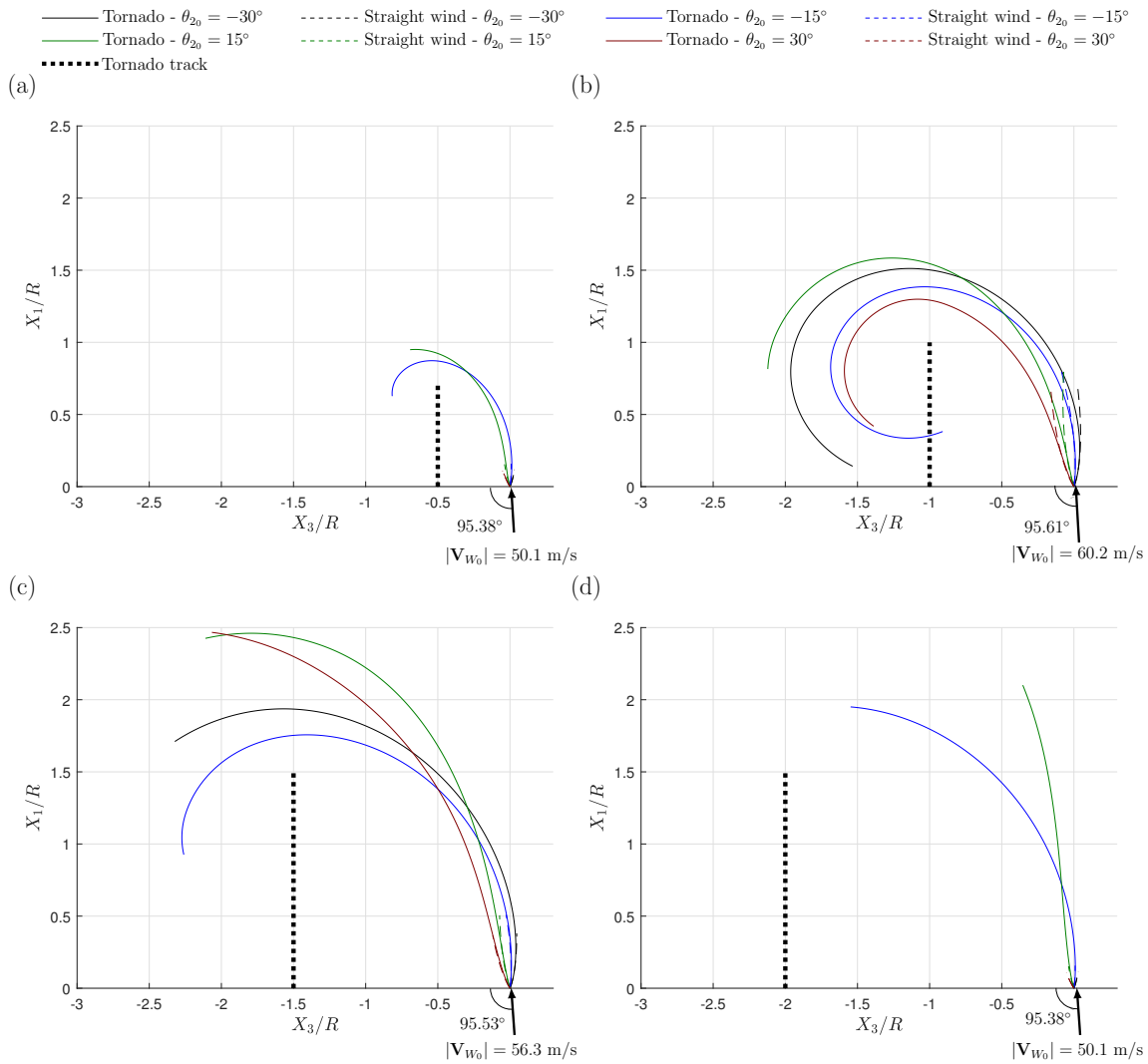

Figure 6.9: Windborne debris trajectory for the medium tornado case and the corresponding straight wind case: (a) $|X_{T3}/R| = 0.5$, (b) $|X_{T3}/R| = 1$, (c) $|X_{T3}/R| = 1.5$, and (d) $|X_{T3}/R| = 2$.

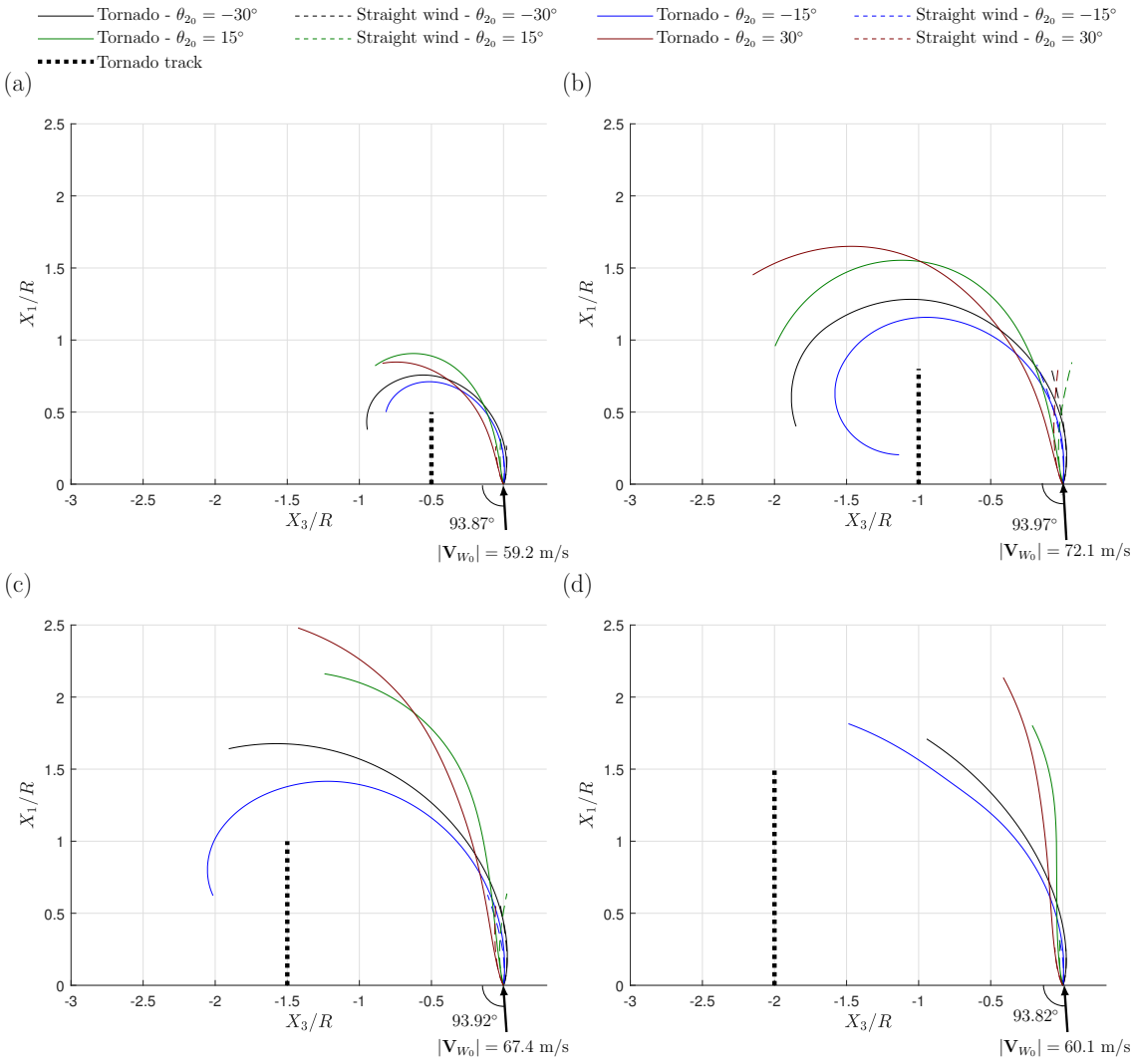

Figure 6.10: Windborne debris trajectory for the large tornado case and the corresponding straight wind case: (a) $|X_{T3}/R| = 0.5$, (b) $|X_{T3}/R| = 1$, (c) $|X_{T3}/R| = 1.5$, and (d) $|X_{T3}/R| = 2$.

6.5 Conclusions

A 3D 6DOF debris trajectory model is presented for describing debris flight in tornado wind fields. The proposed solution strategy is based on a predictor-corrector time-marching scheme. For each time step, the time-marching scheme solves the equations of motion while updating the wind velocity according to a translating tornado wind field model. This update is essential for modeling debris flight in tornadoes as opposed to hurricanes for which the wind field can be approximated using straight line winds. The model is used to estimate the trajectory of a typical plywood roof sheathing panel under various initial conditions and tornadoes of various sizes. The aim is to compare the trajectories generated from tornado wind fields with those generated by straight line winds. The results show that there is a significant difference in trajectories generated by tornado wind fields as opposed to straight line winds. This significant difference clearly illustrates the limits of assuming straight line winds when modeling the flight of debris due to tornado winds.

CHAPTER VII

Summary, Key Contributions and Future Directions

7.1 Summary

This dissertation provides computational frameworks and numerical models that can be used to quantify the resilience of residential wooden buildings against hurricanes and tornadoes. Hurricane-imposed risks and the performance of the residential residential buildings subject to hurricane winds is quantified using a physics-based vulnerability model. The vulnerability model accounts for damage from dynamic wind pressure and impact of windborne debris, including exogenous windborne debris. Resilience of residential wooden buildings subject to hurricane winds is estimated by integrating the developed vulnerability model with a probabilistic recovery model.

Hurricanes are typically associated with heavy precipitation which can result in significant damage to the built environment due to the leakage of rainwater into buildings (i.e. wind-driven rain). If rainfall persists over long periods of time, the failure of the drainage systems will potentially lead to inland flooding. Therefore, hurricane rainfall on residential communities is then incorporated into a framework to quantify its impact on residential wooden buildings. The framework estimates water ingress due to wind-driven rain and inland flooding. Each of the wind-driven rain and inland flooding hazards is of a different nature and requires different mitigation

actions.

Finally, the problem of estimating the damage caused by windborne debris in tornadoes is addressed. Four main items are required to be identified: (1) the nature of debris objects (i.e. mass and shape), which can be identified from damage surveys and field studies; (2) the number of debris objects flying in the wind field, which can be estimated using a pressure damage moel; (3) the landing location; and (4) the impact energy or momentum. To identify the landing location and impact energy or momentum of the windborne debris, this dissertation provides a six-degree-of-freedom (6DOF) debris trajectory model.

These frameworks can be used by decision-makers to compare the current resilience level of residential wooden buildings with target levels, identify gaps, and select the most effective ameliorative strategies.

7.2 Key Contributions

The key contributions of this research work can be summarized as follows:

1. A methodology to account for the effect of exogenous windborne debris while estimating the damage of residential neighborhoods subject to hurricanes is presented.
2. A comprehensive set of hurricane fragility curves are developed for residential wooden buildings that account for the damage from dynamic wind pressure and the impact of windborne debris.
3. The resilience of residential wooden buildings subject to hurricane winds is quantified probabilistically.
4. The impact of hurricane rainfall on residential communities is modeled comprehensively considering both wind-driven rain and inland flooding.

5. The trajectory of windborne debris in tornado wind field is modeled using a 6DOF trajectory model.

7.3 Future Directions

7.3.1 A holistic multi-hazard approach for hurricane resilience

Hurricanes are typically associated with multiple hazards: strong winds, heavy precipitation, storm surge, and even tornadoes. A more comprehensive approach to quantify the resilience of a community against hurricanes is to develop frameworks that are capable of modeling the impact of all hazards. In particular, the developed hurricane vulnerability model can be extended to estimate damage to the built environment due to heavy precipitation and storm surge. With the aim of quantifying community resilience, it is crucial to consider the inevitable interdependencies between the critical infrastructure systems that constitute the community.

7.3.2 Tornado resilient communities

Within the wind engineering field, most of the attention has been focused on the impact of synoptic windstorms (e.g. hurricanes) on structures. Non-synoptic winds, particularly tornadoes, are considered of low-occurrence probability which has hindered the inclusion of tornadic loading provisions in current building codes. Recently, research on tornadoes has increased with a focus on understanding their impact on a community and identifying appropriate mitigation actions. Within this context, there is an opportunity to advance the state-of-the-art of this emerging research field. Estimating tornado damage using high-fidelity engineering-based models that consider interdependencies between various community systems as well as simulating the recovery process will provide insights on a community's response to this severe localized storms. As a result, a community's resilience against tornadoes can be

quantified which is an essential step to mitigate their consequences.

7.3.3 Accelerating the estimation of the community resilience

Besides the intellectual challenges posed by modeling the interdependent response of various community systems to windstorms (e.g. hurricane and tornadoes), there are massive computational challenges that can severely hinder progress in this research area. However, these computational challenges can be addressed with robust GPU computing algorithms that are capable of providing efficient solutions. The advantage of using GPU computing is the ability to accelerate simulations while preserving the level-of-fidelity of the developed models.

With the aim of providing computational tools that can provide real-time resilience quantification (i.e. simulation time in order of seconds), there is a substantial advantage to considering data-driven models and machine learning algorithms. In particular, Kriging surrogate models (metamodels) can be used to establish a computationally inexpensive input/output relationship based on the database generated from the aforementioned high-fidelity models. These computationally inexpensive models will ultimately arm decision-makers with tools for the identification of optimum mitigation strategies as well as targeted intervention plans.

BIBLIOGRAPHY

(2012), *Disaster Resilience: A National Imperative*, The National Academies Press, Washington, DC.

Abdelhady, A. U., S. M. Spence, and J. McCormick (2019a), Realizing hurricane resilient communities through distributed computing, in *Routledge Handbook of Sustainable and Resilient Infrastructure*, pp. 134–151, Routledge.

Abdelhady, A. U., S. M. Spence, and J. McCormick (2019b), Probabilistic Quantification of Hurricane Resilience of Communities through a Distributed Simulation Platform, in *13th International Conference on Applications of Statistics and Probability in Civil Engineering (ICASP13)*, Seoul, South Korea.

Abdelhady, A. U., S. M. Spence, and J. McCormick (2020), A framework for the probabilistic quantification of the resilience of communities to hurricane winds, *Journal of Wind Engineering and Industrial Aerodynamics*, *206*, 104,376.

Abdelhady, A. U., S. M. Spence, and J. McCormick (2021a), A resilience-based assessment of the performance of residential communities subject to hurricane hazard, in *11th International Structural Engineering and Construction Conference (ISEC11)*, Cairo, Egypt.

Abdelhady, A. U., S. M. Spence, and J. McCormick (2021b), Modeling the effect of exogenous windborne debris in hurricanes, *Engineering Structures*, *Submitted*.

Abdelhady, A. U., S. M. Spence, and J. McCormick (2021c), Risk and fragility

assessment of residential wooden buildings subject to hurricane winds, *Structural Safety*, *Submitted*.

Abdelhady, A. U., S. M. Spence, and J. McCormick (2021d), A framework for the estimate of water ingress due to hurricane rainfall, *Building and Environment*, *Under Preparation*.

Abdelhady, A. U., S. M. Spence, and J. McCormick (2021e), A three-dimensional six-degree-of-freedom windborne debris trajectory model for tornadoes, *Journal of Wind Engineering and Industrial Aerodynamics*, *Submitted*.

Abdelhady, A. U., S. M. Spence, and J. McCormick (2022), Towards more resilient communities: A probabilistic framework for the quantification of hurricane resilience, in *13th International Conference on Structural Safety & Reliability (ICOSSAR 2021-2022)*, Shanghai, China.

Abdelhady, A. U., et al. (2019c), A Distributed Computing Platform for Community Resilience Estimation, in *13th International Conference on Applications of Statistics and Probability in Civil Engineering (ICASP13)*, Seoul, South Korea.

Ahmad, S., and K. Kumar (2001), Interference effects on wind loads on low-rise hip roof buildings, *Engineering Structures*, *23*(12), 1577–1589.

Akanbi, A. A., and N. D. Katopodes (1988), Model for flood propagation on initially dry land, *Journal of Hydraulic Engineering*, *114*(7), 689–706, doi: 10.1061/(ASCE)0733-9429(1988)114:7(689).

ASCE/SEI 7-16 (2017), *Minimum design loads and associated criteria for buildings and other structures*, American Society of Civil Engineers, Reston, VA.

Aven, T. (2011), On some recent definitions and analysis frameworks for risk, vulnerability, and resilience, *Risk Analysis*, *31*(4), 515–522.

Baker, C., and M. Sterling (2019), Are tornado vortex generators fit for purpose?, *Journal of Wind Engineering and Industrial Aerodynamics*, *190*, 287–292.

Baker, C. J. (2007), The debris flight equations, *Journal of Wind Engineering and Industrial Aerodynamics*, *95*(5), 329–353.

Baker, C. J., and M. Sterling (2017), Modelling wind fields and debris flight in tornadoes, *Journal of Wind Engineering and Industrial Aerodynamics*, *168*, 312–321.

Baker, C. J., and M. Sterling (2018), A conceptual model for wind and debris impact loading of structures due to tornadoes, *Journal of Wind Engineering and Industrial Aerodynamics*, *175*, 283–291.

Beason, W. L., G. E. Meyers, and R. W. James (1984), Hurricane related window glass damage in Houston, *Journal of Structural Engineering*, *110*(12), 2843–2857.

Begnudelli, L., and B. F. Sanders (2006), Unstructured grid finite-volume algorithm for shallow-water flow and scalar transport with wetting and drying, *Journal of Hydraulic Engineering*, *132*(4), 371–384.

Best, A. C. (1950), The size distribution of raindrops, *Quarterly Journal of the Royal Meteorological Society*, *76*(327), 16–36.

Bhamra, R., S. Dani, and K. Burnard (2011), Resilience: the concept, a literature review and future directions, *International Journal of Production Research*, *49*(18), 5375–5393.

Blocken, B., and J. Carmeliet (2004), A review of wind-driven rain research in building science, *Journal of Wind Engineering and Industrial Aerodynamics*, *92*(13), 1079–1130.

Blocken, B., and J. Carmeliet (2010), Overview of three state-of-the-art wind-driven rain assessment models and comparison based on model theory, *Building and Environment*, *45*(3), 691–703.

Bourque, L. B., J. M. Siegel, M. Kano, and M. M. Wood (2006), Weathering the Storm: The Impact of Hurricanes on Physical and Mental Health, *The ANNALS of the American Academy of Political and Social Science*, *604*(1), 129–151.

Bruneau, M., et al. (2003), A framework to quantitatively assess and enhance the seismic resilience of communities, *Earthquake Spectra*, *19*(4), 733–752.

Burton, H. V., G. Deierlein, D. Lallemant, and T. Lin (2016), Framework for incorporating probabilistic building performance in the assessment of community seismic resilience, *Journal of Structural Engineering*, *142*(8).

Burton, H. V., S. B. Miles, and H. Kang (2018), Integrating performance-based engineering and urban simulation to model post-earthquake housing recovery, *Earthquake Spectra*, *34*(4), 1763–1785.

Burton, H. V., H. Kang, S. B. Miles, A. Nejat, and Y. Zhengxiang (2019), A framework and case study for integrating household decision-making into post-earthquake recovery models, *International Journal of Disaster Risk Reduction*, *37*.

Census Reporter (2017), Miami-Dade County, FL.

Ceskavich, R., and M. Sasani (2018), Methodology for Evaluating Community Resilience, *Natural Hazards Review*, *19*(1), 04017,021.

Choi, E. C. C. (1993), Simulation of wind-driven-rain around a building, *Journal of Wind Engineering and Industrial Aerodynamics*, *46-47*(C), 721–729.

Choi, E. C. C. (1994), Determination of wind-driven-rain intensity on building faces, *Journal of Wind Engineering and Industrial Aerodynamics*, *51*(1), 55–69.

Cimellaro, G. P., A. M. Reinhorn, and M. Bruneau (2010), Framework for analytical quantification of disaster resilience, *Engineering Structures*, *32*, 3639–3649.

Congressional Budget Office (2019), Expected costs of damage from hurricane winds and storm-related flooding.

Dao, T. N., and J. W. Van De Lindt (2010), Methodology for wind-driven rainwater intrusion fragilities for light-frame wood roof systems, *Journal of Structural Engineering*, *136*(6), 700–706.

Datin, P. L., D. O. Prevatt, and W. Pang (2011), Wind-uplift capacity of residential wood roof-sheathing panels retrofitted with insulating foam adhesive, *Journal of Architectural Engineering*, *17*(4), 144–154.

Deborah D'Souza (2019), Hurricane Dorian: Measuring the Economic Impact.

Di Giammarco, P., E. Todini, and P. Lamberti (1996), A conservative finite elements approach to overland flow: the control volume finite element formulation, *Journal of Hydrology*, *175*(1), 267 – 291.

Disse, M., T. G. Johnson, J. Leandro, and T. Hartmann (2020), Exploring the relation between flood risk management and flood resilience, doi: 10.1016/j.wasec.2020.100059.

Dong, Y., and Y. Li (2016), Risk-based assessment of wood residential construction

subjected to hurricane events considering indirect and environmental loss, *Sustainable and Resilient Infrastructure*, *1*(1-2), 46–62.

Edwards, R., J. G. La Due, J. T. Ferree, K. Scharfenberg, C. Maier, and W. L. Coulbourne (2013), Tornado intensity estimation: Past, present, and future, *Bulletin of the American Meteorological Society*, *94*(5), 641–653.

Ellingwood, B. R., D. V. Rosowsky, Y. Li, and J. H. Kim (2004), Fragility assessment of light-frame wood construction subjected to wind and earthquake hazards, *Journal of Structural Engineering*, *130*(12), 1921–1930.

Emanuel, K. (2005), Increasing destructiveness of tropical cyclones over the past 30 years, *nature*, *436*(4), 686–688.

Espinel, Z., J. P. Kossin, S. Galea, A. S. Richardson, and J. M. Shultz (2019), Forecast: Increasing mental health consequences from atlantic hurricanes throughout the 21st Century, *Psychiatric Services*, *70*(12), 1165–1167.

Gavanski, E., B. Kordi, G. A. Kopp, and P. J. Vickery (2013), Wind loads on roof sheathing of houses, *Journal of Wind Engineering and Industrial Aerodynamics*, *114*, 106–121.

Ge, H., U. K. D. Nath, and V. Chiu (2017), Field measurements of wind-driven rain on mid-and high-rise buildings in three Canadian regions, *Building and Environment*, *116*, 228–245.

Gillmeier, S., M. Sterling, H. Hemida, and C. Baker (2018), A reflection on analytical tornado-like vortex flow field models, *Journal of Wind Engineering and Industrial Aerodynamics*, *174*, 10–27.

Gottardi, G., and M. Venutelli (2008), An accurate time integration method for simplified overland flow models, *Advances in Water Resources*, *31*(1), 173 – 180.

Grayson, J. (2014), Building envelope failure assessment of residential developments subjected to hurricane wind hazards, Ph.D. thesis, Clemson University.

Grayson, J. M., W. Pang, and S. Schiff (2012a), Three-dimensional probabilistic wind-borne debris trajectory model for building envelope impact risk assessment, *Journal of Wind Engineering and Industrial Aerodynamics*, *102*, 22–35.

Grayson, J. M., W. Pang, and S. Schiff (2013), Building envelope failure assessment framework for residential communities subjected to hurricanes, *Engineering Structures*, *51*, 245–258.

Grayson, M., W. Pang, and S. Schiff (2012b), Three-dimensional probabilistic wind-borne debris trajectory model for building envelope impact risk assessment, *Journal of Wind Engineering and Industrial Aerodynamics*, *102*, 22–35.

Guo, Y., and J. van de Lindt (2019), Simulation of Hurricane Wind Fields for Community Resilience Applications: A Data-Driven Approach Using Integrated Asymmetric Holland Models for Inner and Outer Core Regions, *Journal of Structural Engineering*, *145*(9), 04019,089.

Gurley, K., et al. (2005), *Florida public hurricane loss projection model, engineering team final report*, International Hurricane Research Center Florida International University, Miami, FL.

Haggag, M., M. Ezzeldin, W. El-Dakhakhni, and E. Hassini (2020), Resilient cities critical infrastructure interdependence: a meta-research, *Sustainable and Resilient Infrastructure*, pp. 1–22.

Haimes, Y. Y. (2009), On the definition of resilience in systems, *Risk Analysis*, *29*(4), 498–501.

Han, Z., D. Ma, B. Hou, and W. Wang (2020), Seismic resilience enhancement of urban water distribution system using restoration priority of pipeline damages, *Sustainability (Switzerland)*, *12*(3), doi:10.3390/su12030914.

Harriet Torry, and Sarah Chaney (2018), Big Storms Leave Small Marks on the U.S. Economy - WSJ.

Hassan, E. M., H. N. Mahmoud, and B. R. Ellingwood (2020), Resilience of School Systems Following Severe Earthquakes, *Earth's Future*, *8*(10).

HAZUS-MH 2.1 (2003), *Multi-hazard loss estimation methodology, earthquake model, technical manual (HAZUS-MH 2.1)*, Department of Homeland Security, Federal Emergency Management Agency (FEMA), Mitigation Division, Washington, D.C.

He, J., F. Pan, and C. S. Cai (2017), A review of wood-frame low-rise building performance study under hurricane winds, *Engineering Structures*, *141*, 512–529.

Holland, G. J. (1980), An analytic model of the wind and pressure profiles in hurricanes., *Monthly Weather Review*, *108*(8), 1212–1218.

Holmes, J. D. (2017), *Wind Loading of Structures*, CRC Press, USA.

Holmes, J. D., C. W. Letchford, and N. Lin (2006), Investigations of plate-type windborne debris - part II: Computed trajectories, *Journal of Wind Engineering and Industrial Aerodynamics*, *94*(1), 21–39.

Horritt, M. S. (2002), Evaluating wetting and drying algorithms for finite element models of shallow water flow, *International Journal for Numerical Methods in Engineering*, *55*(7), 835–851.

Hosseini, S., K. Barker, and J. E.Ramirez-Marquez (2016a), A review of definitions and measures of system resilience, *Reliability Engineering and System Safety*, *145*, 47–61.

Hosseini, S., K. Barker, and J. E. Ramirez-Marquez (2016b), A review of definitions and measures of system resilience, *Reliability Engineering and System Safety*, *145*, 47–61.

Huang, S. H., and Q. S. Li (2010), Numerical simulations of wind-driven rain on building envelopes based on Eulerian multiphase model, *Journal of Wind Engineering and Industrial Aerodynamics*, *98*(12), 843–857.

ISO (1997), Hygrothermal performance of buildings — Climatic data — Part 3: calculation of a driving rain index for vertical surfaces from hourly wind and rain data, Draft prEN 13013-3, *Tech. rep.*, International Organization for Standardization.

Ivanov, V. Y., E. R. Vivoni, R. L. Bras, and D. Entekhabi (2004), Catchment hydrologic response with a fully distributed triangulated irregular network model, *Water Resources Research*, *40*(11).

Ivanov, Y. V., et al. (2021), Breaking Down the Computational Barriers to Real-Time Urban Flood Forecasting, *AGU Advances*, *Submitted*.

Jain, V. K., R. Davidson, and D. Rosowsky (2005), Modeling changes in hurricane risk over time, *Natural Hazard Review*, *6*(2), 88–96.

Jakobsen, F., and H. Madsen (2004), Coparison and further development of parametric tropical cyclone models for storm surge modelling, *Journal of Wind Engineering and Industrial Aerodynamics*, *92*, 375–391.

Kim, J., A. Warnock, V. Y. Ivanov, and N. D. Katopodes (2012), Coupled modeling of hydrologic and hydrodynamic processes including overland and channel flow, *Advances in Water Resources*, *37*, 104 – 126.

Koordinates (2021), Houston, Texas Building Footprints - Harris County — GIS Map Data — City of Houston, Texas — Koordinates.

Kosiba, K., and J. Wurman (2010), The three-dimensional axisymmetric wind field structure of the Spencer, South Dakota, 1998 Tornado, *Journal of the Atmospheric Sciences*, *67*(9), 3074–3083.

Kubilay, A., D. Derome, B. Blocken, and J. Carmeliet (2013), CFD simulation and validation of wind-driven rain on a building facade with an Eulerian multiphase model, *Building and Environment*, *61*, 69–81.

Kubilay, A., D. Derome, B. Blocken, and J. Carmeliet (2014), Numerical modeling of turbulent dispersion for wind-driven rain on building facades, *Environmental Fluid Mechanics*, *15*(1), 109–133.

Kubilay, A., D. Derome, and J. Carmeliet (2017), Analysis of time-resolved wind-driven rain on an array of low-rise cubic buildings using large eddy simulation and an eulerian multiphase model, *Building and Environment*, *114*, 68–81.

Kyle Grammatica (), Impact of Hurricanes on the Environment — Fish and Wildlife Foundation of Florida.

Lee, K. H., and D. V. Rosowsky (2005), Fragility assessment for roof sheathing failure in high wind regions, *Engineering Structures*, *27*(6), 857–868.

Li, Y., and B. R. Ellingwood (2006), Hurricane damage to residential construction

in the US: Importance of uncertainty modeling in risk assessment, *Engineering Structures*, *28*(7), 1009–1018.

Lin, N., and E. Vanmarcke (2010a), Windborne debris risk analysis - part I. introduction and methodology, *Wind and Structures*, *13*(2), 191–206.

Lin, N., and E. Vanmarcke (2010b), Windborne debris risk analysis - part I. introduction and methodology, *Wind and Structures*, *13*(2), 191–206.

Lin, N., C. Letchford, and J. Holmes (2006), Investigation of plate-type windborne debris - part I: Experiments in wind tunnel and full scale, *Journal of Wind Engineering and Industrial Aerodynamics*, *94*(2), 51–76.

Lin, N., E. Vanmarcke, and S.-C. Yau (2010a), Windborne debris risk analysis-part II. application to structural vulnerability modeling, *Wind and Structures*, *13*(2), 207–220.

Lin, N., E. Vanmarcke, and S.-C. Yau (2010b), Windborne debris risk analysis - part II. application to structural vulnerability modeling, *Wind and Structures*, *13*(2), 207–220.

Lu, X., W. Liao, D. Fang, K. Lin, Y. Tian, C. Zhang, Z. Zheng, and P. Zhao (2020), Quantification of disaster resilience in civil engineering: A review, *Journal of Safety Science and Resilience*, *1*(1), 19–30.

Marshall, T. P. (2002), Tornado damage survey at Moore, Oklahoma, *Weather and Forecasting*, *17*(3), 582–598.

Maruyama, T. (2011), Simulation of flying debris using a numerically generated tornado-like vortex, *Journal of Wind Engineering and Industrial Aerodynamics*, *99*, 249–256.

Masoomi, H., and J. W. van de Lindt (2018), Restoration and functionality assessment of a community subjected to tornado hazard, *Structure and Infrastructure Engineering*, *14*(3), 275–291.

Masoomi, H., M. R. Ameri, and J. W. Van De Lindt (2018), Wind performance enhancement strategies for residential wood-frame buildings, *Journal of Performance of Constructed Facilities*, *32*(3).

Masters, F. J., K. R. Gurley, N. Shah, and G. Fernandez (2010), The vulnerability of residential window glass to lightweight windborne debris, *Engineering Structures*, *32*(4), 911–921.

McClymont, K., D. Morrison, L. Beevers, and E. Carmen (2020), Flood resilience: a systematic review, *Journal of Environmental Planning and Management*, *63*(7), 1151–1176.

McDonald, J. R. (1990), Impact resistance of common building materials to tornado missiles, *Journal of Wind Engineering and Industrial Aerodynamics*, *36*(PART 2), 717–724.

Meerow, S., J. P. Newell, and M. Stults (2016), Defining urban resilience: A review.

Memari, M., N. Attary, H. Masoomi, H. Mahmoud, J. W. van de Lindt, S. F. Pilkington, and M. R. Ameri (2018), Minimal Building Fragility Portfolio for Damage Assessment of Communities Subjected to Tornadoes, *Journal of Structural Engineering*, *144*(7), 4018,072.

Miles, S. B., and S. E. Chang (2006), Modeling community recovery from earthquakes, *Earthquake Spectra*, *22*(2), 439–458.

Minor, J. E. (1994), Windborne debris and the building envelope, *Journal of Wind Engineering and Industrial Aerodynamics*, *53*(1-2), 207–227.

Mitchell, T., and K. Harris (2012 (accessed April 30, 2018)), *Resilience: A risk management approach, Background note*, Overseas Development Institute (odi), London, UK.

National Oceanic and Atmospheric Admenstiration (NOAA) (2017), Hurricane Harvey 2017 Data Archive.

NCEI (2017), NEXRAD Products — National Centers for Environmental Information (NCEI) formerly known as National Climatic Data Center (NCDC).

NOAA (2013), *National coastal population report: Population trends from 1970 to 2020*, National Oceanic and Atmospheric Adminstration, Washington, DC.

NOAA Satellite Imagery of Hurricane Harvey (2017), NOAA National Environmental Satellite, Data, and Information Service (NESDIS).

Nofal, O. M., and J. W. Van De Lindt (2020), Probabilistic Flood Loss Assessment at the Community Scale: Case Study of 2016 Flooding in Lumberton, North Carolina, *ASCE-ASME Journal of Risk and Uncertainty in Engineering Systems, Part A: Civil Engineering*, *6*(2), 05020,001.

Nofal, O. M., and J. W. van de Lindt (2020), Understanding flood risk in the context of community resilience modeling for the built environment: research needs and trends, *Sustainable and Resilient Infrastructure*, pp. 1–17.

Ouyang, Z., and S. M. J. Spence (2019), A performance-based damage estimation framework for the building envelope of wind-excited engineered structures, *Journal of Wind Engineering and Industrial Aerodynamics*, *186*, 139 – 154.

Ouyang, Z., and S. M. J. Spence (2020), A performance-based wind engineering framework for envelope systems of engineered buildings subject to directional wind and rain hazards, *Journal of Structural Engineering*, *146*(5), 04020,049.

Pita, G., J.-P. Pinelli, K. Gurley, and J. Mitrani-Reiser (2015), State of the art of hurricane vulnerability estimation methods: A review, *Natural Hazards Review*, *16*(2), 1–16.

Raji, F., I. Zisis, and J. P. Pinelli (2020), Experimental Investigation of Wind-Driven Rain Propagation in a Building Interior, *Journal of Structural Engineering*, *146*(7), 04020,114.

Redmann, G. H., J. R. Radbill, J. E. Marte, P. Dergarabedian, and F. E. Fendell (1978), Wind field and trajectory models for tornado-propelled objects, *Tech. Rep. NASA-CR-158775*, NASA.

Rhodes, J., C. Chan, C. Paxson, C. E. Rouse, M. Waters, and E. Fussell (2010), The Impact of Hurricane Katrina on the Mental and Physical Health of Low-Income Parents in New Orleans, *American Journal of Orthopsychiatry*, *80*(2), 237–247.

Ribeiro, P. J. G., and L. A. Pena Jardim Gonçalves (2019), Urban resilience: A conceptual framework, doi:10.1016/j.scs.2019.101625.

Richards, P. J., N. Williams, B. Laing, M. Mccarty, and M. Pond (2008a), Numerical calculation of the three-dimensional motion of wind-borne debris, *Journal of Wind Engineering and Industrial Aerodynamics*, *96*, 2188–2202.

Richards, P. J., N. Williams, B. Laing, M. McCarty, and M. Pond (2008b), Numerical calculation of the three-dimensional motion of wind-borne debris, *Journal of Wind Engineering and Industrial Aerodynamics*, *96*, 2188–2202.

Robert M. Horkovich (2017), The Environmental Impact of Hurricanes – Risk Management.

Rosowsky, D. V. (2020), Defining resilience, *Sustainable and Resilient Infrastructure*, *5*(3), 125–130.

Sallenger, A. (), Hurricane Impacts on the Coastal Environment - USGS Fact Sheet.

Sanders, B. F. (2008), Integration of a shallow water model with a local time step, *Journal of Hydraulic Research*, *46*(4), 466–475.

Sediek, O. A., S. El-Tawil, and J. McCormick (2020), Dynamic Modeling of In-Event Interdependencies in Community Resilience, *Natural Hazards Review*, *21*(4), 04020,041.

Sen, M. K., S. Dutta, G. Kabir, N. N. Pujari, and S. A. Laskar (2021), An integrated approach for modelling and quantifying housing infrastructure resilience against flood hazard, *Journal of Cleaner Production*, *288*, 125,526.

Sharma, N., A. Tabandeh, and P. Gardoni (2017), Resilience analysis: a mathematical formulation to model resilience of engineering systems, *Sustainable and Resilient Infrastructure*.

Sharma, N., A. Tabandeh, and P. Gardoni (2018), Resilience analysis: a mathematical formulation to model resilience of engineering systems, *Sustainable and Resilient Infrastructure*, *3*(2), 49–67.

Shih, T. H., W. W. Liou, A. Shabbir, Z. Yang, and J. Zhu (1995), A new $k-\epsilon$ eddy viscosity model for high reynolds number turbulent flows, *Computers and Fluids*, *24*(3), 227–238.

sigma (2017), *Natural catastrophes and man-made disasters in 2016: A year of widespread damages*, sigma 2/2017, Swiss Re., London.

Simiu, E., and M. Cordes (1976), Tornado-borne missile speeds, *Tech. Rep. PB–253111*, National Bureau of Standards, Washington, D.C. (USA).

Stochino, F., C. Bedon, J. Sagaseta, and D. Honfi (2019), Robustness and resilience of structures under extreme loads, doi:10.1155/2019/4291703.

Straube, J. (1997), Moisture control and enclosure wall systems, Ph.D. thesis, University of Waterloo, Waterloo, Ontario, Canada.

Strobl, E. (2011), The Economic Growth Impact of Hurricanes: Evidence From U.S. Coastal Counties, *The Review of Economics and Statistics*, *93*(2), 575–589.

Surry, D., and J. X. Lin (1995), The effect of surroundings and roof corner geometric modifications on roof pressures on low-rise buildings, *Journal of Wind Engineering and Industrial Aerodynamics*, *58*(1-2), 113–138.

Tachikawa, M. (1983), Trajectories of flat plates in uniform flow with application to wind-generated missiles, *Journal of Wind Engineering and Industrial Aerodynamics*, *14*(1-3), 443–453.

Tachikawa, M. (1988), A method for estimating the distribution range of trajectories of wind-borne missiles, *Journal of Wind Engineering and Industrial Aerodynamics*, *29*(1-3), 175–184.

Tanamachi, R. L., H. B. Bluestein, W. C. Lee, M. Bell, and A. Pazmany (2007), Ground-based velocity track display (GBVTD) analysis of W-band Doppler radar data in a tornado near Stockton, Kansas, on 15 May 1999, *Monthly Weather Review*, *135*(3), 783–800.

Tanner, L. J. (2002), Tornado damage in Happy, Texas, *Tech. rep.*, Wind Science and Engineering Research Center, Texas Tech University, Lubbock, Texas.

Teng, J., A. J. Jakeman, J. Vaze, B. F. Croke, D. Dutta, and S. Kim (2017), Flood inundation modelling: A review of methods, recent advances and uncertainty analysis, *Environmental Modelling and Software*, *90*, 201–216.

Tokyo Polytechnic University (2007), Aerodynamic database of non-isolated low-rise buildings.

Unnikrishnan, V. U., and M. Barbato (2016), Performance-Based Comparison of Different Storm Mitigation Techniques for Residential Buildings, *Journal of Structural Engineering*, *142*(6), 04016,011.

USGS (2017), USGS 08074540 Little Whiteoak Bayou at Trimble St, Houston, TX.

USGS (2021), The National Map - Data Delivery.

van de Lindt, J. W., and T. N. Dao (2009), Performance-based wind engineering for wood-frame buildings, *Journal of Structural Engineering*, *135*(2), 169–177.

van de Lindt, J. W., et al. (2020), Community Resilience-Focused Technical Investigation of the 2016 Lumberton, North Carolina, Flood: An Interdisciplinary Approach, *Natural Hazards Review*, *21*(3), 04020,029.

Vickery, P. J., and L. A. Twisdale (1995a), Prediction of hurricane wind speeds in the United States, *Journal of Structural Engineering*, *121*(11), 1691–1699.

Vickery, P. J., and L. A. Twisdale (1995b), Wind-field and filling models for hurricane wind speed predicitons, *Journal of Structural Engineering*, *121*(11), 1700–1709.

Vickery, P. J., P. F. Skerlj, and L. A. Twisdale (2000), Simulation of hurricane risk in the U.S. using empirical track model, *Journal of structural engineering*, *126*(10), 1222–1237.

Vickery, P. J., J. Lin, P. F. Skerlj, L. A. Twisdale, and K. Huang (2006a), HAZUS-MH Hurricane Model Methodology. I: Hurricane Hazard, Terrain, and Wind Load Modeling, *Natural Hazards Review*, *7*(2), 82–93.

Vickery, P. J., P. F. Skerlj, J. Lin, L. A. T. Jr., M. A. Young, and F. M. Lavelle (2006b), HAZUS-MH hurricane model methodology. II: Damage and loss estimation, *Natural Hazards Review*, *7*(2), 94–103.

Vutukuru, K. S., M. Moravej, A. Elawady, and A. G. Chowdhury (2020), Holistic testing to determine quantitative wind-driven rain intrusion for shuttered and impact resistant windows, *Journal of Wind Engineering and Industrial Aerodynamics*, *206*, 104,359.

Walker, G. R. (2011), Modelling the vulnerability of buildings to wind-a review, *Canadian Journal of Civil Engineering*, *38*(9), 1031–1039.

Wang, H., W. Song, and Y. Chen (2019), Numerical simulation of wind-driven rain distribution on building facades under combination layout, *Journal of Wind Engineering and Industrial Aerodynamics*, *188*(February), 375–383.

Webster, P. J., G. J. Holland, J. A. Curry, and H.-R. Chang (2005), Increasing destructiveness of tropical cyclones over the past 30 years, *Science*, *309*(5742), 1844–1846.

Weller, H. G., G. Tabor, H. Jasak, and C. Fureby (1998), A tensorial approach to

computational continuum mechanics using object-oriented techniques, *Computers in physics*, *12*(6), 620–631.

Wetsman, N. (2019), Connecting the dots on hurricanes and mental health issues — Popular Science.

Wills, J. A. B., B. E. Lee, and T. A. Wyatt (2002), A model of wind-borne debris damage, *Journal of Wind Engineering and Industrial Aerodynamics*, *90*, 555–565.

Woods, D. D. (2015), Four concepts for resilience and the implications for the future of resilience engineering, *Reliability Engineering and System Safety*, *141*, 5–9.

Yau, S. C. (2011), Wind hazard risk assessment and management for structures, Ph.D. thesis, Princeton University.

Yau, S. C., N. Lin, and E. Vanmarcke (2011), Hurricane damage and loss estimation using an integrated vulnerability model, *Natural Hazards Review*, *12*(4), 184–189.

Zhang, S., K. Nishijima, and T. Maruyama (2014), Reliability-based modeling of typhoon induced wind vulnerability for residential buildings in Japan, *Journal of Wind Engineering and Industrial Aerodynamics*, *124*, 68–81.